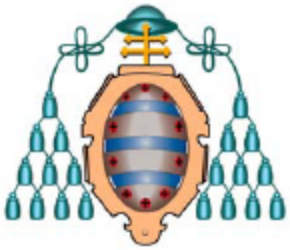

UNIVERSIDAD DE OVIEDO

DEPARTAMENTO DE FÍSICA

Influencia de la morfología y la estructura cristalina en las propiedades magnéticas de películas delgadas de Co

Borja Presa Ordiz

Junio 2012

A Irene, mi mujer,
que con tanta convicción
me ha animado a escribir esta tesis.

Índice general

Índice de figuras

Capítulo 3:

Índice de tablas

Capítulo 4:

Agradecimientos

En primer lugar debo expresar mi agradecimiento a mis directores, Javier Fernández Calleja y Mª del Carmen Contreras Sanz, por haberme permitido trabajar en su grupo de investigación y por su gran ayuda aportada en todo momento durante estos años. También he de reconocer mi agradecimiento al profesor Rafael Matarranz Fernández por la inestimable ayuda en los cálculos numéricos.

También quiero mostrar mi gratitud al resto de personas que de una forma u otra han contribuido al desarrollo de esta tesis: Yves Huttel, Alfonso Cebollada, Montserrat García, Kevin O'Grady y Luis Eugenio Fernández.

Y finalmente aunque no cite explícitamente sus nombres, les dedico este trabajo a mi familia y amigos, ya que ellos son la verdadera fuente de toda inspiración porque sin su apoyo y paciencia nada de esto sería posible.

Resumen

Para determinar la influencia de la morfología y la estructura cristalina en las propiedades magnéticas de películas delgadas de Co se llevó a cabo la presente tesis. Las diferentes características físicas de las muestras se consiguieron modificando las condiciones de fabricación de éstas.

Se fabricaron películas delgadas de Co policristalino mediante una técnica de pulverización catódica que permite variar el tamaño del grano mediante el control de la velocidad de deposición. Los espesores de Co estudiados varían desde 10 a 170 nm. El tamaño del grano aumenta al aumentar el espesor depositado y como consecuencia la anisotropía evoluciona desde una anisotropía uniáxica en el plano muy bien definida para granos pequeños hasta un estado isótropo en el caso de granos más grandes. El aumento del tamaño del grano implica un aumento del campo coercitivo y de la intensidad del anclaje de las paredes de dominio, tal como se observa en las medidas de Susceptibilidad Transversal (ST). Este último parámetro determina el campo al cual tiene lugar la inversión de la imanación y es por tanto fundamental en la descripción de los materiales para memorias RAM.

Por otra parte, se fabricaron películas delgadas de Co nanoestructurado en forma de islas. Este crecimiento se consiguió depositando Co sobre Si_3N_4 mediante pulverización catódica a 550 °C. Las islas se depositaron con un recubrimiento de Pt (magnéticamente polarizable) o de Au (no polarizable) con el fin de estudiar el efecto de la interacción entre partículas. Tanto el tamaño medio de las islas (D) como la dispersión de la distribución de tamaños aumentan con el espesor nominal, debido a la unión de islas vecinas. Las medidas de ST ponen de manifiesto que las muestras son isótropas en el plano debido a un crecimiento del Co en fase hcp sin textura. Tanto el campo de anisotropía como el campo coercitivo aumentan con el tamaño medio de las islas siguiendo una ley D^6, de acuerdo con las predicciones del modelo de anisotropía aleatoria para sistemas tridimensionales. El papel del recubrimiento se pone de manifiesto en el comportamiento magnético de las muestras, llegándose a observar comportamiento superparamagnético a temperatura ambiente en el caso de muestras recubiertas con Au, siendo ferromagnéticas sus homólogas recubiertas con Pt.

Con el fin de estudiar la morfología, estructura cristalina y propiedades magnéticas de Co crecido epitaxialmente, se fabricaron tricapas de V/Co/MgO y Co/V/MgO. Se obtiene de esta manera Co(001) fcc sobre MgO y Co hcp sobre V. El Co hcp crece con el eje c en el plano, obteniéndose dos dominios, cada uno con el eje c a 90° del otro. En ambos casos las muestras presentan anisotropía biáxica en el plano, como es de esperar dada la estructura cristalina obtenida. En ambos casos, para un espesor de la capa de Co de 2 nm, el valor obtenido de la anisotropía a partir de medidas de ST, es mucho más pequeño que el correspondiente al Co en volumen. Para espesores de Co de 20 nm se obtiene sin embargo un valor de la constante de anisotropía próximo al del Co volúmico (en el caso de Co fcc) y las muestras de Co hcp no se pueden saturar a lo largo del eje difícil. Todo ello conduce a que en las etapas iniciales del crecimiento el Co crece de manera discontinua, de manera que la anisotropía magnética viene determinada por las tensiones y la anisotropía de forma. Al aumentar el espesor de Co, la anisotropía magnética está dominada por la anisotropía magnetocristalina del mismo. Además, las muestras de Co fcc con 2 nm de Co presentan una anisotropía uniáxica inducida que desaparece para espesores mayores, cuya aparición se asocia al sustrato, dato que redunda en la discontinuidad de la capa de Co en las primeras etapas de crecimiento. Es interesante el hecho de que una capa de V crecida sobre el Co fcc produce una disminución del campo coercitivo, es decir, el V favorece la inversión de la imanación. Los ciclos de histéresis a lo largo del eje difícil del Co hcp presentan una inesperada asimetría. El estudio de los ciclos de histéresis a campos altos y de los ciclos FC y ZFC a 5 K permite concluir que los procesos de imanación a lo largo del eje difícil tienen lugar mediante rotación de la imanación a campos elevados seguido de desplazamiento de paredes a campos más bajos. La asimetría desaparece cuando se alcanza la saturación.

Abstract

The aim of this work is to investigate the influence of morphology and crystallographic structure on the magnetic properties of Co thin films. In order to attain the objectives targeted, Co thin films with different morphologies were fabricated and characterized. Different morphologies were attained by modifying the deposition conditions.

Polycrystalline Co thin films were grown by sputtering, Co grain size being controlled by controlling the deposition rate growth. Thickness values range between 10 and 170 nm. Grain size increases with increasing thickness. As a result, the anisotropy of the samples evolves from a well-defined in plane anisotropy for the thinner samples to an isotropic state in the case of the thicker ones. The coercive force and the intensity of the domain wall pinning also increase with the grain size, as shown by Transverse Susceptibility (TS) measurements. The latter parameter is vital in MRAM materials since it determines the switch of the magnetization.

Co islands were grown by sputtering at 550 °C on Si_3N_4. The islands were subsequently capped with a Pt layer (magnetically polarizable) or with a Au layer (non polarizable). Both the mean grain size (D) and the grain size dispersión increase with increasing thickness, due to percolation. According to TS measurements the samples are isotropic in-plane, in agreement with hcp without texture growth of Co. Both the anisotropy field and the coercive force depend on D according to a D^6 law, typical of 3-dimensional systems in the framework of the random magnetic anisotropy model. Interparticle interaction was investigated by using Pt or Au capping layers. While Pt capped films were ferromagnetic at room temperature, the Au capped counterparts were superparamagnetic.

V/Co/MgO and Co/V/MgO trilayers were fabricated in order to study the properties of epitaxial fcc and hcp Co. fcc Co(001) is grown on MgO and hcp Co is grown on V. Two hcp domains were obtained with the c-axis in plane and at 90° from each other. In both cases in-plane fourfold anisotropy was obtained, as expected. For Co thickness of 2 nm the value of the anisotropy is too low to be attributed to Co magnetocrystalline anisotropy. For fcc Co thickness of 20 nm, a value of the anisotropy

close to that of bulk Co is obtained, while hcp Co 20-thick samples could not be saturated along the hard axis. Moreover, 2-nm thick fcc Co samples exhibit a superimposed uniaxial anisotropy. In conclusion, the Co layer is not continuously at the early stages of growth, and contributions from stress and shape anisotropy are expected to the magnetic anisotropy value. A V layer on the Co layer diminishes the coercive force, i.e., it favors the magnetization reversal.

In the case of hcp Co, an expected asymmetry was observed in the hysteresis loops along the hard axis. According to high field hysteresis loops and FC and ZFC hysteresis loops at 5 K, the magnetization reversal takes place via magnetization reversal al high fields and domain wall displacement at lower fields. Only when magnetic saturation is attained, the asymmetry vanishes.

Capítulo 1

Introducción

1.1 Antecedentes

El desarrollo de nuevas tecnologías ha dado lugar a la fabricación y caracterización de materiales de dimensiones nanométricas[1,2]

El término nanoestructuras caracteriza a materiales cuyo tamaño estructural varía desde 1 a 100 nm. Ejemplos de nanoestructuras magnéticas artificiales son los nanohilos, nanotubos, películas delgadas, sistemas multicapa y sistemas nanoparticulados. El comportamiento magnético de las nanopartículas está directamente relacionado con su tamaño. Por debajo de un diámetro crítico, las partículas tienden a formar monodominios, ya que la formación de paredes de dominio requeriría un gasto energético mayor. El tamaño crítico suele ser de unas decenas de nanómetros y está relacionado tanto con la naturaleza del material como con anisotropías que presente dicho sistema[3,4].

En estas escalas, la relación superficie/volumen es tan elevada que afecta drásticamente su comportamiento magnético. La interacción entre las partículas juega un papel relevante en este tipo de sistemas. Se pueden llegar a observar y medir algunos efectos cuánticos, como por ejemplo el "tunneling" cuántico de momento magnético y la interacción RKKY en sistemas tricapa FM/M/FM, donde M representa un metal no magnético y FM un material ferromagnético[5,6,7].

En los sistemas multicapa, las interacciones entre los espines en las intercaras influyen de manera decisiva en el comportamiento del material. Un ejemplo de ello sería el canje, que aunque conocido desde hace 50 años en sistemas multicapa, también se ha observado en las fronteras de grano en sistemas nanoparticulados[8,9,10]. Estas características entre otras son responsables de que las propiedades magnéticas en los sistemas nanoestructurados no sean las mismas que en los materiales masivos.

Las aplicaciones de los sistemas granulares son múltiples y variadas, tanto en sistemas de grabación magnética, en sensores magnéticos o en biomedicina[11,12,13,14]. El poder diseñar y optimizar los sistemas nanoestructurados, despierta gran interés tanto desde el punto de vista de la investigación aplicada como en la ciencia básica, ya que comprender el comportamiento de este tipo de sistemas resulta primordial para optimizar sus propiedades. La capacidad de fabricar materiales magnéticos en forma de láminas delgadas con morfologías diversas ha dado lugar al descubrimiento de nuevos fenómenos físicos, acompañado de un exhaustivo desarrollo teórico. Todo ello ha favorecido el desarrollo de un gran número de nuevas aplicaciones tecnológicas. Las propiedades físicas de las láminas delgadas dependen de que ésta sea continua o formada por agregados de estructuras nanométricas y en este último caso dependen también del tamaño, distribución e interacción de las nanoestructuras que la forman. El Cobalto es unos de los elementos magnéticos por excelencia, y bien él solo o en aleación con otros elementos, es un componente básico de los dispositivos magnéticos. Así, por ejemplo, películas delgadas de Co se usan como capa libre en las uniones de efecto túnel, capas de partículas de Co se utilizan en sensores magnéticos y multicapas formadas por capas de Co separadas por capas de metal de transición no magnético se han utilizado para obtener acoplamiento oscilante.

1.2 Motivación

La motivación del trabajo se encuentra en el amplio espectro de aplicaciones tecnológicas de las películas delgadas de Co. A continuación detallamos el interés tecnológico del Co en las morfologías estudiadas en esta tesis.

Las películas delgadas de Co policristalino forman parte de uniones de efecto túnel de $La_{0.67}Sr_{0.33}MnO_3/SrTiO_3/Co$ [15] y de $Ni_{81}Fe_{19}/AlO_x/Co$ [16]. Estas estructuras forman los ladrillos con los que se fabrican estructuras más complejas que conforman dispositivos como cabezas lectoras o memorias RAM. En las uniones de efecto túnel los procesos de inversión de la imanación de los electrodos magnéticos son importantes porque, primero, para conseguir un valor lo más elevado posible de la magnetorresistencia ha de conseguirse un alineamiento antiparalelo perfecto y uniforme

de los momentos de los electrodos. Segundo, en el caso de los dispositivos para memorias RAM es deseable que la inversión de la imanación tenga lugar en un pequeño margen de campo magnético. Además, la inversión de cada elemento debe ser reproducible. Por último, los procesos de imanación en el electrodo libre deben tener lugar por rotación coherente.

Las nanoestructuras de Co crecidas sobre Si_3N_4, formadas por islas de dimensiones nanométricas de Co, se integran como componentes de microsensores ópticos[17]. Estos sensores están formados por una guía de ondas. La alteración de una propiedad física o química en el entorno de la guía induce un cambio en las características de propagación de la luz en la guía. Dicho cambio se traduce en un cambio de potencia transmitida o en cambios de fase. Detectando estos últimos, pueden identificarse las alteraciones de las propiedades físicas y/o químicas en las proximidades de la guía de ondas. Los dispositivos mencionados estarían construidos con guías de ondas cuyo núcleo es de Si_3N_4. Si sobre el núcleo de la guía se deposita un material de alta actividad magnetoóptica, las alteraciones producidas sobre éste alterarán las características de propagación de la luz en la guía. Estos dispositivos pueden utilizarse como detectores de campo magnético o como moduladores magnetoópticos[18] o como biosensores[19]. En todos los casos las nanoestructuras ferromagnéticas de Co son unas de las más destacadas candidatas para ser utilizadas como capa sensora. Ello motiva el estudio de nanopartículas de Co sobre Si_3N_4.

Por último, el interés en las bicapas V/Co y Co/V crecidas por epitaxia sobre MgO viene motivada por la importancia de la naturaleza de la interfaz V-Co y de los espesores de las capas de V y Co en fenómenos como el canje oscilatorio, la magnetorresistencia gigante y la superconductividad que puede presentarse en multicapas de dichos compuestos. Así por ejemplo, se ha detectado acoplamiento antiferromagnético entre las capas de Co separadas por una capa de V de 9 Å [20], si bien en otros casos se ha encontrado acoplamiento ferromagnético independiente del espesor de la capa de V [21]. Por otra parte, el acoplamiento entre las capas en multicapas de V/Co parece depender fuertemente de la estructura de cada una de las capas así como de la rugosidad de la interfaz V–Co [22]. Por último, cabe citar que las propiedades superconductoras de las multicapas de V/Co, y especialmente la temperatura de transición, oscilan con el espesor de la capa de Co [23]. En general, las propiedades

magnéticas y magnetoópticas del sistema Co/V/MgO son muy sensibles a los espesores de las capas y la naturaleza de las intercaras[24].

1.3 Objetivos

El objetivo de este trabajo es estudiar cómo la morfología y la estructura cristalina determinan las propiedades magnéticas de películas delgadas de Co. Las propiedades magnéticas a las que nos referimos son básicamente la anisotropía magnética y los procesos de inversión de la imanación, propiedades determinantes para su aplicación tecnológica, como se relató anteriormente.

La consecución del objetivo enunciado arriba ha requerido el cumplimiento de unos objetivos parciales, siendo éstos:

- Fabricación de películas delgadas de Co nanocristalino (no epitaxial) con diferentes tamaños de grano.
- Caracterización magnética de las películas delgadas de Co nanocristalino mediante medidas de la ST y de los ciclos de histéresis.
- Caracterización estructural de películas delgadas de Co nanocristalino mediante difracción de rayos X, AFM y TEM.
- Fabricación de películas delgadas de Co crecido en forma de islas (no epitaxial) con diferentes tamaños de las islas y con *cappings* magnéticamente polarizables y no polarizables.
- Caracterización magnética de las películas delgadas de Co crecido en forma de islas mediante medidas de la ST, ciclos de histéresis y medidas de curvas FC/ZFC.
- Caracterización estructural de películas delgadas de Co crecido en forma de islas mediante difracción de rayos X y AFM.
- Fabricación de películas delgadas de Co crecido por epitaxia en las fases hcp o fcc.

- Caracterización magnética de las películas delgadas de Co epitaxial mediante medidas de ST y ciclos de histéresis a temperatura ambiente y a 350 K y ciclos de histéresis FC y ZFC a 5 K.
- Caracterización estructural de las películas delgadas de Co epitaxial mediante difracción de rayos X.

1.4 Estructura de la memoria

Con todo lo anterior, la estructura de la memoria se atiene al esquema siguiente, que resume los sistemas estudiados:

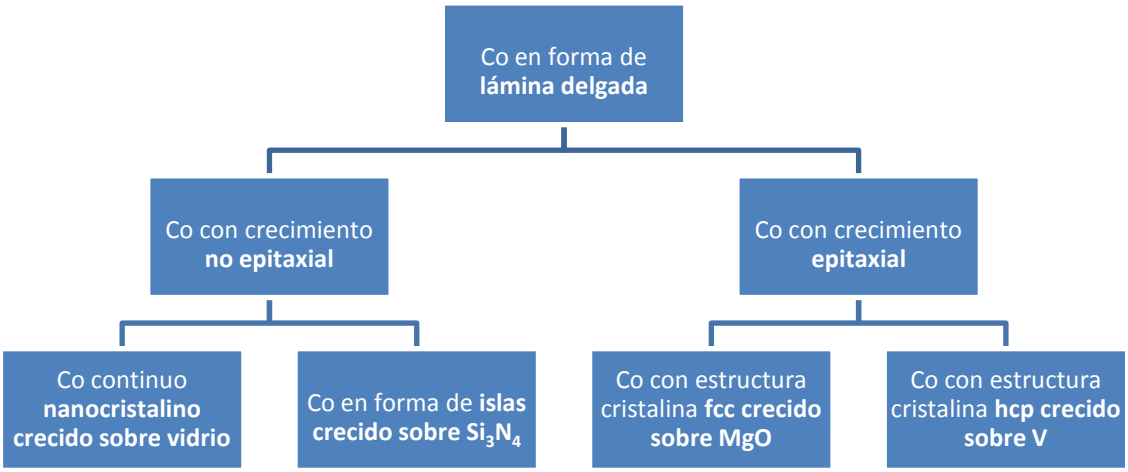

Así, en el capítulo 2 se presentan los resultados obtenidos sobre Co nanocristalino crecido sobre vidrio y la correspondiente publicación.

El capítulo 3 está dedicado al Co crecido en forma de islas sobre Si_3N_4, con el resumen de los resultados y la publicación a la que dieron lugar.

El capítulo 4 comprende los resultados de Co crecido por epitaxia, ya sea Co fcc obtenido al crecer Co epitaxialmente sobre MgO o Co hcp obtenido al crecer Co epitaxialmente sobre V. Se añaden las dos publicaciones a las que dieron lugar los resultados.

Para finalizar se presentan a continuación las conclusiones y la bibliografía, refiriéndose ésta última exclusivamente a aquellas llamadas desde el texto no comprendidas en los artículos que acompañan a esta memoria.

Para cada publicación se ha consultado la estadística del año en que fue publicada en el *Journal Citation Reports* de la *Web of Knowledge*. A continuación se detallan el factor de impacto y la clasificación de cada revista en su categoría en el año de publicación de los trabajos presentados en esta tesis.

Año 2006, **JOURNAL OF APPLIED PHYSICS** tiene un Factor de Impacto de **2.316**. La tabla siguiente muestra el ranking de esta revista en sus categorías basado en el índice de Impacto.

Categoría	**Total de revistas científicas en la categoría**	**Posición en el ranking**	**Cuartil en la categoría**
PHYSICS, APPLIED	84	14	Q1

Año 2007, **JOURNAL OF APPLIED PHYSICS** tiene un Factor de Impacto de **2.171**. La tabla siguiente muestra el ranking de esta revista en sus categorías basado en el índice de Impacto.

Categoría	**Total de revistas científicas en la categoría**	**Posición en el ranking**	**Cuartil en la Categoría**
PHYSICS, APPLIED	94	17	Q1

Año 2007, **JOURNAL OF PHYSICS D: APPLIED PHYSICS** tiene un Factor de Impacto de **2.200**.

La tabla siguiente muestra el ranking de esta revista en sus categorías basado en el índice de Impacto.

Categoría	Total de revistas científicas en la categoría	Posición en el ranking	Cuartil en la Categoría
PHYSICS, APPLIED	94	15	Q1

Año 2008, **IEEE TRANSACTIONS ON MAGNETICS** tiene un Factor de Impacto de **1.129**.

La tabla siguiente muestra el ranking de esta revista en sus categorías basado en el índice de Impacto.

Categoría	Total de revistas científicas en la categoría	Posición en el ranking	Cuartil en la Categoría
ENGINEERING, ELECTRICAL & ELECTRONIC	229	110	Q2
PHYSICS, APPLIED	95	59	Q3

Capítulo 2

Co policristalino crecido sobre vidrio

Artículo I

Artículo publicado en la revista IEEE TRANSACTIONS ON MAGNETICS: "Magnetic Properties of Nanocrystalline Co Thin Films Grown on Glass"

2.1Resumen

En primer lugar se crecieron láminas delgadas de Co sobre un substrato amorfo (vidrio) a temperatura ambiente y mediante un sistema de sputtering denominado HiTUS. Los espesores depositados fueron de 10 a 170 nm. La presión base se fijó en $3 \cdot 10^{-7}$ mbar y la presión de Ar en $3 \cdot 10^{-3}$ mbar. La velocidad de deposición fue de 0.6 Å/s. Se utilizó Ta (3 nm) como capa protectora para evitar la oxidación.

De los datos estructurales se demuestra que las láminas son policristalinas, con nanocristales para los espesores más pequeños. No hay formación de islas ni de estructuras epitaxiales como en los otros sistemas de Co estudiados. Los patrones de XRD muestran que las láminas son policristalinas con fase principalmente hcp. A medida que aumenta el espesor de Co se desarrolla la textura <001> hcp. En cambio, para espesores menores de 80 nm, los máximos observados en el diagrama son muy anchos por lo que se deduce que las láminas están formadas por granos cristalinos muy pequeños sin textura. Se detectó también la presencia de una pequeña cantidad de Co con fase cristalina fcc. Las constantes cristalinas se calcularon por medio de un ajuste teórico encontrándose solo una variación del 2% respecto al valor en masivo. También se calculó el tamaño del grano cristalino hcp, evolucionando desde tamaños más pequeños que 5 nm hasta 26 nm para las muestras con mayor espesor. El cristal fcc mantuvo un tamaño casi constante en torno a 3 nm para todos los espesores, indicando que esta fase metaestable se mantiene gracias a la energía de superficie.

Por otro lado, para confirmar la naturaleza ultrafina de los granos se obtuvieron imágenes TEM mostrando una distribución de granos propia de una muestra policristalina. También se examinó la superficie de las láminas mediante AFM. Los resultados mostraron que la rugosidad aumenta con el espesor nominal de Co además de favorecer la creación de estructuras columnares más estrechas.

Las propiedades magnéticas de las láminas nanocristalinas de Co fueron investigadas mediante susceptibilidad transversal. Esta técnica nos proporcionó más información que los clásicos ciclos de histéresis sobre los procesos de inversión de la imanación.

Para sistemas como las láminas nanocristalinas de Co aquí estudiadas, donde el proceso de inversión de la imanación es controlado por movimiento de paredes de los dominios magnéticos, la susceptibilidad transversal revela detalles de la fuerza con la cual las paredes se anclan en los bordes de los granos. Por tanto, se obtuvieron valores tanto del campo coercitivo como del máximo campo de anclaje para los dominios. También se detectó la existencia de una anisotropía uniáxica en el plano, particularmente acentuada para muestras con espesores menores de 50 nm de Co. De los datos analizados quedó claro que el valor de H_C en la dirección del eje fácil es siempre consistentemente mayor que el del eje difícil. Además, el valor del campo de anclaje llega a ser incluso el doble del campo coercitivo, lo que se traduce en que la coercitividad se encuentra aproximadamente en el 50% del camino que necesita la muestra según la distribución de energía para atravesar todos los puntos de anclaje de las paredes. Esto implica que la medida de H_C no es un buen método para conocer el campo magnético necesario para invertir completamente la imanación, lo cual tiene importantes implicaciones en el funcionamiento de dispositivos MRAM.

El campo de anclaje y H_C aumentan conforme aumenta el espesor de cobalto en estos sistemas nanocristalinos. Este efecto puede deberse a un incremento en la densidad de fronteras de granos como ha sido demostrado por AFM y TEM, dando lugar esta estructura policristalina 3-D a un enorme número de puntos de anclaje para las paredes de Néel formadas en estas láminas.

2.2 Artículo I

2788 IEEE TRANSACTIONS ON MAGNETICS, VOL. 44, NO. 11, NOVEMBER 2008

Magnetic Properties of Nanocrystalline Co Thin Films Grown on Glass

Borja Presa[1], Rafael Matarranz[1], Mariá Carmen Contreras[1], Javier Fernández Calleja[1], Luis Eugenio Fernandez-Outon[2], and Kevin O'Grady[2]

[1]Departamento de Física, Universidad de Oviedo, Oviedo 33007, Spain
[2]Department of Physics, The University of York, York YO10 5DD, U.K.

Co thin films have been deposited by sputtering on glass substrates. The film thickness ranges from 10 to 170 nm. Structural results show that the films are polycrystalline with a dominant hcp structure. An ultrafine distribution of crystallites with diameters about 5 nm is found for the thinnest samples, which is also detected by a smooth surface. The grain size grows as the thickness increases in consequence an evolution occurs from a well-defined uniaxial anisotropy to a more isotropic behavior. This gives rise to an increase in the coercivity, domain wall pinning strength, and its dispersion. The magnetization reversal mechanism is also influenced by the film thickness. Using transverse susceptibility measurements we have found that the maximum domain wall pinning strength increases significantly as the film thickness increases.

Index Terms—**Co thin film, magnetic anisotropy, magnetization reversal, transverse susceptibility.**

I. Introduction

THE physical and magnetic properties of single and multilayered Co thin films are of interest from both the fundamental and the applied point of view. For example, a thin Co film is often used as a free layer in magnetic tunnel junctions (MTJs) such as $La_{0.67}Sr_{0.33}MnO_3/SrTiO_3/Co$ [1] and $Ni_{81}Fe_{19}/AlO_x/Co$ [2]. MTJs have provided a convenient environment to study the spin-polarized electronic structure of thin films and have already been applied in magnetic memories and read heads [3]. However, a complete study of the magnetic anisotropy and the switching behavior of Co thin films is required to improve the performance of MTJs. Moreover, the magnetic properties of Co thin films depend greatly on the methods and conditions of preparation [4]. The coercivity is affected significantly by structural parameters such as particle size, texture, surface roughness, and crystallographic structure. Kharmouche *et al.* [5] detected a sharp increase in the in-plane coercivity of evaporated hcp Co thin films for thicknesses above 130 nm. Chen *et al.* [6] found two distinct types of behavior of the magnetostriction and coercivity depending on the thickness of Co films when all the films had the same fcc structure independent of the thickness.

In this work we report on an analysis of the evolution of the structural and magnetic properties of Co thin films with increasing thickness from 10 nm to 170 nm. In particular we have correlated transverse susceptibility (TS) studies across the whole reversal process to conventional hysteresis loops to determine full details of the magnetization reversal process. The domain wall pinning strength has been extracted from the transverse susceptibility showing the origin of the coercivity. This is correlated to the physical microstructure of the films and particularly to the grain size which has been controlled. Hence our work is a significant extension to that of Alameda *et al.* [7].

Digital Object Identifier 10.1109/TMAG.2008.2001506

Color versions of one or more of the figures in this paper are available online at http://ieeexplore.ieee.org.

II. Experimental Procedures

The films were grown on glass substrates at room temperature (RT) using a HiTUS sputtering system. This system has been shown to allow control of grain size in thin films via control of the growth rate without the use of artificial effects such as seed layers and substrate heating allowing unique samples to be prepared [8]. For all samples the base pressure achieved was 3×10^{-7} mbar and the Ar process pressure was 3×10^{-3} mbar. The deposition rate was 0.6 Å/s. A 3-nm-thick Ta capping layer was grown to avoid oxidation. The crystallographic structure of the films was studied *ex-situ* by X-ray diffraction (XRD) using CuK_α radiation. The ultrafine nature of the grains was confirmed by transmission electron microscopy (TEM) as well as XRD. The surface morphology of the films was imaged by atomic force microscopy (AFM). Magnetic properties were measured by a transverse magneto-optical Kerr effect (MOKE) to obtain the major hysteresis loops and the transverse susceptibility (TS). TS measurements consist of the application of a small alternating magnetic field H_T and an orthogonal steady field H_{DC} both in the film plane. The Kerr signal is proportional to the component of the magnetization parallel to $H_T(M_T)$. If the amplitude of H_T is small, M_T is proportional to the susceptibility which is measured as a function of H_{DC}. H_T had a frequency of 127 Hz and an rms value of 0.4 Oe. All measurements were made at 293 K.

III. Results and Discussion

A. Crystallographic and Grain Size Analysis

Fig. 1 shows the XRD pattern of the Co thin films with different thicknesses. The data reveal that the films are polycrystalline with mainly an hcp phase due to the presence of the (100), (002), and (101) diffraction peaks located at values of 2θ equal to 41.7°, 44.5°, and 47.4° respectively. From this data we believe that the films develop hcp $\langle 001\rangle$ texture as the thickness increases. For thinner Co films with $t < 80$ nm we observed broad peaks characteristic of very small grains within clear texture. This is based on the increase in intensity of the (002) hcp peak with thickness which is proportionally greater than that for the other peaks. The presence of some fcc phase was detected

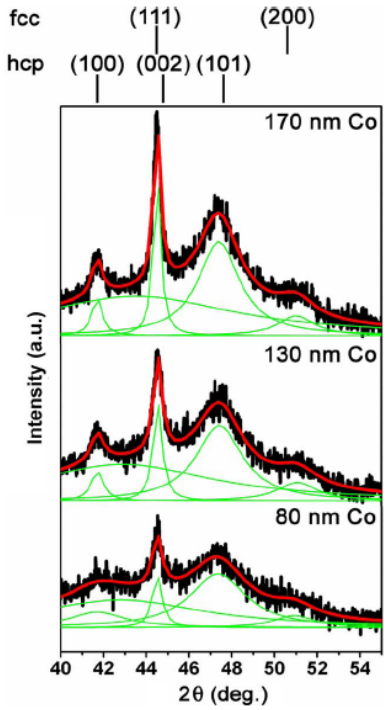

Fig. 1. X-ray diffraction spectra for Co samples with different thicknesses (black line). The fit (red line) is an overlap of five different functions (green lines).

from a broad peak at $2\theta = 51.0°$. We believe the peak around 44.5° is a combination of the hcp (002) and the fcc (111) reflections. These data were fitted using an overlap of the three peaks of the hcp phase and the two peaks of the fcc phase. The lattice constants obtained from the fit are $a = 2.50$ Å and $c = 4.08$ Å for the hcp structure and $a = 3.61$ Å for the fcc structure. These values agree with those for the bulk within 2%. The crystallite size was estimated using the Scherrer formula [9]. The crystallite size has been found to increase with increasing thickness for the preferred orientations. For the (002) reflection, the crystallite sizes are 16 nm, 20 nm, and 26 nm for samples with Co thickness equal to 80 nm, 130 nm, and 170 nm respectively. For thicknesses below 50 nm the crystallite size is less than 5 nm. In the case of the grains corresponding to the (100) hcp orientation the evolution is similar with crystallite sizes equal to 3 nm, 13 nm, and 17 nm. However, the grain size remains almost constant at around 4 nm measured from the (101) hcp reflection. For the fcc reflections, the size determined is smaller than that for the hcp grains and does not depend on the film thickness. With typical values around 3 nm for both reflections. This is in agreement with theoretical studies which suggest that surface energy can stabilize the fcc phase below a critical size of 20 nm [10]. In order to confirm this ultrafine nature of the grains, bright-field TEM images were obtained for a 20-nm-thick Co film (see Fig. 2). The lateral grain size (D_L) was measured in this sample counting over 500 grains. The grain size distribution and the fit to the log-normal function are shown in the inset of Fig. 2. From the fit we obtain the mean grain size $D_L = 5.3$ nm and the standard deviation of ln D, $\sigma = 0.41$.

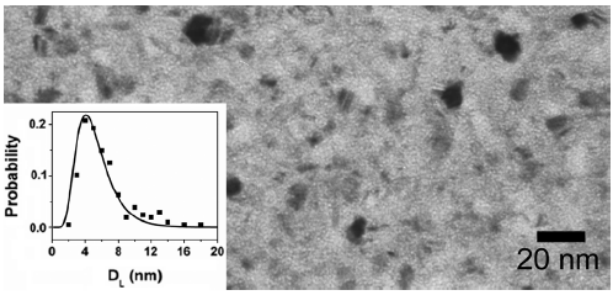

Fig. 2. Plane-view TEM for 20-nm-thick Co film. The inset shows the particle size distribution (squares) and the log-normal fit (line).

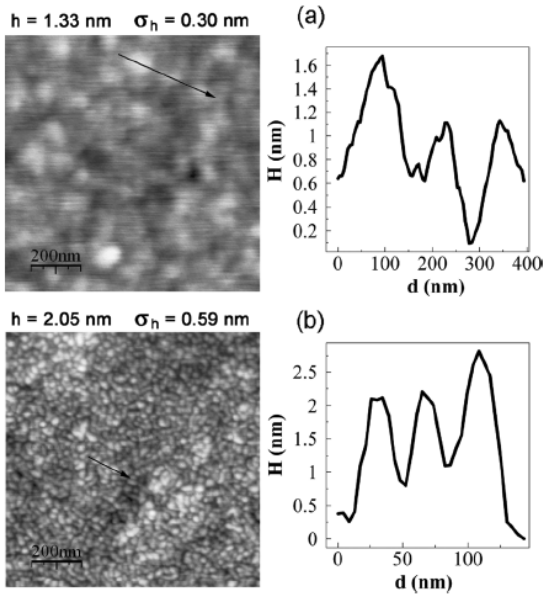

Fig. 3. AFM images and the corresponding line scans of Co thin films with thicknesses equal to (a) 10 nm and (b) 150 nm.

Fig. 3 shows AFM images of the films and surface roughness scans determined using a commercial programme WSxM [11]. The data show that the size distribution of the features is wide with the average size decreasing with increased thickness. Of course each feature recorded by the AFM may contain several crystallites and hence a correlation to the X-ray crystallite size is not expected. However the reduction in feature size indicates the development of columnar grains supporting the development of the hcp texture in the thicker films.

B. Magnetic Properties

The magnetic properties of the samples were investigated by measuring transverse Kerr loops while simultaneously measuring the transverse susceptibility (TS). The Kerr loops give the DC magnetic properties of a ferromagnetic thin film but do not provide further information on the magnetization reversal processes. Using the capability to do simultaneous transverse susceptibility measurements allows more detailed information about the processes ongoing in the material.

Previously TS measurements have been used to determine the magnetic properties of a wide range of materials including par-

ticulate systems and thin films. The technique provides information about the reversal processes in a DC field (H_{DC}) by probing the ability of the magnetic moment of the system to respond to a small AC field (H_T) applied perpendicular to the DC field. Hence changes in the component of magnetization or its stiffness along the direction of H_{DC} induce changes in M_T leading to a series of well defined peaks in the behavior of dM_T/dH_T. Independent of the magnetization reversal mechanism the TS will exhibit a well defined peak at the field at which the magnetization is zero, i.e., the coercivity, H_C.

In the case of uniaxial particulate materials with a significant degree of easy axis alignment, when H_{DC} is applied parallel to the hard magnetization direction, the magnetic moment of each grain exhibits an instability at the anisotropy field $H_{DC} = \pm H_K$ at which the moment points in the hard direction. At this point the transverse AC field has its maximum effect on the moment and TS rises dramatically. However as H_{DC} is increased further, the coupling between the moment of the single domain particle and the field increases thereby inhibiting the ability of the AC field to affect the moment. Hence a well defined peak or cusp in the variation of TS with H_{DC} is observed.

For systems where the magnetization reversal mechanism is controlled by domain wall motion such as those examined here the TS measurements reveal details of the strength of the pinning of the walls for example at grain boundaries. The measured coercivity of a magnetic material is a manifestation of a balance between reversible and irreversible changes in the magnetic state as shown by (1).

$$M_{REV}(H_C) + M^{-}_{IRR}(H_C) = M^{+}_{IRR}(H_C) \qquad (1)$$

Where M^{-}_{IRR} and M^{+}_{IRR} indicate those fractions of the material which have and have not undergone an irreversible transition in the field H_C.

In the case of bulk-like thin films, the coercive point will be such that certain walls will have broken away from domain wall pins and crossed other pins so that a removal of the field would not allow them to return to their original position. However the reversible component will be a manifestation of elastic excursions of the domain walls whilst it remains pinned at pinning sites. In TS experiments the effect of the DC field applied orthogonal to H_T will be to progressively unpin the domain walls from their pinning sites. This has the effect of increasing the value of M along the direction of H_{DC} but in moderate fields it also has the effect of allowing the domain walls to move in such a manner as to follow the AC field applied perpendicular to H_{DC}. This has the effect of increasing the value of TS in a similar manner to that which is observed in particulate systems. As H_{DC} is increased further the increased coupling between the magnetization of the film and the DC field causes TS to fall. In this way a peak or cusp is produced.

The magnetization process in a bulk-like film is almost entirely by domain wall motion. The TS measurement of the second peak beyond the coercivity is indicative of the maximum domain wall pinning strength in the material.

Fig. 4 shows the variation of the TS with H_{DC} along the easy and hard axis of the samples for different film thicknesses. The

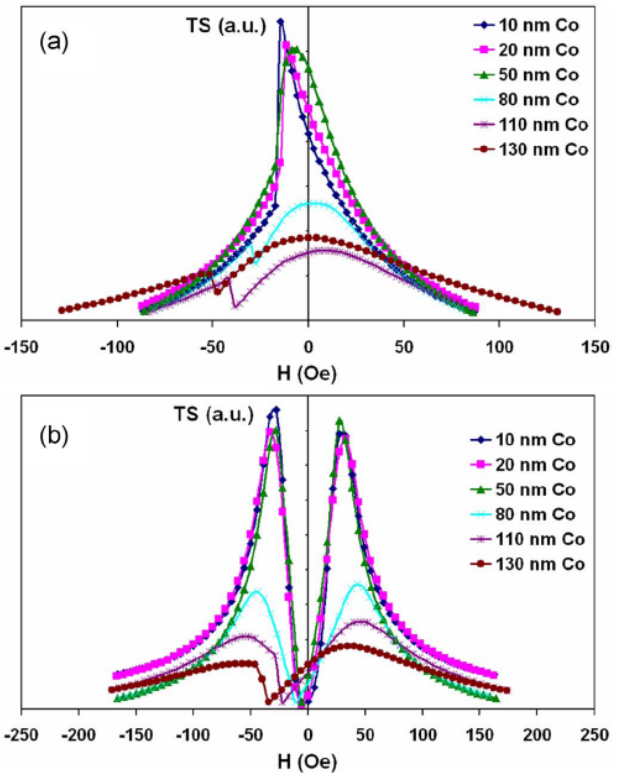

Fig. 4. TS with the bias field H along the (a) easy and (b) hard axis of magnetization for different Co nominal thicknesses.

data seen in the figures are entirely consistent with the description of the behavior given above. The single peak detected in Fig. 4(a) is indicative of the presence of an in-plane easy axis which is particularly marked for samples of thickness less than 50 nm. Along the hard axis two marked peaks are observed as expected [12].

The existence of the in-plane anisotropy does not appear to be crystallographic in origin since there is no evidence for preferential orientation of the c-axes in the X-ray data. There are several possible sources of the in-plane anisotropy including surface roughness [13], stress [14] or possible slight oblique incidence during deposition [15]. From the data available in this work we are unable to establish which effect caused the development of the easy direction. Fig. 5 shows the variation of the coercivities along the easy and hard directions together with the value of the marked peak from Fig. 4(b). This peak occurs at a field H_P which is the maximum pinning field present in the sample. From the data in Fig. 5 it is clear that the coercivity along the easy axis (H_{CE}) is consistently larger than that along the hard axis (H_{CH}). Domains do not form as readily along the hard axis as expected. Both coercivity peaks are also consistent with the value of H_P which to a good approximation is twice the value of H_{CE}. This would indicate that the coercivity lies approximately 50% of the way across the energy barrier distribution arising from the domain wall pins. The true mean of the energy barrier distribution occurs at the remanent coercivity H_{CR} but the two quantities are approximately the same when the reversible

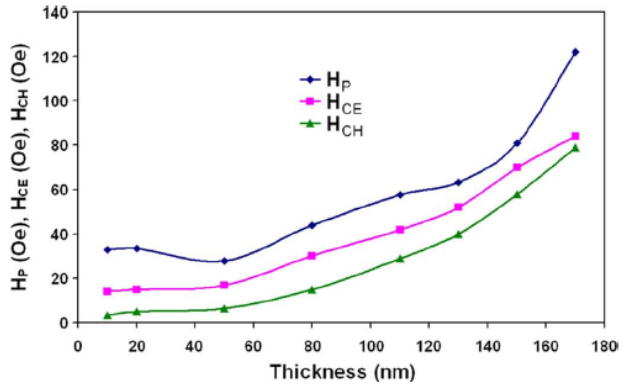

Fig. 5. Evolution of the maximum pinning field (H_P) and the coercivity of the easy (H_{CE}) and hard (H_{CH}) axes of magnetization as a function of Co thickness.

component of magnetization is small. The TS data in Fig. 4 indicate that the reversible component is small at fields around the coercivity.

It is also clear that the coercivity and H_P increase substantially with the film thickness. This is presumably because of the increased density of grain boundaries within the material. The crystallographic data and the grain size data obtained from TEM indicate that for films of thickness greater than 10 nm a multiplicity of layers of small grains occur in these samples rather than columnar growth. This 3-D polycrystalline structure would provide an enormous number of pinning sites for the Néel walls that will form in these films. Indeed for the thicker films it is even possible that some cross-tie walls might form. The onset of this type of domain formation may be responsible for the steep rise in H_P at around 160 nm.

IV. Conclusion

In this work we have used TS measurements to undertake a detailed evaluation of the magnetization processes occurring in Co thin films. We find that due to stress and other anomalies occurring during film preparation, uniaxial anisotropy can be formed in the film which have a significant influence on the domain wall processes. Generally the grain sizes are small providing a plethora of domain wall pinning sites contributing to the high coercivity commonly observed in Co based materials. In particular our TS measurements have shown that the maximum domain wall pinning field is approximately twice the coercivity. This implies that the coercivity is not a good measure of the field required to completely switch such films in devices such as MRAM cells.

Acknowledgment

This work was supported in part by the Universidad de Oviedo and by project MAT2007-66162-C02-01. The work of B. Presa was supported by the "Plan de Ciencia, Tecnología e Innovación 2006-2009 del Principado de Asturias" under Grant BP05-15.

References

[1] I. J. Vera Marún, F. M. Postma, J. C. Lodder, and R. Jansen, "Tunneling magnetoresistance with positive and negative sign in $La_{0.67}Sr_{0.33}MnO_3/SrTiO_3/Co$ junctions," *Phys. Rev. B*, vol. 76, p. 064426, 2007.

[2] N. D. Hughes and R. J. Hicken, "Correlation of tunnel magnetoresistance with magnetic switching in $Co/AlO_x/Ni_{81}Fe_{19}$ cross-strip structures," *J. Phys. D: Appl. Phys.*, vol. 35, pp. 3153–3160, 2002.

[3] S. A. Wolf, A. Y. Chtchelkanova, and D. M. Treger, "Spintronics: A retrospective and perspective," *IBM J. Res. Dev.*, vol. 50, pp. 101–110, 2006.

[4] W. Yang, D. N. Lambeth, and D. E. Laughlin, "Dependence of Co anisotropy constants on temperature, processing, and underlayer," *J. Appl. Phys.*, vol. 87, pp. 6884–6886, 2000.

[5] A. Kharmouche, S. M. Chérif, A. Bourzami, A. Layadi, and G. Schmerber, "Structural and magnetic properties of evaporated Co/Si(100) and Co/glass thin films," *J. Phys. D: Appl. Phys.*, vol. 37, pp. 2583–2587, 2004.

[6] Y. T. Chen, S. U. Jen, Y. D. Yao, J. M. Wu, C. C. Lee, and A. C. Sun, "Magnetic properties of face-centered cubic Co films," *IEEE Trans. Magn.*, vol. 42, pp. 278–282, 2006.

[7] J. M. Alameda and F. Lopez, "Transverse susceptibility and structure constant in cobalt thin films," *Phys. Stat. Solidi A-App. Res.*, vol. 69, no. 2, pp. 757–765, 1982.

[8] M. Vopsaroiu, G. Vallejo Fernandez, M. J. Thwaites, J. Anguita, P. J. Grundy, and K. O'Grady, "Deposition of polycrystalline thin films with controlled grain size," *J. Phys. D: Appl. Phys.*, vol. 38, pp. 490–496, 2005.

[9] B. E. Warren, *X-Ray Diffraction*. Boston, MA: Dover, 1990.

[10] O. Kitakami, H. Sato, Y. Shimada, F. Sato, and M. Tanaka, "Size effect on the crystal phase of cobalt fine particles," *Phys. Rev. B*, vol. 56, pp. 13849–13854, 1997.

[11] Nanotec Electronica SL [Online]. Available: www.nanotec.es

[12] R. Matarranz, M. C. Contreras, G. Pan, B. Presa, J. A. Corrales, and J. F. Calleja, "Transverse susceptibility of nanoparticle systems: The effect of interaction, dispersion, and texture," *J. Appl. Phys.*, vol. 99, p. 08Q504, 2006.

[13] M. Li, Y. P. Zhao, G. C. Wang, and H. G. Min, "Effect of surface roughness on magnetization reversal of Co films on plasma-etched Si(100) substrates," *J. Appl. Phys.*, vol. 83, pp. 6287–6289, 1998.

[14] D. Spoddig, C. Urban, D. H. You, U. Köhler, and R. Meckenstock, "Strong uniaxial anisotropies of iron grown on UHV cleaved InAs(110) investigated by correlated scanning tunneling microscopy and ferromagnetic resonance," *J. Appl. Phys.*, vol. 99, p. 08J704, 2006.

[15] Y. Park, E. E. Fullerton, and S. D. Bader, "Growth-induced uniaxial in-plane magnetic anisotropy for ultrathin Fe deposited on MgO(001) by oblique-incidence molecular beam epitaxy," *Appl. Phys. Lett.*, vol. 66, pp. 2140–2142, 1995.

Manuscript received March 03, 2008. Current version published December 17, 2008. Corresponding author: B. Presa (e-mail: presaborja.uo@uniovi.es).

Capítulo 3

Co nanoestructurado en forma de islas crecido sobre Si_3N_4

Artículo II

Artículo publicado en la revista JOURNAL OF APPLIED PHYSICS: "Morphological and Magnetic Properties of Co Nanoparticle Thin Films Grown on Si_3N_4"

3.1 Resumen

El siguiente paso fue depositar películas de Co a elevada temperatura intentando así crear nanopartículas, lo cual implicará un comportamiento magnético completamente distinto. Las muestras fueron obtenidas por sputtering triodo con una presión base en la cámara principal de alrededor de 10^{-9} mbar. La presión de trabajo con el Ar ionizado fue establecida en $4 \cdot 10^{-4}$ mbar. Para favorecer la formación de nanopartículas el substrato se calentó hasta los 550º C. También es importante resaltar la existencia de 100 nm de buffer de Si_3N_4 amorfo depositado sobre los substratos cristalinos de Si(100). Este buffer amorfo impide la epitaxia y predisposición a la orientación cristalina de las nanopartículas. Con estas condiciones el ritmo de deposición observado para el Co fue de 0.37 Å/s. Las nanopartículas se cubrieron por un elemento magnéticamente polarizable (Au) o por un elemento altamente polarizable (Pt) lo cual modificó la interacción magnética entre partículas. Las propiedades morfológicas de las muestras fueron analizadas mediante AFM ex situ, mientras que las características estructurales se obtuvieron con XRD ex situ. Las propiedades magnéticas en el plano fueron estudiadas mediante susceptibilidad transversal y ciclos de histéresis, y fuera del plano mediante efecto Kerr polar. Las muestras estudiadas son: Pt (2 nm)/Co(t nm)/Si_3N_4 y Au(2 nm)/Co(t' nm) /Si_3N_4 con t = 2, 3, 5 y 10 nm y t' = 2 y 10 nm, siendo t y t' el espesor nominal, es decir, el espesor de la capa de Co para el tiempo

de deposición usado en cada una cuando la temperatura de deposición es tal que el crecimiento fuera en forma de capa continua.

Los resultados de AFM muestran un patrón nanoestructurado bien definido para las muestras con espesores nominales por debajo de los 5 nm de Co, evidenciando un claro crecimiento en forma de islas en 3D. A medida que se deposita más cantidad de Co comienza a cubrirse toda el área del substrato, las nanopartículas incrementan su tamaño y terminan percolando. El diámetro de las partículas varía desde 12.5 nm para un espesor nominal de Co de 2 nm hasta los 84.1 nm para 15 nm de Co. Por otro lado, la rugosidad de las láminas, definida como la distancia vertical media que recorre la punta en las medidas de AFM, varía desde 1.0 nm hasta 10.8 nm. Merece la pena puntualizar que el comportamiento del diámetro de las nanopartículas y de la rugosidad frente al espesor de Co es diferente. Mientras el diámetro de la nanopartícula incrementa a medida que se deposita más Co, la rugosidad alcanza un máximo para 10 nm de espesor nominal, mostrando que a partir de un tiempo de deposición determinado el Co cubre por completo todo el substrato decreciendo así el recorrido vertical realizado por la punta. También se calcularon las desviaciones estándar del diámetro de las nanopartículas y de la rugosidad obteniendo resultados similares a los anteriormente expuestos: mientras la desviación del diámetro aumenta con el espesor debido a la percolación entre las nanopartículas, la desviación de la rugosidad alcanza un máximo. Además las muestras con nanopartículas más pequeñas muestran una distribución de tamaños más homogénea debido a que no se ha iniciado la percolación. Finalmente, otro punto destacable de las medidas de AFM para un mismo espesor de Co pero distinto recubrimiento (Au o Pt) es la diferencia en rugosidad, siendo aproximadamente el doble para las láminas delgadas con recubrimiento de Pt. Parece que el Pt tiende a cubrir sólo la parte alta de las nanopartículas, mientras que el Au puede penetrar entre ellas. Esto es debido a la diferente difusión atómica del Au y Pt sobre la superficie de Co.

La estructura cristalina del Co se estudió mediante XRD. Los datos muestran que el Co cristalizó en la fase hcp sin apenas ningún tipo de textura. Los picos de difracción son más intensos y estrechos a medida que el espesor nominal de Co aumenta, lo cual revela que el tamaño del grano cristalino aumenta con el espesor.

Se estudiaron los ciclos de histéresis tanto en el plano como en la dirección perpendicular al plano de las muestras. En la dirección perpendicular al plano se realizaron ciclos Kerr polar. Para todos los tamaños de nanopartículas de Co se observaron unos ciclos de histéresis con una baja remanencia y bajo campo coercitivo, lo cual indica que la imanación se encuentra principalmente en el plano de la película delgada. Sin embargo, se detecta un incremento gradual del campo de saturación a medida que aumenta el espesor nominal de Co, esto se corresponde con una transición desde un sistema de nanopartículas poco conectadas a un sistema percolado de agregados mayores, como se demostró por AFM. Los diferentes recubrimientos (Au o Pt) produjeron una pequeña diferencia en el proceso de imanación, siendo ligeramente menor el campo de saturación para las muestras con recubrimiento de Pt, probablemente debido a la formación de una anisotropía perpendicular en la interfaz Co/Pt.

Los estudios de los procesos de imanación en el plano indicaron una primera e importante conclusión: todas las láminas delgadas mostraron un comportamiento magnético isótropo, es decir, la forma de los ciclos de histéresis no dependen de la dirección en la cual se aplica el campo magnético. Esta falta de ejes de imanación fáciles y difíciles está relacionada con la distribución sin textura de las nanopartículas. En el caso de las muestras con recubrimiento de Au, hay procesos de rotación involucrados en la inversión de la imanación, hasta el punto de que la lámina con las nanopartículas más pequeñas (espesor nominal de 2 nm) tiene un comportamiento cercano al superparamagnetismo. Eso se puede explicar calculando la energía de activación para las nanopartículas. En el caso de las muestras más delgadas esta energía no es suficiente para superar con creces la energía térmica, con lo cual el estado de equilibrio de la imanación fluctúa en el tiempo. Esta es la razón por la cual las muestras más delgadas con recubrimiento de Au presentan tendencia a un comportamiento superparamagnético, mientras que cuando el tamaño de las nanopartículas aumenta se detecta un comportamiento plenamente ferromagnético con un alto campo coercitivo.

Por otro lado, el uso de Pt como recubrimiento de las nanopartículas tuvo un drástico efecto en las propiedades magnéticas. La primera es que incluso las láminas delgadas con las nanopartículas más pequeñas muestran un claro comportamiento ferromagnético. Esto es debido a la diferente polarizabilidad del Au y Pt, de forma que, las nanopartículas recubiertas con Pt están magnéticamente conectadas. Esto produce un

aumento del volumen magnético efectivo de las partículas al estar fuertemente conectadas, lo que produce un aumento de la energía de activación, superando así la energía térmica. Con espesores nominales de Co pequeños y recubrimiento de Pt, la anisotropía efectiva es pequeña y se observa un comportamiento característico de materiales magnéticamente blandos debido a un promediado de la anisotropía local. Cuando el tamaño de las partículas aumenta los procesos de inversión de la imanación se vuelven más complicados involucrando más rotaciones lo que repercute en un aumento de la coercitividad. Esto es debido a que el vector imanación está más fuertemente ligado al eje de la anisotropía local, alcanzándose la saturación para campos magnéticos más elevados. Estos comportamientos del campo coercitivo y de la anisotropía efectiva fueron estudiados dentro del modelo de anisotropía aleatoria, demostrando que, a pesar de la poca esfericidad de las partículas, éstas crecen en un modo más próximo a estructuras tridimensionales.

Las medidas de susceptibilidad transversal, mucho más sensibles que los ciclos de histéresis, mostraron también que los procesos magnéticos son isótropos dentro del plano de las muestras. La susceptibilidad transversal para la muestra de 2 nm de Co con recubrimiento de Au tiene un solo máximo redondeado en torno a H = 0, lo que nos evidencia que la muestra en volumen es todavía ferromagnética pero su estado está cercano al superparamagnetismo. En cambio para un espesor mayor de Co, el campo de anisotropía efectiva ya es detectado en forma de dos máximos. En función de la posición relativa de estos máximos y de su anchura se obtuvieron extrapolaciones sobre la interacción entre partículas y la dispersión de la anisotropía. Por un lado, la interacción puede ser fácilmente modificada por medio del tipo de recubrimiento. Si se usa un material altamente polarizable como el Pt, las nanopartículas quedan conectadas magnéticamente, promoviendo un aumento del volumen magnético efectivo, y por consiguiente aumentando la temperatura de bloqueo propia del sistema nanoestructurado en ausencia de recubrimiento. Sin embargo, si se usa un material poco polarizable como el Au, las nanopartículas de Co quedan prácticamente desconectadas, de forma que la temperatura de bloqueo es más baja. Esta es la razón por la cual mientras 2 nm de Co con recubrimiento de Pt es claramente ferromagnético, con Al tiende al superparamagnetismo. Estos resultados fueron corroborados mediante curvas de imanación FC / ZFC, como se muestra en las figuras 1, 2 y 3. Como estos resultados no forman parte de la publicación presentada, se estudian con más detalle en lo que

sigue. Para la obtención de las curves ZFC, las muestras son enfriadas hasta 5 K en ausencia de campo magnético, y posteriormente se mide el momento magnético en un campo H = 100 Oe calentando la muestra desde 5 K hasta la temperatura ambiente. Para la obtención de las curvas FC se mide el momento magnético de las muestras en un campo magnético H = 100 Oe al enfriarlas desde la temperatura ambiente hasta 5 K. Puede observarse que las dos muestras (Au / Co (2nm) y Pt / Co (3nm)) presentan el típico comportamiento superparamagnético: las dos curves FC y ZFC coinciden para temperaturas por encima de una temperatura de bifurcación T_b y además las curvas ZFC exhiben un máximo a una temperatura T_m. En el caso ideal de un sistema formado por partículas idénticas no interactuante, ambas temperaturas coinciden con la temperatura de bloqueo T_B. La diferencia entre T_b y T_m se debe a una distribución de temperaturas de bloqueo, debida a su vez a una distribución de tamaños de las partículas[25, 26]. De acuerdo a las curvas FC / ZFC, la temperatura de bloqueo parece ser inferior a la temperatura ambiente, es decir, las tres muestras deberían ser superparamagnéticas a temperatura ambiente, lo que estaría en contradicción con los resultados de la susceptibilidad transversal. Sin embargo, esto es un efecto del campo magnético aplicado durante las medidas, pues es bien conocido que dicho campo magnético disminuye la barrera de potencial, desplazando el máximo de las curvas FC/ZFC hacia temperaturas más bajas[27, 28].

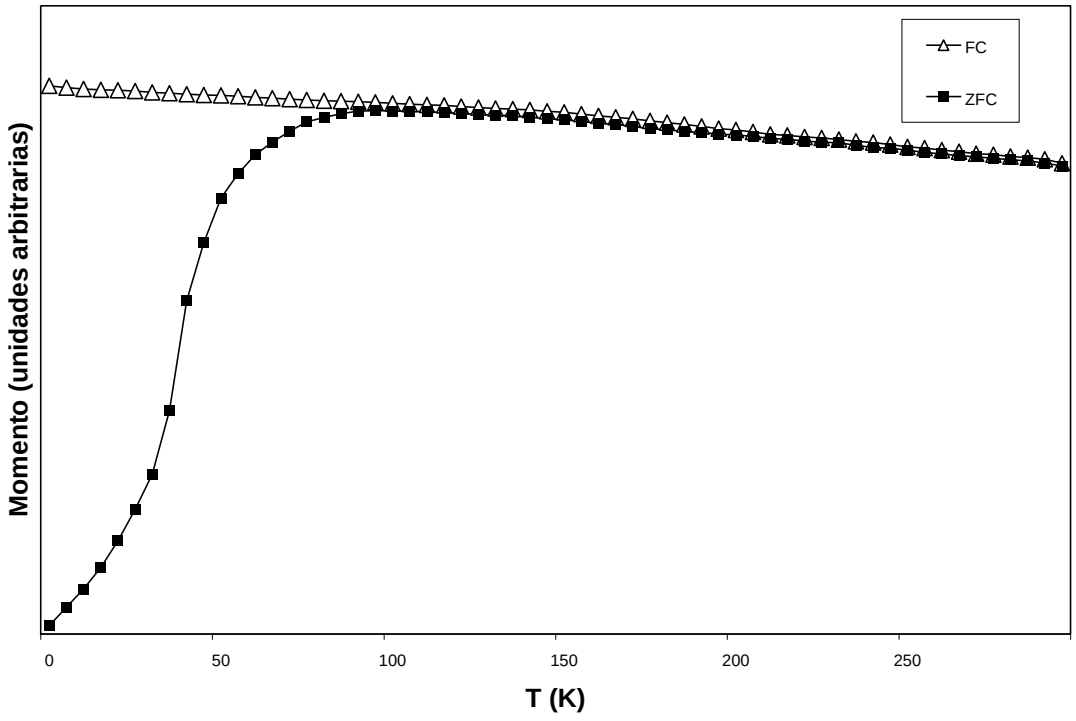

FIG.1.Curvas ZFC/FC para nanopartículas de Co con espesor nominal de 3 nm cubiertas por un capping de Pt.

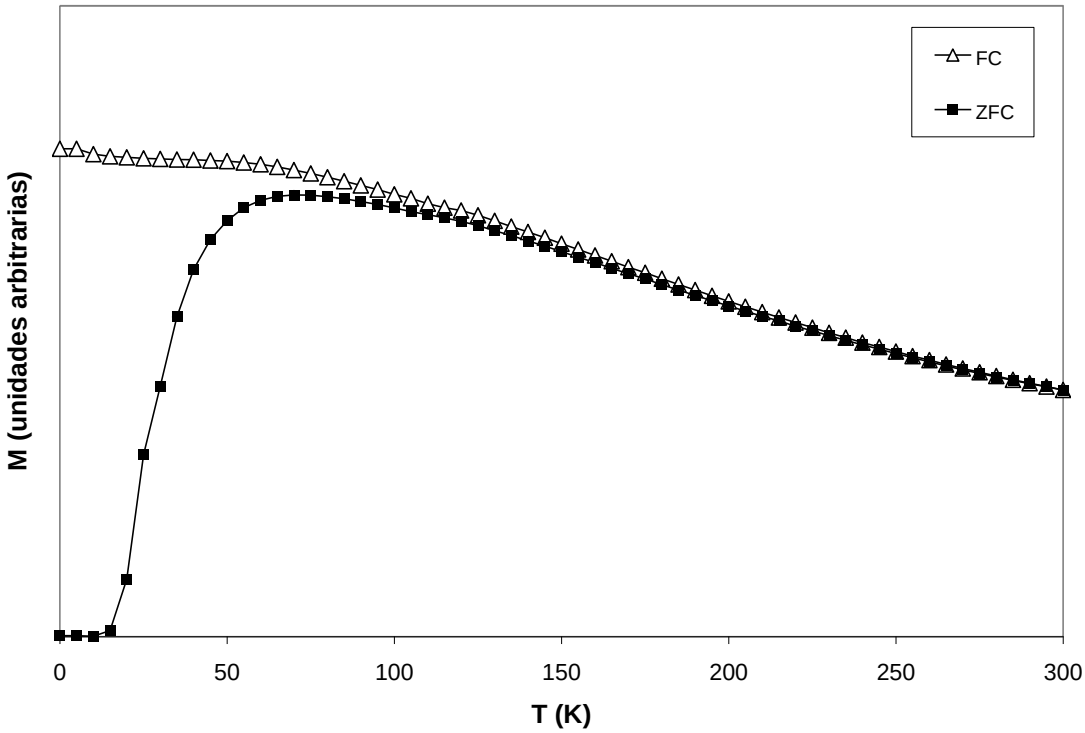

FIG.2.Curvas ZFC/FC para nanopartículas de Co con espesor nominal de 2 nm cubiertas por un capping de Au.

Por otro lado, también se evidenció que la dispersión en el campo de anisotropía está estrechamente relacionada con la dispersión en el tamaño de las partículas observado por AFM.

3.2 Artículo II

JOURNAL OF APPLIED PHYSICS **102**, 053901 (2007)

Morphological and magnetic properties of Co nanoparticle thin films grown on Si_3N_4

B. Presa[a] and R. Matarranz
Departamento de Física, Facultad de Ciencias, Universidad de Oviedo, Calvo Sotelo S/N, 33007 Oviedo, Spain

C. Clavero and J. M. García-Martín
Instituto de Microelectrónica de Madrid-IMM (CNM-CSIC), Isaac Newton 8 (PTM), 28760 Tres Cantos, Madrid, Spain

J. F. Calleja and M. C. Contreras
Departamento de Física, Facultad de Ciencias, Universidad de Oviedo, Calvo Sotelo S/N, 33007 Oviedo, Spain

(Received 6 February 2007; accepted 14 July 2007; published online 4 September 2007)

The morphological and magnetic properties of Co nanoparticles deposited by triode sputtering on Si_3N_4 at 550 °C are reported. The nominal thickness of Co ranges from 2 up to 15 nm, and two different capping layers, Au and Pt, are used. The nanoparticles were characterized by x-ray diffraction and atomic force microscopy. Morphological and structural studies show that the nanoparticles grow in a well-defined nanostructured pattern and adopt a hexagonal closed packed crystalline structure. Moreover, the average particle size and the particle size dispersion increase as the thickness increases, due to percolation. Experimental characterization of effective anisotropy field was carried out with transverse susceptibility. Transverse susceptibility measurements reveal an in-plane isotropic magnetic behavior. Both the effective anisotropy field and the coercive field increase as the particle size increases, following a D^6 dependence, which is typical for three-dimensional structures in the framework of the random anisotropy model. The relationship between the particle size distribution and the anisotropy field distribution is shown, explaining the significant dependence of the magnetic behavior on the Co layer thickness. On the other hand, different capping layers give rise to a change in the magnetic response due to the modification of the interparticle interaction. © *2007 American Institute of Physics*. [DOI: 10.1063/1.2775172]

I. INTRODUCTION

One of the most interesting problems in modern condensed matter physics is the study of nanostructures, especially magnetic low-dimensional systems. In such systems, structural properties (crystallographic structure, particle size, and texture) deeply affect magnetic properties such as anisotropy, coercivity, and magnetization reversal process. Research on these systems has led to the development of new technological applications such as ultrahigh-density computer disk drives[1,2] and magnetic sensors.[3,4] For example, Co nanoparticles,[5,6] Co nanocolumns,[7] and Co-based alloys[8] have attracted a lot of attention in the past decade since they may be good candidates for high-density storage media. A critical feature is the reduced particle size which causes thermal relaxation of magnetic moments[9] and a modification of the effective anisotropy through interparticle interaction.[10]

Measurement of the transverse susceptibility (χ_T) at room temperature has proven to be a very powerful technique to obtain the effective anisotropy field, the interparticle interaction, texture, and anisotropy field distribution in nanostructured systems.[11–13] The value of the effective anisotropy field depends on several parameters such as the intrinsic anisotropy constant K_1 of the particles, their volume V, and the temperature T that produces the thermal fluctuations. The activation energy required to reverse the particle's magnetization is given by K_1V. Therefore, if k_BT is not small enough compared to K_1V, the period of stability of the particle's magnetization will not be long enough for the particle to be used as a magnetic bit. Then the system is said to be superparamagnetic. Lowering the superparamagnetic limit requires new ways of enhancing the anisotropy of the magnetic bits.

Recently, Spinu *et al.*[14,15] have pointed out the influence of temperature in the χ_T response of nanoparticle systems, distinguishing between the blocked and superparamagnetic states for fixed activation energy. Nevertheless, another interesting point of view for this problem is to change the activation energy of the particles, varying their volumes or even changing the capping layer, for fixed temperature, as it is well known that the capping layer can produce an enhancement of the magnetic anisotropy due to interparticle interaction.[16] In this work, two different capping layers, Au and Pt, are used. Pt polarization has been widely studied by means of x-ray magnetic circular dichroism (XMCD),[17] Kerr spectroscopy,[18,19] and *ab initio* simulations in Co/Pt interfaces and multilayers. In all the cases, the polarization of the Pt atoms has been observed when they make contact with a Co surface, due to orbital hybridization between Co 3*d* and Pt 5*d*, giving rise to a perpendicular magnetic anisotropy in

[a]Electronic mail: presaborja.uo@uniovi.es

the Co/Pt interface. Suzuki *et al.*[17] observed a total magnetic moment of 0.61 μ_B/atom for the Pt atoms at the interface and an exponential decrease of the magnetic moment from the interface. The polarization of the Au atoms has also been studied when they make contact with a Co surface.[20] In this case, the induced magnetic moment of Au was very small, about one order of magnitude smaller than that of Pt.

The present paper is focused on the magnetic properties of $Co/Si_3N_4/Si(100)$ thin films. Both the role of Co nanoparticle size and the influence of the kind of capping layer used are investigated. In order to characterize the physical properties of the Co nanoparticles, x-ray diffraction (XRD) and atomic force microscopy (AFM) were used. The correlation between morphology, especially the mean particle size and the particle size dispersion, and the magnetic properties is discussed.

II. EXPERIMENT

The samples were grown in an ultrahigh vacuum multichamber with triode sputtering facility (base pressure about 10^{-9} mbar, work pressure $P_{Ar}=4\times10^{-4}$ mbar, and deposition rates 0.50, 0.37, and 0.30 Å/s for Au, Co, and Pt, respectively). Co deposition was performed at 550 °C in order to favor the formation of nanoparticles. Si(100) substrates covered with a 100-nm-thick Si_3N_4 buffer layer were used. A 2-nm-thick capping layer was grown by sputtering, at room temperature, to obtain a conformal growing. The capping layer material was chosen to be a low polarizable material (Au) or a highly polarizable one (Pt). Particle size and physical contact between them were controlled by deposition time and studied with AFM. Particle size in the film plane was obtained for all samples by measuring and counting the particles' diameter using a Zeiss particle size analyzer. More details regarding particle size analysis can be found elsewhere.[21] Roughness analysis of the samples was done with the free commercial program WSXM.[22]

The magnetic properties of the samples were obtained from χ_T measurements performed by a transverse magneto-optical Kerr effect. This basically consists of the application of a small alternating magnetic field H_1 and an orthogonal steady field H, both in the film plane, as can be seen in Fig. 1. The Kerr signal is proportional to the component of the magnetization parallel to H_1 (ΔM). If the amplitude of H_1 is small enough, ΔM is proportional to the susceptibility, and then this magnitude, in a direction parallel to H_1, is measured as a function of H. In our case, H_1 had a frequency of 127 Hz. The same experimental setup was used to obtain the magneto-optical transverse Kerr hysteresis loops of the samples. Also polar Kerr spectra were acquired with a maximum field of 1.6 T applied in the perpendicular direction.

III. RESULTS AND DISCUSSION

A. Morphological and structural properties

AFM results for the Au and Pt capped samples are shown in Figs. 2 and 3, respectively. The particle size distribution was fitted to a log-normal distribution. *Ex situ* AFM measurements were performed in capped samples and reveal a well-defined nanostructured pattern without any coalescence for the thinner Co layers. This real space microscopic characterization technique allowed us to get direct evidence of the three-dimensional (3D) growth for these structures: uncovered substrate areas were observed and therefore excess of material accumulated on top of the particles. For low coverage, Co aggregates into small nanoparticles that increase their size and percolate with increasing deposition time. The mean particle size (D) ranges from 12.5 up to 84.1 nm and the mean roughness (H) ranges from 1.0 up to 10.8 nm. H is the mean value of the vertical distance covered by the tip in the AFM measurements. The values of D, H, and the corresponding standard deviations (σ_D and σ_H) are displayed in Table I. The nominal thickness of Co (t_{Co}) corresponds to that of a continuous and flat Co film if grown on the same substrate but at lower temperature [giving rise to two-dimensional (2D) growth]. Since a 2-nm-thick capping layer covers the nanoparticles, H does not correspond exactly to the mean nanoparticle height. It is worth pointing out that the behaviors of D and H are different: while D increases

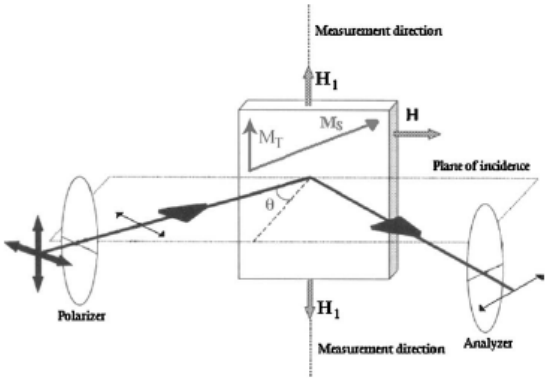

FIG. 1. Schematic diagram of the magneto-optical experimental setup used for the measurement of the transverse susceptibility and the hysteresis loops. The transverse component of the magnetization M_T is measured as a function of H_1 (hysteresis loop) or as a function of H (transverse susceptibility).

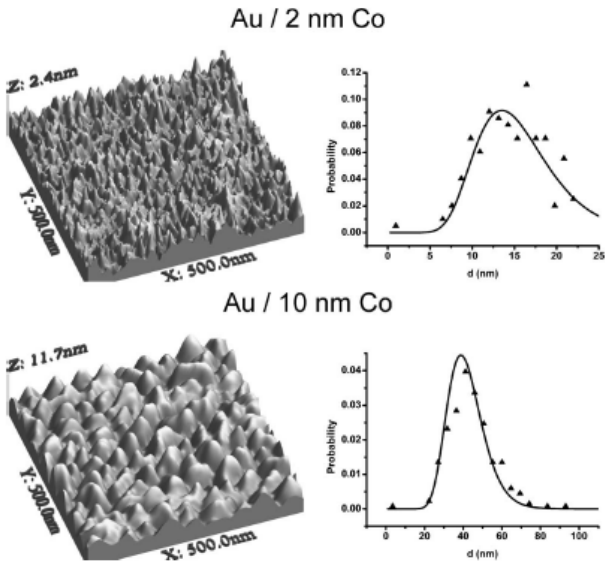

FIG. 2. 3D AFM images and nanoparticle size distributions of Au capped samples with different Co nominal thicknesses.

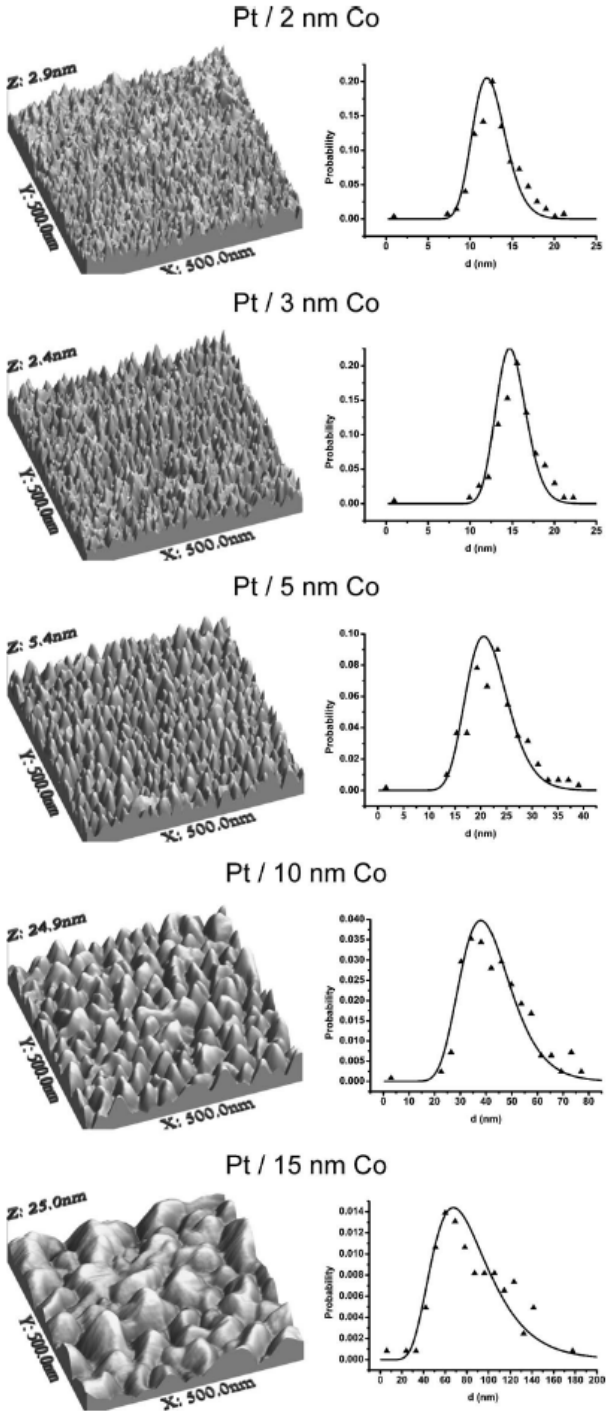

FIG. 3. 3D AFM images and nanoparticle size distributions of Pt capped samples with different Co nominal thicknesses.

with increasing amounts of Co, as expected, H reaches a maximum for 10-nm-thick Co layer. This is due to the fact that when the deposition time is increased, the nanoparticles grow completely, filling up the substrate (see Figs. 2 and 3). Similar features are obtained with the corresponding standard deviations: while σ_D increases due to the percolation between nanoparticles, σ_H reaches a maximum with increasing Co thickness. Moreover, the results of the analysis of the AFM images show that D and σ_D are always greater than H and σ_H, respectively. The samples with smaller nanoparticles show a homogeneous size distribution; this implies a narrower anisotropy field distribution, as will be shown in the next section. On the other hand, a slight difference in the morphological results is obtained between the two capping layers. It is worth noting that the Au capped thin film with a Co nominal thickness of 10 nm shows less roughness than the Pt capped one (see the reduction of both H and σ_H in Table I). It seems that platinum tends to cover the top of the nanoparticles, whereas gold may enter deeper between them. This might be due to the different surface diffusion of Au and Pt atoms in Co.

TABLE I. Co nominal thickness (t_{Co}), mean particle size (D), mean roughness (H), and the corresponding standard deviations (σ_D and σ_H) for Co nanoparticle thin films.

Capping layer	t_{Co} (nm)	D (nm)	σ_D (nm)	H (nm)	σ_H (nm)
Au	2	15.6	4.9	1.0	0.3
	10	41.8	9.6	5.2	1.6
Pt	2	12.5	2.0	1.4	0.3
	3	15.0	1.8	1.1	0.3
	5	21.8	4.2	2.4	0.8
	10	41.9	10.9	10.8	3.8
	15	84.1	33.3	9.5	3.7

Ex situ XRD measurements show that Co mainly crystallizes in its hexagonal metallic phase without texture since the $(10\bar{1}0)$, (0002), and $(10\bar{1}1)$ hcp Co diffraction peaks are observed for thicknesses down to 5 nm. As expected, the intensity and width of these peaks evolve with the Co nominal thickness, being more intense and narrower for the thicker samples. This reveals an increase of the grain size, in agreement with other similar systems.[23]

B. Magnetic properties

The magnetic properties of the samples were investigated by measuring polar Kerr loops, transverse Kerr loops, and χ_T at room temperature. These techniques allow us to have a complete characterization of the magnetic process either in the film plane or out of plane. In the case of polar Kerr loops, the magnetic field $H_\perp$ is applied perpendicular to the film plane and the Kerr rotation angle of the light is measured. This Kerr rotation is proportional to the magnetization parallel to $H_\perp$. The resulting hysteresis loops are displayed in Fig. 4. Loops with a low remanence and coercive field are found in all the samples, typical of a system with in-plane magnetization. However, the effect of the Co nominal thickness is present in the measurements. A gradual increase of the saturation field can be seen in Fig. 4, corresponding to the transition from a system with small magnetically isolated nanoparticles to a percolated system with large aggregates (as observed by AFM). Consequently, the magnetic size of the nanoparticles in the direction perpendicular to the substrate plane exerts influence on the effective anisotropy energy out of plane. On the contrary, the capping layer has only a slight influence on the magnetization process. The saturation field of the Pt capped samples seems to be slightly lower than that of Au capped ones, prob-

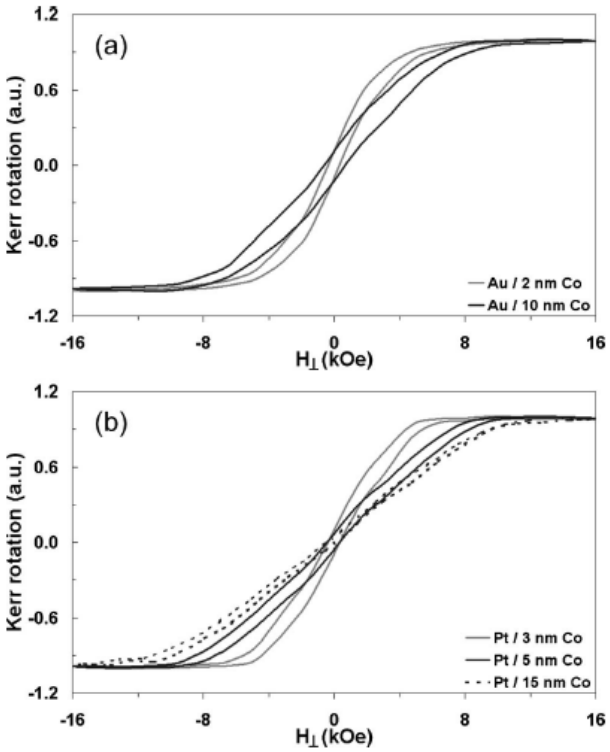

FIG. 4. (a) Hysteresis loops measured in the polar Kerr configuration for Au capped samples with Co nominal thicknesses of 2 and 10 nm. (b) Hysteresis loops measured in the polar Kerr configuration for Pt capped samples with Co nominal thicknesses of 3, 5, and 15 nm.

ably due to the formation of perpendicular anisotropy in the Co/Pt interface.[18] However, the capping layer has much more influence in the in-plane magnetization process as will be shown later on.

In order to investigate the in-plane magnetization, transverse Kerr hysteresis loops were measured for all the samples along several directions. Isotropic magnetic behaviors were obtained, i.e., the shape of the hysteresis loop does not depend on the direction in which the magnetic field H_1 is applied. Therefore, there is a lack of easy and hard magnetization axes. This is related to the fact that Co nanoparticles, grown on an amorphous buffer layer (Si_3N_4) at 550 °C, form a randomly oriented system. Figure 5(a) displays the transverse Kerr hysteresis loops for the samples with Au capping layer. The results for the samples with Pt capping layer can be seen in Fig. 5(b). Unfortunately, in this case, it was not possible to saturate the samples with nominal thicknesses of 10 and 15 nm in our experimental setup, observing only the Rayleigh region. The coercivity data have been included in Table II.

In the case of Au capped samples [see Fig. 5(a)], there are rotations involved in the magnetization reversal. Moreover, the hysteresis loop of the sample with a Co nominal thickness of 2 nm shows a behavior close to a superparamagnetic state. Let us consider, in a rough approximation, the nanoparticles in the shape of an oblate spheroid, $D/2$ being its major axis and $(H+t_{Co})/2$ its minor axis. In this case, the volume of a particle is given by $\pi D^2(H+t_{Co})/6$. The values of $\alpha(=K_1V/k_BT)$ at room temperature are included in Table II

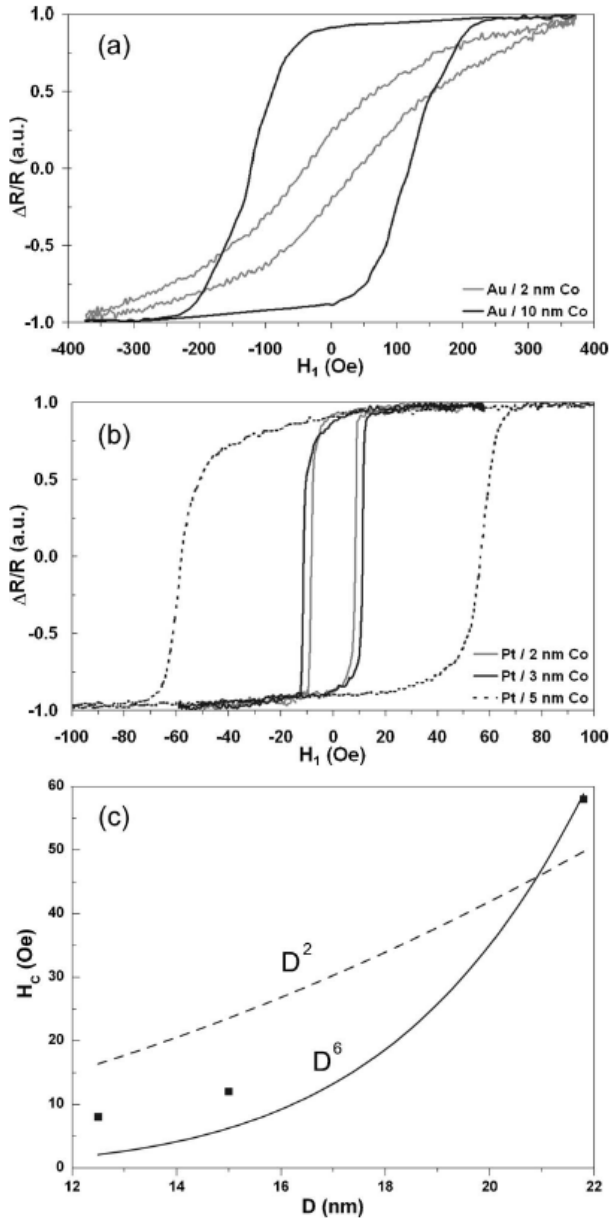

FIG. 5. (a) Hysteresis loops measured in the transverse Kerr configuration for Au capped samples with Co nominal thicknesses of 2 and 10 nm. (b) Hysteresis loops measured in the transverse Kerr configuration for Pt capped samples with Co nominal thicknesses of 2, 3, and 5 nm. (c) Dependence of Pt capped Co nanoparticles' coercivity on particle size with the corresponding fits to D^6 law (solid line) and D^2 law (dashed line).

for each nanoparticulated sample, K_1 being the magnetic anisotropy constant[24] of bulk Co ($K_1=4.1\times10^5$ J/m^3). This ratio between the activation and thermal energies allows us to determine the transition from one equilibrium state to the other. For example, the medium thermal stability criterion is given by $\alpha\geq60$, which defines a thermally stable state for a ten year period.[25] In our case, the α values are low for the thinner samples. This is the reason why the Au capped sample with a Co nominal thickness of 2 nm has a high superparamagnetic component. However, when the particle size increases, a ferromagnetic behavior is observed [see Fig. 5(a)], as expected. Magnetization rotations are involved in

the magnetization reversal of the Au capped sample with a Co nominal thickness of 10 nm. It also exhibits a high coercivity, typical of a ferromagnetic state.

On the other hand, the Pt capping layer has a drastic effect on the magnetic properties of the Co nanoparticles, as can be seen in Fig. 5(b). Even the thinner samples show a clear ferromagnetic behavior. This is due to the different polarizability of Au and Pt. Hence, while the nanoparticles of Pt capped samples are magnetically connected via the capping, the nanoparticles of Au capped samples must be disconnected. When Pt is used, an increase of the effective magnetic volume of the particles is promoted and so it is easier to overcome the thermal instability. When the particle size increases, the magnetization reversal becomes more complicated, involving more rotations, showing a sharp increase in the coercivity [see Fig. 5(b)]. For low Co nominal thickness, the effective anisotropy is small and soft magnetism is observed due to a scaling down of the local anisotropy. However, when the particle size increases, the magnetization vector is more strongly constrained by the orientation of the local anisotropy and saturation of the magnetization is harder to achieve. The magnetic anisotropy in polycrystalline ferromagnetic films is well described by the random anisotropy model (RAM). According to this model,[26] when the particle size is smaller than the exchange length, the effective anisotropy energy K_{eff} variation with the particle size follows $D^{2/3}$, D^2, and D^6 laws for one-dimensional, two-dimensional, and three-dimensional structures, respectively. Moreover, in this framework, the coercivity is proportional to K_{eff}. In Fig. 5(c) we have plotted H_C vs D for the samples with t_{Co}=2, 3, and 5 nm, with Pt capping layer. The corresponding fits to D^2 (dashed line) and D^6 (solid line) laws have been applied to the experimental data, which are closer to D^6 dependence. Although Co nanoparticles always have a mean particle size bigger than the mean height, the ratio between D and H is around 10, yielding a growth mode closer to three dimensions. This behavior of H_C is completely different from that which can be obtained when the deposition is performed at room temperature. In such a case, a continuous thin film growth is promoted. For example, Kharmouche *et al.*[27] achieved a constant coercivity around 10 Oe for a wide range of thickness in Co films deposited at room temperature on glass, which is another amorphous substrate.

We now turn to the χ_T measurements, which provide a fairly accurate description of the magnetic anisotropies involved in a system and a picture of the magnetization reversal mechanism along the direction in which the steady field H is applied. Let us keep in mind that while the transverse hysteresis loop is a representation of M_T vs H_1, χ_T is a representation of dM_T/dH_1 vs H. Accordingly, any small change in the component of the magnetization along H induces a small change in M_T, which can be detected as a peak in the dM_T/dH_1. This response makes χ_T a very sensitive technique to detect the magnetic anisotropy in a nanoparticulated system. In the case of noninteracting uniaxial randomly oriented single-domain particle systems, the Stoner-Wohlfarth model predicts characteristic peaks in the field dependence of the χ_T located at $\pm H_K$ and $-H_C$.[28] Pareti and Turilli[29] provided the first experimental confirmation in polycrystalline samples of $BaFe_{12}O_{19}$. However, the effect of interparticle interaction, anisotropy field dispersion, and texture complicates the behavior of these systems.[11,13,30–33]

TABLE II. Co nominal thickness (t_{Co}), coercivity (H_C), effective anisotropy field ($H_{K,\text{eff}}$), and the parameter α ($=K_1V/k_BT$) at room temperature for Co nanoparticle thin films.

Capping layer	t_{Co} (nm)	H_C (Oe)	$H_{K,\text{eff}}$ (Oe)	α
Au	2	35	⋯	38
	10	120	200	1380
Pt	2	8	10	28
	3	12	21	47
	5	58	77	183

According to the experimental χ_T curves, all the samples exhibit a magnetic isotropic behavior, i.e., the shape of the χ_T curve does not depend on the direction in which the steady field H is applied. The χ_T was always measured from positive to negative saturation. In Fig. 6(a) we have displayed the χ_T measurements for Au capped samples. The most characteristic feature of the χ_T curve for the Au capped sample with t_{Co}=2 nm is that it has only one rounded peak located at H=0. Moreover, let us remember that the transverse Kerr hysteresis loop for this sample was close to an S shape. Similar results have been obtained by other authors[14,34,35] on nanostructured systems. For example, Spinu *et al.*[34] observed a rounded peak around H=0 in the χ_T response of Co nanoparticles, dispersed in a wax matrix, when the system was below but close to the average blocking temperature. These results show that this sample is still ferromagnetic at room temperature but it is close to the superparamagnetic state. Finally, the sample with a Co nominal thickness of 10 nm and Au capping layer shows a χ_T curve different from the other. The expected peak at $-H_C$ is absent due to the anisotropy field dispersion, which produces the broadening of the peaks detected in the effective anisotropy field.[11] This broadening can mask the expected peak at $-H_C$. From the position of the peaks, we have obtained the effective anisotropy field ($H_{K,\text{eff}}$), which has been included in Table II.

It is important to mention that the drastic effect of the Pt capping layer has also been detected in the χ_T measurements, as can be seen in Fig. 6(b). In this case, the expected peaks in $\pm H_{K,\text{eff}}$ are always detected, even in the thinner samples. When the Co nominal thickness is increased, the peaks are more broadened and the position around H=0 becomes less symmetric. There is also an increase of the asymmetry in the peak heights. These features are related to the anisotropy field dispersion and the interparticle interaction. As was shown in the morphological studies, σ_D increases as t_{Co} increases, so σ_D exerts an influence on the anisotropy field dispersion. As a consequence, the magnetization reversal takes place in a wider range of magnetic-field values. Interparticle interaction is controlled by the distance between particles and the surface contact. In Fig. 6(c) we have plotted $H_{K,\text{eff}}$ vs D for the samples with t_{Co}=2, 3, and 5 nm, with Pt capping layer. Once more, the experimental data are closer to D^6 dependence, which is in agreement with the RAM for a 3D system. However, these $H_{K,\text{eff}}$ values are too low com-

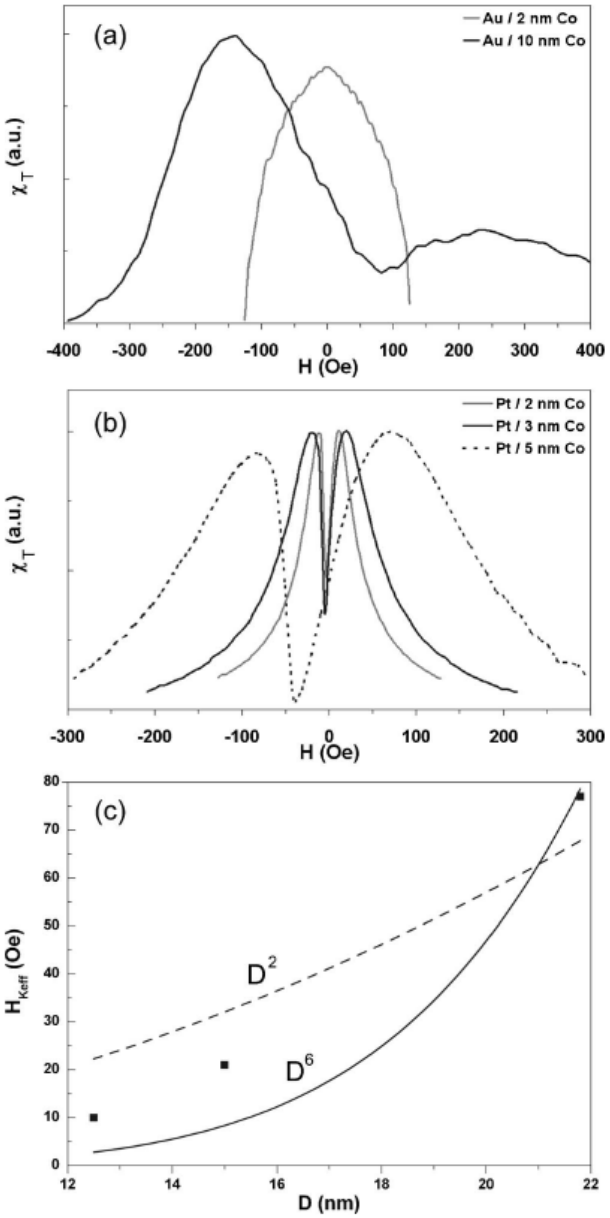

FIG. 6. (a) Transverse susceptibility for Au capped samples with Co nominal thicknesses of 2 and 10 nm. (b) Transverse susceptibility for Pt capped samples with Co nominal thicknesses of 2, 3, and 5 nm. (c) Dependence of Pt capped Co nanoparticles' effective anisotropy field on particle size with the corresponding fits to D^6 law (solid line) and D^2 law (dashed line).

pared to that of the effective anisotropy predicted by this model.[26] For example, for Co nanocrystalline particles with a correlation length of 4 nm, the RAM predicts an effective anisotropy field of 1600 Oe. Therefore we have to take into account the effect of the relaxation of the particle magnetic moments. In our case, the α values are lower for the thinner samples (see Table II), so the thermal energies will affect the effective anisotropy observed at room temperature. When the Co nominal thickness is increased, the activation energy increases, showing a higher effective anisotropy field. This implies that the Pt capped samples with $t_{Co}=10$ and 15 nm have enough activation energy so that the peaks in the χ_T are detected closer to the anisotropy field of bulk Co. That is the

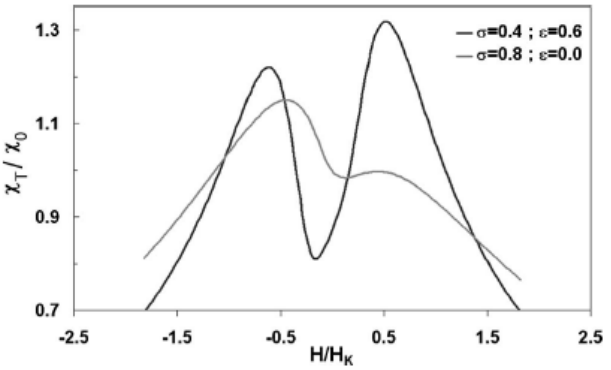

FIG. 7. Theoretically determined χ_T plots for a randomly oriented nanoparticle system with two different values of the anisotropy field dispersion (σ) and interparticle interaction (ε) according to the model described in Ref. 13.

reason why they were not detected with the magnetic fields attained in our experiment. This behavior in the χ_T measurements is similar to that obtained by Spinu *et al.*[14,15] by varying the temperature in magnetic nanoparticle systems of Fe and γ-Fe_2O_3. The idea is the same, so a change of the magnetic volume or the temperature leads to a change of the parameter α.

It is worth mentioning that valuable information can be obtained from a close study of the shape of the peaks of χ_T curves. Let us compare χ_T for the Pt capped, 5 nm Co sample with χ_T for the Au capped, 10 nm Co sample. First of all, while the peak at $H=H_{K,\text{eff}}$ is higher than the peak at $H=-H_{K,\text{eff}}$ for the Pt capped sample, the reversed is observed in the case of the Au capped one [see Figs. 6(a) and 6(b)]. Secondly, the peaks of the Au capped sample are more broadened than those of the Pt capped one due to a higher anisotropy dispersion in the former sample. This can be attributed to the fact that the particle size dispersion has more than doubled when the Co nominal thickness is increased from 5 to 10 nm, as can be seen in Table I. All these features can be qualitatively explained by a theoretical model described elsewhere.[13] In this model, the effects on the χ_T of the anisotropy field dispersion (σ), interparticle interaction (ε), and texture (σ_ϕ and σ_θ) have been studied. In Fig. 7, we have calculated the χ_T for a randomly oriented nanoparticle system with two different values of σ and ε. In the first case, a system with strong interparticle interaction ($\varepsilon=0.6$), representing the case of Pt/Co thin film, is considered. In the second case, the χ_T is calculated without interparticle interaction ($\varepsilon=0$) and with twice the anisotropy field dispersion, representing the case of Au/Co thin film, in agreement with the change of ε and σ from one sample to the other. The correlation between experimental and theoretical χ_T data shows two important features. On the one hand, the anisotropy field dispersion is intrinsically related to the particle size dispersion. On the other hand, the interparticle interaction can be strongly modified by the capping layer. A highly polarizable capping layer (like Pt) can connect magnetically the Co nanoparticles, promoting an increase of the effective magnetic volume, and so be used for decreasing the blocking temperature of a nanostructured system. However, a low polarizable capping layer (like Au) does not produce a magnetic connection among nanoparticles. That is the reason

why the sample Au/2 nm Co tends to the superparamagnetic state, whereas the sample Pt/2 nm Co exhibits a clear effective anisotropy field.

IV. CONCLUSIONS

We have presented a study on the properties of Co nanoparticles grown on Si_3N_4. The system has a clear 3D growth due to the high temperature of the substrate during deposition. For nominal thicknesses up to 5 nm, Co nanoparticles exhibit a narrow distribution of sizes. However, the percolation between nanoparticles occurs for thicker samples, giving rise to an increase in the particle size distribution. We have shown that the effective magnetic anisotropy depends dramatically on the particle size, the distribution of sizes, and the magnetic interaction among the nanoparticles. The interparticle interaction can be controlled by the capping layer, so that when a highly polarizable material (Pt) is used, a strong magnetic interaction between the nanoparticles is observed. This can be used as a means of changing the effective magnetic anisotropy in nanostructured systems.

ACKNOWLEDGMENTS

This work was supported in part by Universidad de Oviedo. One of the authors (B.P.) gratefully thanks Dr. Luis Eugenio Fernandez-Outon and Dr. Gonzalo Vallejo-Fernandez for the support received in the particle size analysis. Also, B.P. acknowledges financial support received from Gobierno del Principado de Asturias under Grant No. BP05-015. J.M.G.M. wishes to thank the financial support from CSIC under Project No. PIE 200650 130. C.C. acknowledges the Ministerio de Educación y Ciencia and FPI program for financial support.

[1]S. Sun and C. B. Murray, J. Appl. Phys. **85**, 4325 (1999).
[2]V. F. Puntes, P. Gorostiza, D. M. Aruguete, N. G. Bastus, and A. P. Alivisatos, Nat. Mater. **3**, 263 (2004).
[3]S. Sun, C. B. Murray, D. Weller, L. Folks, and A. Moser, Science **287**, 1989 (2000).
[4]V. F. Puntes, K. M. Krishnan, and A. P. Alivisatos, Science **291**, 2115 (2001).
[5]C. G. Zimmermann, M. Yeadon, K. Nordlund, J. M. Gibson, R. S. Averback, U. Herr, and K. Samwer, Phys. Rev. Lett. **83**, 1163 (1999).
[6]C. D'Orléans *et al.*, Phys. Rev. B **67**, 220101(R) (2003).
[7]F. Tang, D.-L. Liu, D.-X. Ye, Y.-P. Zhao, T.-M. Lu, G.-C. Wang, and A. Vijayaraghavan, J. Appl. Phys. **93**, 4194 (2003).
[8]X. Du, M. Inokuchi, and N. Toshima, J. Magn. Magn. Mater. **299**, 21 (2006).
[9]Y. Shiratsuchi, M. Yamamoto, Y. Endo, D. Li, and S. D. Bader, J. Appl. Phys. **94**, 7675 (2003).
[10]F. Luis *et al.*, Phys. Rev. B **65**, 094409 (2002).
[11]A. Hoare, R. W. Chantrell, W. Schmitt, and A. Eiling, J. Phys. D **26**, 461 (1993).
[12]L. Spinu *et al.*, Appl. Phys. Lett. **86**, 012506 (2005).
[13]R. Matarranz, M. C. Contreras, G. Pan, B. Presa, J. A. Corrales, and J. F. Calleja, J. Appl. Phys. **99**, 08Q504 (2006).
[14]L. Spinu, H. Srikanth, E. E. Carpenter, and C. J. O'Connor, J. Appl. Phys. **87**, 5490 (2000).
[15]L. Spinu, H. Srikanth, J. A. Wiemann, S. Li, J. Tang, and C. J. O'Connor, IEEE Trans. Magn. **36**, 3032 (2000).
[16]F. Luis *et al.*, J. Appl. Phys. **99**, 08G705 (2006).
[17]M. Suzuki *et al.*, Phys. Rev. B **72**, 054430 (2005).
[18]C. Train, P. Beauvillain, V. Mathet, G. Pénissard, and P. Veillet, J. Appl. Phys. **86**, 3165 (1999).
[19]Y. P. Lee, K. W. Kim, R. Gontarz, and Y. V. Kudryavtsev, Curr. Appl. Phys. **1**, 451 (2001).
[20]F. Wilhelm *et al.*, Phys. Rev. B **69**, 220404(R) (2004).
[21]M. Vopsaroiu, G. Vallejo Fernandez, M. J. Thwaites, J. Anguita, P. J. Grundy, and K. O'Grady, J. Phys. D **38**, 490 (2005).
[22]Nanotec Electronica SL™, www.nanotec.es
[23]J. Arbiol, F. Peiró, A. Cornet, C. Clavero, A. Cebollada, G. Armelles, and Y. Huttel, Appl. Phys. Lett. **86**, 032510 (2005).
[24]R. C. O'Handley, *Modern Magnetic Materials: Principles and Applications* (Wiley, New York, 2000).
[25]S. H. Charap, P. L. Lu, and Y. He, IEEE Trans. Magn. **33**, 978 (1997).
[26]G. Herzer, Mater. Sci. Eng., A **133**, 1 (1991).
[27]A. Kharmouche, S.-M. Chérif, A. Bourzami, A. Layadi, and G. Shmerber, J. Phys. D **37**, 2583 (2004).
[28]A. Aharoni, E. H. Frei, S. Shtrikman, and D. Treves, Bull. Res. Counc. Isr., Sect. A: Math., Phys. Chem. **6**, 215 (1957).
[29]L. Pareti and G. Turilli, J. Appl. Phys. **61**, 5098 (1987).
[30]Ch.-R. Chang and J.-S. Yang, Appl. Phys. Lett. **65**, 496 (1994).
[31]L. Spinu, C. J. O'Connor, and H. Srikanth, IEEE Trans. Magn. **37**, 2188 (2001).
[32]L. Spinu, C. Cimpoesu, L. Stoleriu, and A. Stancu, IEEE Trans. Magn. **39**, 2516 (2003).
[33]P. Poddar, H. Srikanth, S. A. Morrison, and E. E. Carpenter, J. Magn. Magn. Mater. **288**, 443 (2005).
[34]L. Spinu, Al. Stancu, L. D. Tung, J. Fang, P. Postolache, H. Srikanth, and C. J. O'Connor, J. Magn. Magn. Mater. **242–245**, 604 (2002).
[35]J. F. Calleja, M. C. Contreras, R. Matarranz, E. Navarro, Y. Huttel, A. Cebollada, and G. Armelles, J. Appl. Phys. **97**, 104302 (2005).

Capítulo 4

Bicapas Co/V y V/Co crecidas epitaxialmente sobre MgO

Artículo III

Artículo publicado en la revista JOURNAL OF APPLIED PHYSICS: "Structural and Magnetic Properties of V/Co_{fcc} Co_{hcp}/V Bilayers Grown on MgO(100): A Comparative Study"

Artículo IV

Artículo publicado en la revista JOURNAL OF PHYSICS D: APPLIED PHYSICS: "Fourfold Magnetic Anisotropy, Coercivity and Magnetization Reversal of Co/V Bilayers Grown on MgO(001)"

4.1 Resumen

Otro bloque de esta tesis consistió en la fabricación de láminas delgadas de Co con una estructura epitaxial. Para ello fue indispensable la elección de un substrato cristalino. En definitiva, se trata de analizar la influencia que tiene la estructura cristalina del cobalto en la anisotropía magnética de láminas delgadas epitaxiales del tipo V/Co y Co/V. El sustrato escogido fue MgO(001). Estos substratos son comerciales y en el laboratorio se sometieron a una inmersión en alcohol isopropílico (C_3H_8O) para disolver las primeras capas de la superficie eliminando posibles residuos. Posteriormente se calentaron durante 30 minutos a 450ºC en la campana de UHV para eliminar los restos del alcohol. El MgO se escogió como substrato por la similitud del parámetro de red con el de los metales Co y V en comparación con el que producirían otros substratos como el Si. Además el MgO posee excelentes propiedades como barrera de difusión atómica y como aislante eléctrico. En el crecimiento de sistemas

epitaxiales en forma de lámina delgada es muy importante partir siempre de una superficie idéntica, fácilmente reproducible y con el menor número de defectos para que éstos no influyan de una manera aleatoria en los proceses magnéticos del sistema. Por estas razones, se depositó en todos los casos una capa buffer de MgO sobre los substratos comerciales MgO(001) debidamente tratados. En este caso se creó una interfaz homoepitaxial. El crecimiento de la capa buffer se hizo mediante ablación láser de un blanco monocristalino de MgO(001) rotatorio. El espesor depositado para todas las muestras, calibrado mediante perfilómetro, fue de 80 Å con un ritmo de deposición de 8 Å/min. Para prevenir la oxidación de las muestras, se depositó en todas mediante sputtering triodo una capa de Al de un espesor de 30 Å a temperatura ambiente. El ritmo de deposición fue de 20 Å/min. Además el aluminio presenta una baja polarizabilidad con lo cual no jugará un papel muy importante en los procesos magnéticos del sistema Co/V.

La estructura cristalográfica de las muestras ha sido investigada por difracción de rayos X ex-situ. Se han realizado barridos simétricos ($2\theta/\omega$) y asimétricos (ϕ) para estudiar la forma de crecimiento en dirección perpendicular al plano de la muestra y las relaciones epitaxiales entre las diferentes capas. A modo de resumen, las relaciones epitaxiales encontradas en cada sistema, la estructura cristalina del compuesto y su dirección de crecimiento son:

$$Co(001)_{fcc}[100]||MgO(001)[100]$$

$$Co(11\bar{2}0)_{hcp}[0001]||V(001)_{bcc}[100]||MgO(001)[110]$$

$$Co(11\bar{2}0)_{hcp}[0001]||V(001)_{bcc}[010]||MgO(001)[1\bar{1}0]$$

Cuando el cobalto se crece sobre óxido de magnesio exhibe una estructura cristalina fcc, mientras que si está depositado sobre vanadio su estructura es la hcp. Este cambio tan drástico afectará de manera fundamental a las propiedades magnéticas de estos sistemas.

Los ciclos de histéresis de todas las láminas se han medido mediante efecto Kerr transversal explorando en todas las direcciones los procesos de imanación dentro del

plano de la película. Fuera del plano, mediante efecto Kerr polar, no se encontró señal remanente de imanación en ninguna muestra, indicando una fuerte anisotropía de forma debido a la estructura en 2D de los sistemas que coloca a la imanación siempre en el plano de la película.

Cuando el espesor de Co fcc es de 100 Å, se obtiene una clara anisotropía magnética biáxica con dos ejes fáciles a lo largo de las direcciones $[110]_{Co}$ y $[1\bar{1}0]_{Co}$, mientras que los ejes difíciles se disponen en las direcciones $[100]_{Co}$ y $[010]_{Co}$. Esto es lo esperado en compuestos con estructura cristalina cúbica centrada en las caras, como en el caso del Níquel, cuyos ejes de fácil imanación son las familias <111>. En el caso presente estas direcciones se encuentran fuera del plano de la película y por tanto debido a la anisotropía de forma la imanación no se coloca en esta dirección. Los siguientes ejes de fácil imanación son las familias <110> que sí se encuentran en el plano de la muestra, mientras que los ejes difíciles son las aristas del cubo <100>. Como se observa en el ciclo de histéresis del eje fácil para 100 Å de Co fcc la inversión de la imanación se produce de un modo muy abrupto pasando de un estado de saturación a otro en sentido contrario en un margen muy pequeño de campo magnético aplicado, lo cual implica que el proceso dominante es el desplazamiento de paredes mediante la nucleación y posterior propagación de paredes de dominio de 90º o 180º. Cuando el campo magnético se aplica a lo largo de alguna dirección difícil, conforme se va disminuyendo desde un estado de saturación la imanación se va reduciendo por rotaciones coherentes hasta un valor próximo de $M_S/2^{1/2}$ (valor de la imanación remanente en el caso ideal). Una vez alcanzado el valor de campo negativo correspondiente al campo coercitivo ($H_C \approx 10$ Oe), la imanación se invierte abruptamente a lo largo del eje fácil hasta alcanzar el valor de $-M_S/2^{1/2}$ debido a la nucleación de dominios orientados a lo largo de los ejes fáciles con su posterior propagación de paredes. Aumentando todavía más la magnitud del campo aplicado, la imanación rotará reversiblemente hasta alcanzar la dirección del eje difícil. Este comportamiento implica que para un espesor nominal de 100 Å de cobalto el sistema se comporta de un modo continuo, es decir, aunque exista un cierto crecimiento granular todo el sistema está magnéticamente conectado entre sí permitiendo un rápido desplazamiento de paredes a través de él.

Todo lo contrario ocurre en los sistemas de 30 Å Al / 20 Å Co / MgO(001) y 30 Å Al / 15 Å V / 20 Å Co / MgO(001) donde, a través de los ciclos de histéresis, no es posible detectar una clara anisotropía magnética en el plano. Esto es típico de un crecimiento en forma de islas magnéticas sobre la superficie de MgO las cuales no están todas ellas en contacto directo entre sí, impidiendo la inversión total de la imanación a través de un desplazamiento de paredes, de forma que cada isla con su propia anisotropía contribuye a los procesos magnéticos. El campo coercitivo según las direcciones $[110]_{Co}$, $[1\bar{1}0]_{Co}$, $[100]_{Co}$ y $[010]_{Co}$ es aproximadamente de 20 Oe en todos los casos, además no es observada una modificación apreciable debido a la presencia de vanadio sobre cobalto.

Los ciclos de histéresis medidos para el sistema $Co(11\bar{2}0)_{hcp}$ / $V(001)_{bcc}$ / MgO(001) muestran dos claros ejes de fácil imanación a lo largo de las direcciones $[110]_{MgO}$ y $[1\bar{1}0]_{MgO}$ las cuales se corresponden con los ejes ‘c’ del cobalto hcp crecido sobre las aristas del vanadio bcc. Para espesores de 40 Å, 100 Å y 200 Å de cobalto se observa una pequeña asimetría del ciclo de histéresis a lo largo de las direcciones de difícil imanación ($[100]_{MgO}\|[110]_{V}$ y $[010]_{MgO}\|[1\bar{1}0]_{V}$), ya que los campos coercitivos no coinciden en las dos ramas del ciclo. Como se demostrará posteriormente mediante medidas de susceptibilidad transversal, esto es debido a la no saturación según estas direcciones, de forma que se están describiendo ciclos de histéresis menores. Se observa una anisotropía magnética biáxica, con los ejes fáciles paralelos a los ejes ‘c’ de cada uno de los dominios hcp, indicando una distribución de volúmenes de ambos dominios, en concordancia con los datos de rayos X.

Para un espesor de 20 Å de cobalto hcp se observan unos ciclos de histéresis menos cuadrados que en el caso de las muestras de 40 Å, 100 Å y 200 Å de cobalto hcp. Esto puede indicar un cierto crecimiento en forma de islas no conectadas magnéticamente. Sin embargo, en contraste con el caso de 20 Å Co / MgO(001), aquí la anisotropía magnética es todavía observable en el ciclo de histéresis con una fuerte reducción del campo coercitivo en la dirección $[100]_{MgO}$ comparado con la dirección $[110]_{MgO}$.

En la tabla siguiente se presentan los campos coercitivos de las muestras estudiadas. En los casos en los que aparecen dos valores, ambos corresponden a los valores medidos en cada rama del ciclo (ciclos asimétricos).

Tabla I. Estructura y espesores de las tricapas V/Co/MgO y Co/V/MgO. Campos coercitivos a lo largo del eje fácil (dirección $[110]_{MgO}$) y difícil (dirección $[100]_{MgO}$). En el caso de ciclos de histéresis asimétricos se dan dos valores, cada uno correspondiente a cada rama del ciclo.

		H_C (Oe) $[110]_{MgO}$	H_C (Oe) $[100]_{MgO}$
Co FCC	20 Å Co / MgO	21	23
	15 Å V / 20 Å Co / MgO	20	22
	100 Å Co / MgO	15	9
Co HCP	20 Å Co / 10 Å V / MgO	47	30
	20 Å Co / 20 Å V / MgO	53	45
	20 Å Co / 40 Å V / MgO	70	60
	40 Å Co / 40 Å V / MgO	84	70 / 50
	100 Å Co / 40 Å V / MgO	173	133 / 103
	200 Å Co / 40 Å V / MgO	140	90 / 100

Esta diferencia en el comportamiento entre 20 Å Co / MgO(001) y 20 Å Co / V / MgO(001) radica en la propia diferencia en la anisotropía magnetocristalina de las dos fases del cobalto, dado que la constante de anisotropía uniáxica K_{1U} para el Co hcp es aproximadamente siete veces mayor que la constante de anisotropía K_{1C} para el Co fcc a temperatura ambiente. Por otro lado, se observa que para las muestras 20 Å Co / x Å V / MgO(001) (con x = 10 Å, 20 Å y 40 Å) conforme va disminuyendo el espesor de la capa de vanadio, la muestra se hace magnéticamente más blanda, mostrando una reducción en el campo coercitivo detectado. Esto es explicado fácilmente si se tiene en cuenta que para espesores pequeños de vanadio la capa no será continua, quedando zonas en las cuales el vanadio no crece sobre el óxido de magnesio, de forma que al depositar el cobalto habrá partes de la película en las que crezca en su fase hcp sobre el vanadio, pero habrá otras zonas (las cuales aumentan a medida que el espesor nominal de vanadio decrece) en las que el cobalto crezca en su fase fcc directamente sobre el óxido de magnesio, con lo cual cuanto más volumen de cobalto fcc crezca, la muestra será magnéticamente más blanda. La coexistencia de estas dos fases hcp y fcc del cobalto será puesta de manifiesto otra vez mediante medidas de susceptibilidad

transversal. También se trató de detectar estas fases mediante difracción de rayos X, pero los resultados no fueron concluyentes debido a la poca cantidad de cobalto de las láminas.

Las medidas de susceptibilidad transversal (TS) para el Co fcc muestran una simetría biáxica, como es esperado debido a su propia estructura cristalina, con dos ejes de fácil imanación y dos de difícil imanación alternativamente dispuestos a 45º en el plano de la muestra. Esta anisotropía magnética no pudo ser observada en los ciclos de histéresis para las láminas delgadas de 20 Å de Co fcc, como ya fue mencionado anteriormente. Esto muestra claramente que las medidas de TS son mucho más sensibles que los ciclos de histéresis para detectar la anisotropía magnética. Dependiendo del espesor de Co depositado han sido observados dos comportamientos diferentes. Por un lado, las muestras con 20 Å de Co fcc exhiben unas propiedades similares. Cuando el campo magnético continuo H es aplicado a lo largo de la dirección $[110]_{Co}$ la TS muestra un comportamiento de eje de fácil imanación con un decaimiento de la señal en el rango 15 - 25 Oe correspondiente a su campo coercitivo según esta dirección. Cuando H es aplicado según la dirección $[1\bar{1}0]_{Co}$ la imanación se invierte en el rango 5 - 35 Oe pero el procedimiento no es equivalente puesto que según este eje de fácil imanación se observa un mínimo en la señal de TS. Esto es debido a un alineamiento de la imanación a lo largo de la dirección $[110]_{Co}$ durante el proceso de inversión de la imanación a lo largo del eje $[1\bar{1}0]_{Co}$. Comportamientos similares han sido observados en Fe crecido sobre MgO, dándose como explicación la presencia de una anisotropía uniáxica superpuesta debido a la existencia de pequeños escalones en el substrato de MgO. Este hecho debería observarse en los ciclos de histéresis de forma que el ciclo a lo largo del eje $[1\bar{1}0]_{Co}$ presentaría un pequeño escalón, sin embargo, no pudo ser confirmado de esta forma, mostrándose una vez más la mayor sensibilidad que poseen las medidas de TS. En simulaciones teóricas de TS también fue demostrada la existencia de un mínimo en la TS de un eje fácil cuando existe una anisotropía uniáxica superpuesta sobre otra anisotropía biáxica. Por otro lado, en las medidas de TS a lo largo de los ejes fáciles se puede observar que la imanación se invierte para campos magnéticos ligeramente menores en 15 Å V / 20 Å Co / MgO que para 20 Å Co / MgO, lo cual indica una posible polarización del vanadio favoreciendo la interacción magnética entre granos lo que implica una mayor facilidad en la inversión de la

imanación. Cuando el campo magnético continuo es aplicado a lo largo de las direcciones de difícil imanación ($[100]_{Co}$ y $[010]_{Co}$) se obtienen curvas de TS muy similares para los dos ejes difíciles. Las muestras con 20 Å de Co fcc exhiben un comportamiento casi idéntico con ambos máximos simétricamente dispuestos en ±100 Oe, el cual se corresponde con el campo de anisotropía macroscópica efectiva de las láminas. Estos resultados experimentales fueron comparados con los obtenidos de forma teórica para un monodominio de Co fcc.

En contraposición, para 100 Å de Co fcc se obtuvo un comportamiento distinto al obtenido para 20 Å de Co FCC. Esto ya fue evidenciado desde un principio con los ciclos de histéresis, pero además las medidas de TS aportan nuevas evidencias. La inversión de la imanación a lo largo de los ejes fáciles se produce en un intervalo de campo magnético aplicado mucho menor, entre 14 - 17 Oe para la dirección $[110]_{Co}$ y 10 - 18 Oe para la dirección $[1\bar{1}0]_{Co}$. La TS según el eje difícil $[100]_{Co}$ muestra dos máximos con mucha menos dispersión dispuestos simétricamente en ±230 Oe, de forma que este campo de anisotropía macroscópica efectiva es mayor que el detectado para las dos láminas más delgadas debido a un incremento de la anisotropía magnética. Todos estos resultados indican que para 100 Å de Co fcc el crecimiento es continuo, mientras que para un espesor de 20 Å las láminas son discontinuas. Una prueba clara de este hecho lo evidencia la inversa de la TS, la cual en la región de saturación no depende linealmente con el campo magnético para las muestras con 20 Å de Co fcc. Sin embargo, la inversa de la TS muestra una clara linealidad con el campo magnético aplicado para la lámina de 100 Å de Co FCC. La anisotropía magnética uniáxica superpuesta sigue manifestándose en esta lámina de 100 Å de Co, de forma que las medidas de TS indican claramente que los dos ejes de fácil imanación no son equivalentes.

Mediante medidas de TS se ha puesto de manifiesto que para el sistema Al/Co/V/MgO todas las muestras exhiben una anisotropía magnética macroscópica biáxica en el plano, como es esperado tras conocer su particular estructura. Los ejes de fácil imanación se disponen a lo largo de las direcciones $[110]_{MgO}$ y $[1\bar{1}0]_{MgO}$, las cuales se corresponden con los dos dominios de ejes [0001] del Co hcp. Los ejes de difícil imanación se encuentran según las direcciones $[100]_{MgO}$ y $[010]_{MgO}$, es decir,

alternativamente a 45º de cada eje fácil. Si se mantiene fijo el espesor de Co en 20 Å, a medida que aumenta el espesor de vanadio también crece el campo de anisotropía macroscópica efectiva, pasando de 207 Oe para 10 Å de vanadio a 247 Oe para 40 Å de vanadio. Esto indica que con espesores de la capa de vanadio menores aparecen discontinuidades, de forma que al depositar encima el cobalto habrá zonas en las que crezca en su fase hcp sobre el vanadio y otras zonas donde presentará su fase fcc al depositarse directamente sobre el óxido de magnesio. Cuando aumenta el espesor de vanadio las discontinuidades disminuyen, haciendo que el volumen de Co fcc también disminuya a favor de un aumento del volumen de Co hcp lo que repercute directamente en un incremento de la anisotropía macroscópica efectiva dada la mayor dureza magnética del Co hcp. La coexistencia de estas dos fases del cobalto también ha sido puesta de manifiesto en sistemas de Co/Cr/MgO y Co/Mo/MgO mediante medidas de histéresis magnética. Por otro lado, la inversión de la imanación según los ejes fáciles se produce de una manera suave en un intervalo de campo magnético que ronda los 20 Oe para cada muestra, indicando que la lámina de 20 Å de Co no es continua. Además a medida que aumenta el espesor de la capa de vanadio también aumenta el valor del campo coercitivo, ya que éste está intrínsecamente relacionado con el campo de anisotropía del sistema. Cuando el espesor de la capa de vanadio es de 40 Å ya no se observa ninguna diferencia en los procesos de inversión entre los dos ejes de fácil imanación siendo ambos idénticos, de forma que la anisotropía uniáxica superpuesta ha desaparecido no produciéndose el mínimo característico en la señal de TS, lo que apoya la hipótesis de que esta anisotropía uniáxica superpuesta está inducida por rugosidades o dislocaciones en el ‘buffer’ de óxido de magnesio crecido mediante ablación láser. En conclusión, se puede afirmar que para un espesor de 40 Å de vanadio no habrá discontinuidades en la lámina, con lo cual todo el volumen de cobalto crecido sobre ésta presentará la fase cristalina hcp.

El espesor de cobalto hcp depositado sobre vanadio influye tanto en los procesos de inversión de la imanación como en los valores del campo coercitivo y de la anisotropía magnética. Según los resultados anteriores se supone que para un espesor nominal de 40 Å de vanadio la capa es continua, con lo cual todo el volumen de cobalto crecido sobre este espesor presentará la estructura cristalina hcp. Con lo cual se mantuvo fijo el espesor de V en 40 Å y se varió el espesor de Co. Las láminas delgadas presentaron una anisotropía magnética en el plano con simetría biáxica, además debido

al espesor del 'buffer' de vanadio no fue detectada ninguna anisotropía inducida. Cuando se observa el comportamiento de la TS según el eje de difícil imanación $[100]_{MgO}||[110]_V$ el campo de anisotropía macroscópica efectiva detectado para 20 Å de Co hcp ronda los 250 Oe, mientras que para espesores mayores de cobalto la anisotropía magnética aumenta lo suficiente como para que las láminas no puedan ser saturadas en el dispositivo experimental (el máximo campo magnético alcanzado para la medida de la TS es de 430 Oe) de forma que las medidas de TS se encuentran entre los dos picos de saturación. En este último caso, se observa que los procesos de imanación son asimétricos, hecho característico de la medida de ciclos de histéresis menores. Esta asimetría en el campo coercitivo ya se intuía en los ciclos de histéresis medidos mediante efecto Kerr transversal según la dirección de difícil imanación. Para comprobar de manera definitiva este proceso de asimetría se realizaron medidas de los ciclos de histéresis mediante un SQUID, para 200 Å de Co hcp, según varias direcciones. Cuando el campo magnético aplicado se fijó entre ±250 Oe se obtuvieron los ciclos de histéresis menores con su clara asimetría, donde aún faltan procesos por completar. En cambio, cuando el campo magnético aplicado fue suficientemente elevado (±3000 Oe) se obtuvieron los ciclos de histéresis con una perfecta simetría, indicando que se ha sobrepasado el campo de anisotropía macroscópica efectiva.

Por otro lado, el proceso de inversión de la imanación según los ejes fáciles también está influenciado por el espesor de cobalto depositado. Mientras que para 20 Å de Co hcp la inversión de la imanación tiene lugar en un rango amplio entre 47 - 64 Oe lo que indica una cierta discontinuidad de la capa, para espesores de 40 Å, 100 Å y 200 Å el rango del campo magnético en el cual tiene lugar la inversión de la imanación se hace cada más pequeño, de forma que el salto en la señal de TS es más abrupto debido a un rápido desplazamiento de paredes a través de la lámina. Aunque en este caso la TS no sigue un comportamiento de saturación a campos magnéticos elevados ya que sólo muestra un decaimiento lineal, los procesos magnéticos son simétricos, como también es evidenciado en los ciclos de histéresis. Esta simetría es consecuencia de la microestructura de las muestras ya que el campo coercitivo observado se corresponde con la inversión de la imanación según los dominios de ejes 'c' del cobalto paralelos al campo magnético continuo aplicado, mientras que los otros dominios de ejes 'c' se encuentran en dirección perpendicular, de manera que irán rotando reversiblemente con el campo. También es importante remarcar la pequeña pero apreciable diferencia en el

valor del campo coercitivo según los dos ejes de fácil imanación. Esta circunstancia observada para las muestras con más espesor de Co hcp puede deberse a una diferencia en las constantes de anisotropía magnética entre las dos regiones con los ejes ‘c’ del cobalto perpendiculares, atribuyéndose a una pequeña diferencia en la cantidad de cobalto crecido en ambos dominios, lo cual sería difícilmente detectable mediante barridos asimétricos de rayos X.

4.2 Artículo III

JOURNAL OF APPLIED PHYSICS **100**, 053917 (2006)

Structural and magnetic properties of V/Co_{fcc} and Co_{hcp}/V bilayers grown on MgO(100): A comparative study

J. F. Calleja[a)]
Departamento de Física, Facultad de Ciencias, Universidad de Oviedo, Calvo Sotelo s/n, 33007 Oviedo, Spain

Y. Huttel
Instituto de Ciencia de Materiales de Madrid (ICMM-CSIC), Cantoblanco, 28049 Madrid, Spain

M. C. Contreras
Departamento de Física, Facultad de Ciencias, Universidad de Oviedo, Calvo Sotelo s/n, 33007 Oviedo, Spain

E. Navarro
Departamento de Física de Materiales, Facultad de Físicas, Universidad Complutense, 28040 Madrid, Spain

B. Presa and R. Matarranz
Departamento de Física, Facultad de Ciencias, Universidad de Oviedo, Calvo Sotelo s/n, 33007 Oviedo, Spain

A. Cebollada
Instituto de Microelectrónica de Madrid-IMM (CNM-CSIC), Isaac Newton 8 (PTM), Tres Cantos, 28760 Madrid, Spain

(Received 6 November 2005; accepted 20 July 2006; published online 15 September 2006)

A detailed study of the structure and magnetic properties of V/Co versus Co/V bilayers grown on MgO(001) substrates with cubic and hexagonal Co crystal structures is presented. Co is found to adopt fcc structure when grown on MgO(001), while it adopts hcp structure when grown on V(001). The different magnetocrystalline anisotropy associated with each structure gives rise to different magnetic properties for the otherwise equivalent symmetric Co–V bilayers. © *2006 American Institute of Physics*. [DOI: 10.1063/1.2336496]

I. INTRODUCTION

Of increasing importance in modern technology are magnetic thin films and interfaces involving thin films. On the one hand, effects usually neglected in three dimensional systems may become important as the dimensions of the system perpendicular and parallel to the film surface become very different. On the other hand, the interface is believed to play an important role in, for example, the oscillatory magnetic coupling that is essential for the giant magnetoresistance phenomenon. Magnetic anisotropy is a key parameter in ferromagnetic thin film behavior since it helps to determine the coercivity and the magnetization reversal process. At the same time, the magnetic anisotropy depends on the microscopic structure of the system, in particular in epitaxial films. Moreover, the film growth mode can give rise to the development of nanostructures (islands) in the first steps of the film growth that have a great impact on the magnetic anisotropy.

In the last decade great attention has been paid to the study of V/Co multilayers [1–4] due to the oscillatory exchange through V layers. These studies clearly indicated that a better understanding of the interface magnetism at the V/Co interface is mandatory to understand the physics of this system. The orientation of the magnetization in a ferromagnetic thin film is determined by the competition between different parameters such as shape anisotropy, magnetocrystalline anisotropy, magnetic surface anisotropy, epitaxial strain, etc.[5] The structures of Co [body centered cubic (bcc), face centered cubic (fcc), and hexagonal close packed (hcp)] provide excellent model systems for the study of the influence of the magnetocrystalline anisotropy on the interface anisotropy and its role in the induction of magnetic moment in the V atoms.

In this paper we present a comparative study of the structure, magnetic properties and magnetic anisotropies of the V–Co system formed in two different stacking sequences, namely, Co/V/MgO(100) and V/Co/MgO(100). These sequences give rise to different Co crystalline structures (hcp versus fcc) and therefore to different magnetic behaviors. The paper is organized as follows: In Sec. II we briefly present the experimental details; In Sec. III we present the experimental results including x-ray diffraction, transverse Kerr, and transverse susceptibility results. In Sec. IV we discuss the results and then present the conclusions.

II. EXPERIMENTAL PROCEDURE

The samples were grown in a combined ultrahigh vacuum system (base pressure in the low 10^{-9} mbar) with triode sputtering and laser ablation facilities. The Co and V films were deposited by triode sputtering onto MgO(100)

a)Electronic mail: jfcalleja@uniovi.es

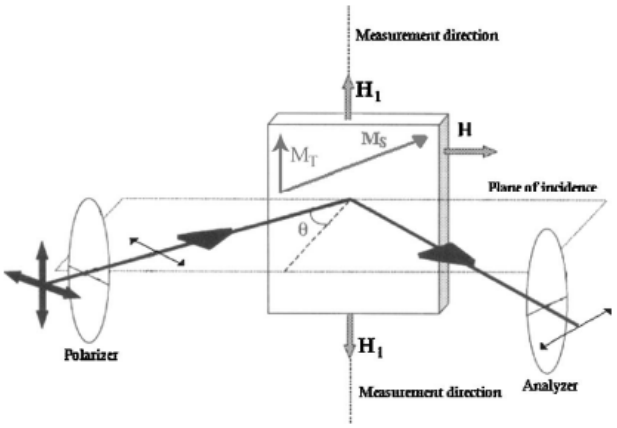

FIG. 1. Geometry of the magneto-optical experimental setup used for the measurement of the transverse susceptibility and hysteresis loops. The transverse component of the magnetization M_t is measured as a function of H_1 (hysteresis loop) or as a function of H (transverse susceptibility).

single crystals at normal incidence. The argon pressure during the sputtering was kept at 4×10^{-4} mbar and the deposition rates were in the range of a few Å/min. Prior to V and Co deposition, an 80 Å MgO buffer layer was grown by laser ablation at 450 °C on the substrate to planarize the surface. Subsequent to the room temperature (RT) deposition of the V and Co, a 30 Å thick Al capping layer was deposited at RT in order to protect the films from oxidation. Different Co crystalline structures were obtained by inverting the deposition sequence of V and Co. As the magnetic anisotropy of the system under study is expected to be mainly determined by the Co crystallographic structure and the Co layer thickness, the samples were tailored as follows. In the case of fcc Co/MgO(001), three systems were investigated: Al/100 Å Co/MgO, Al/20 Å Co/MgO, and Al/15 Å V/20 Å Co/MgO. The last one was chosen in order to investigate the influence of a possible V polarization. In the case of hcp Co/V, the systems under investigation were Al/200 Å Co/40 Å V/MgO and Al/20 Å Co/40 Å V/MgO, with the Co thickness as the varying parameter.

Crystallographic structure, transverse Kerr loops, and magnetic anisotropy were measured after the samples were removed from the vacuum system. The crystallographic structure was investigated using x-ray diffraction (XRD) with a four-circle diffractometer, Cu $K\alpha$ radiation, and 1/4° divergence slits. Both symmetric ($\theta/2\theta$ scans) and asymmetric phi scans (φ scans) have been recorded. The asymmetric phi scans have been recorded selecting an off normal diffraction peak (either from the V or the Co layers) and rotating the sample around its surface normal. This allows us to determine the crystallographic symmetry (if it exists) in the plane of the surface of the structure under study.

The magnetic anisotropy was obtained from transverse susceptibility (TS) measurements which are performed using the transverse magneto-optical Kerr effect. The experimental setup used to obtain the hysteresis loops and the TS is shown in Fig. 1. Two magnetic fields, H_1 and H, can be applied in the plane of the sample. In order to obtain a hysteresis loop only a low frequency magnetic field H_1 is applied. In the

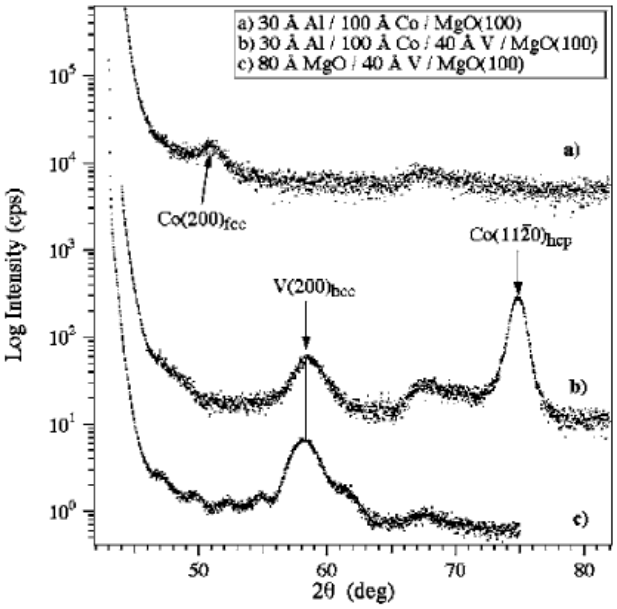

FIG. 2. Selected symmetric XRD scans for the V/MgO(100), Co/MgO(100), and Co/V/MgO(100) structures.

case of transverse susceptibility measurements two magnetic fields are applied: H_1, which in this case is a small amplitude alternating field (the frequency of H_1 used was 127 Hz), and an orthogonal bias field H, both in the film plane. These magnetic fields are produced by two pairs of Helmholtz coils perpendicular to each other. The light from the light source is linearly polarized with the electric vector in the plane of incidence. The magneto-optic Kerr effect produces a small change in the intensity of the reflected light proportional to the component of the magnetization perpendicular to the plane of incidence M_t. The light detected in the photodiode changes accordingly. If the amplitude of H_1 is small enough, the Kerr signal is proportional to the susceptibility, and we obtain the transverse susceptibility as a function of the bias field H. In order to carry out the magnetic characterization of the samples, TS measurements are performed with H applied along different directions, as explained in the following paragraphs. The direction of the sample relative to the magnetic fields is controlled by rotating the sample holder. All the measurements were performed at room temperature.

III. RESULTS

A. X-ray diffraction

The crystallographic structure of the samples has been investigated by means of x-ray diffraction. Both symmetric ($\theta/2\theta$ scans) and asymmetric phi scans (φ scans) have been recorded and the corresponding spectra are displayed in Figs. 2 and 3. Figure 2 displays the symmetric scans for both Co/V/MgO(100) and Co/MgO(100) systems. For reference, we present at the bottom of Fig. 2 the diffraction scan corresponding to 40 Å of V grown on MgO(100) and capped with MgO layer. The intense tail below 50° comes from the MgO(200) diffraction peak. As reported previously[6] the feature located at around 58° corresponds to the V(200) diffrac-

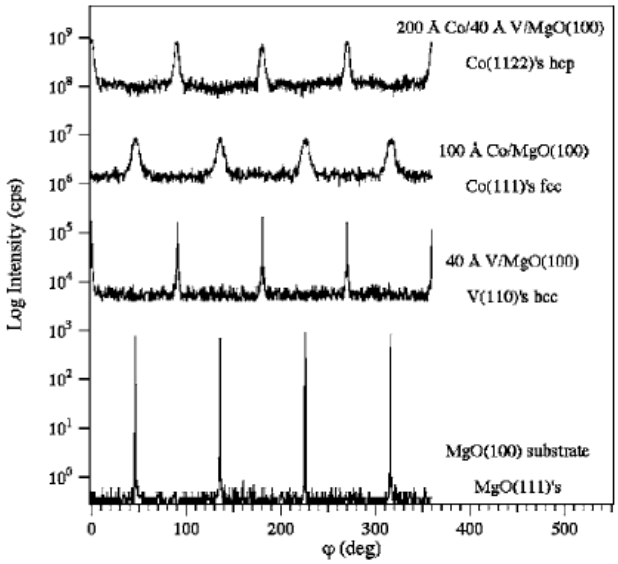

FIG. 3. Representative asymmetric φ scans for MgO(111), V(110), Co(111), and Co($11\bar{2}2$) reflections for different structures grown on MgO(100) substrates. The φ scans illustrate the epitaxial relationships that govern the growth of the structures. See text for details.

tion peak of the body centered cubic V structure. The crystallographic structure of the Co layer deposited on the V layer is illustrated through the scan corresponding to the 30 Å Al/100 Å Co/40 Å V/MgO(100) system. The feature located at 74.8° corresponds to the hcp Co($11\bar{2}0$) diffraction peak, indicating the growth of Co on V in the hcp structure[7] with the *c* axis located in the plane of the surface. As can be observed in Fig. 2, the growth of 100 Å of Co on MgO(100) results in the fcc structure, as revealed by the Co(200) diffraction peak located at 50.8° in the diffraction scan of the 30 Å Al/100 Å Co/MgO(100) sample. Unfortunately, the crystal structure of V on fcc Co in the 30 Å Al/15 Å V/20 Å Co/MgO sample could not be determined, as no signal was detected due to the small amount of V in the sample.

Further characterization of the crystallographic structure is given by the asymmetric φ scans displayed in Fig. 3. As can be observed in the asymmetric φ scan corresponding to the MgO(111) diffraction peak, the MgO substrates display the expected fourfold symmetry. As previously reported,[6,8–10] V grown on MgO(100) also displays a fourfold symmetry with an additional rotation of 45°, leading to the $V(001)_{bcc}[100]\|MgO(001)[110]$ epitaxial relation, i.e., a 45° in-plane rotation of the V[100] directions with respect to the MgO ones. On the other hand, it can be observed that the fcc Co grown on MgO(100) shows a well defined fourfold symmetry that corresponds to the following epitaxial relationship $Co(001)_{fcc}[100]\|MgO(001)[100]$ similar to the one reported for the growth of Co on MgO(100) at 250 °C.[11] As displayed in Fig. 2, when Co is deposited on the initial V/MgO(001) substrate, a Co hcp structure is formed with the *c* axis in the plane of the film. In Fig. 3 the Co($11\bar{2}2$) reflection shows a fourfold symmetry. This is due to the growth of Co($11\bar{2}0$) by simultaneous nucleation of crystalline domains with the (0001) axis aligned with equal probability along the V[100] and [010] directions, and therefore rotated 90° with respect to each other[6] similar to the Co/Mo/MgO(001) system.[12] In this case, the epitaxial relationship for both domains is $Co_{hcp}(11\bar{2}0\|V(001)\|MgO(001)$ for the growth direction, and $Co_{hcp}[0001]\|V[100]\|MgO[110]$ and $Co_{hcp}[0001]\|V[010]\|MgO[1\bar{1}0]$ for the two in-plane orientations. Also it can be noted that the Co($11\bar{2}2$) reflections of the corresponding φ scan have similar intensities, indicating that there are approximately equal volumes of the two hcp Co orientations.

B. Transverse Kerr

Kerr hysteresis loops have been recorded in the transverse geometry, i.e., with the magnetic field in the plane of the sample and perpendicular to the plane of incidence of the light. This geometry allows the measurement of the in-plane magnetization. Panels (a) and (b) of Fig. 4 display the representative Kerr hysteresis loops measured along the $[110]_{MgO}$ and $[100]_{MgO}$ directions for the systems Co/MgO(100) and V/Co/MgO(100), whereas panels (c) and (d) display the Kerr hysteresis loops along the same directions for the Co/V/MgO(100) system. It is interesting to note that no uniaxial in-plane anisotropy could be clearly identified in opposition to similar systems such as fcc Co(110)/MgO(110), 200 Å hcp Co/V/MgO(110), 200 Å hcp Co/Cr/MgO(110), and 200 Å hcp Co/Mo/MgO(110).[13,14] This is simply because the samples were here grown on (001) oriented surfaces [(001) V and MgO], promoting growth with fourfold symmetry. We first concentrate on the Kerr hysteresis loops of the systems Co/MgO(100) and V/Co/MgO(100). Whereas the Kerr hysteresis loops measured at different angles on 100 Å fcc Co/MgO(100) displayed a clear fourfold magnetic symmetry (not shown here), that was not the case for the Kerr hysteresis loops of 20 Å fcc Co/MgO(100) and 15 Å V/20 Å fcc Co/MgO(100). As expected the 100 Å fcc Co/MgO(100) exhibits an easy magnetization axis along the $[110]_{Co}$ axis. The corresponding coercivity along the easy magnetization axis is found to be close to 15 Oe which is considerably lower than the one expected in a thin layer of fcc Co grown on Cu(100).[15] The nonobservation of a clear magnetic in-plane anisotropy for 20 Å fcc Co/MgO(100) and 15 Å V/20 Å fcc Co/MgO(100) might be due to the lack of full continuity of the Co layers, the morphology of which would make it impossible to observe the fcc Co characteristic magnetocrystalline anisotropy. This result suggests the growth of fcc Co islands on the MgO substrate. Additionally, we observe that the growth of 15 Å of V on 20 Å Co/MgO(100) does not significantly modify the coercivity.

We now turn to the Kerr hysteresis loops of the Co/V/MgO(100) system in panels (c) and (d) of Fig. 4. As expected, the Kerr hysteresis loops display a clear easy axis of magnetization along the $[110]_{MgO}$ axis which corresponds also to the *c* axis of the hcp cobalt grown on bcc V. The coercivities of the 200 Å Co/40 Å V/MgO(100) system measured along the $[110]_{MgO}$ and $[100]_{MgO}$ (137 and 96 Oe, respectively) are very similar to the coercivity measured in

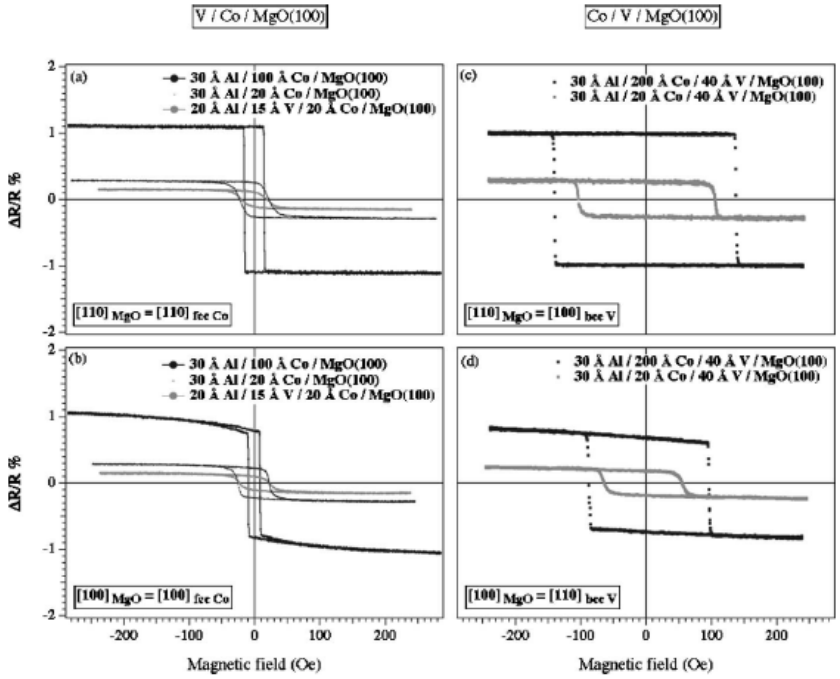

FIG. 4. Representative Kerr hysteresis loops measured in the transverse Kerr configuration for the Al/V/Co/MgO(100) and Al/Co/V/MgO(100) systems along both the $[110]_{MgO}$ and $[100]_{MgO}$ directions. Wavelength of light: 632.8 nm.

similar systems with the same hcp Co structure such as 200 Å Co hcp/Mo/MgO(100) (Ref. 16) and 200 Å Co/50 Å V/MgO(100) (Ref. 14) and much lower than that measured on a thick hcp Co film deposited on GaAs(001).[17] However, in disagreement with Lo *et al.*,[14] we did not observe a clear uniaxial magnetic anisotropy. The absence of uniaxial anisotropy indicates the presence of equal volumes of hcp Co crystals with easy directions 90° apart, leading to a fourfold in-plane magnetic symmetry. Such differences are probably due to the sample preparation, since it is well known that molecular beam epitaxy, electron beam epitaxy, and magnetron sputtering can lead to substantial differences in the growth mode of the evaporated species. Finally, the Co/V system with a thinner Co layer (20 Å Co/40 Å V/MgO) displays a less squared hysteresis loop than those observed for the systems formed with 200 Å of Co, as well as lower coercivities. Interestingly, in contrast to the 15 Å V/20 Å Co/MgO(100) system [panels (a) and (b)], the anisotropy is still observable with a strong reduction of the coercivity in the $[100]_{MgO}$ direction (55 Oe) compared to the $[110]_{MgO}$ direction (105 Oe).

C. Transverse susceptibility

TS measurements provide a fairly accurate description of the magnetic anisotropies involved in a system and a picture of the magnetization reversal mechanism along the direction in which the steady field H is applied. All these features are of interest in the systems under study. Moreover, we will show that TS measurements are much more sensitive than the hysteresis loop in describing these phenomena. In order to understand the information obtained from TS measurements, let us recall some general features of TS. Let us keep in mind that while the hysteresis loop is a representation of M_t vs H_1, TS is a representation of dM_t/dH_1 vs H. Any small change in the component of the saturation magnetization along H induces a small change in M_t which can be detected as a peak in the dM_t/dH_1. In order to understand the information obtained from TS measurements, let us consider the case of a single domain particle with uniaxial anisotropy in which only coherent magnetization rotation is to be considered. If K_u is the anisotropy constant and M_s the saturation magnetization, the anisotropy field is defined as $H_k=2K_u/M_s$. Applying the Stoner-Wohlfarth model,[18] we have calculated hysteresis loops and the corresponding TS for H_1 and H along the hard and easy axes. The results are shown in Fig. 5 (see also Ref. 19). The normalized applied field in Fig. 5 is, following the notation in Fig. 1, $h=H_1/H_k$ for the hysteresis loops [Figs. 5(a) and 5(c)] and $h=H/H_k$ for the TS [Figs. 5(b) and 5(d)]. The calculated TS exhibits singularities at $h=\pm 1$. In real single domain films such singularities become maxima in the detected signal and the position of the maximum for H along the easy axis occurs not for $h=-1$ as in Fig. 5(b) but for the field at which the magnetization reverses, i.e., at the coercive field H_c.[19] Both for H along the easy axis and for H along the hard axis, the inverse of the TS depends linearly on H for high fields for which the sample is saturated.[20,21] The case of a single domain particle with biaxial anisotropy has also been studied theoretically[22] and experimentally.[23] The behavior is similar to the previous one when H is applied either along the easy axis or along the hard axis: a maximum is detected in the former case for $H=-H_c$ and two maxima are detected in the latter case for $h=\pm 1$. The TS in this case also depends linearly on H for high H values.[21] The behavior of the TS is different in the case of particulate media. For thin films, both continuous granular and discontinuous films can be considered as particulate media, the particles being the crystallites in the former case and the islands in the latter case. In those cases, when H is applied along a hard axis two peaks in the

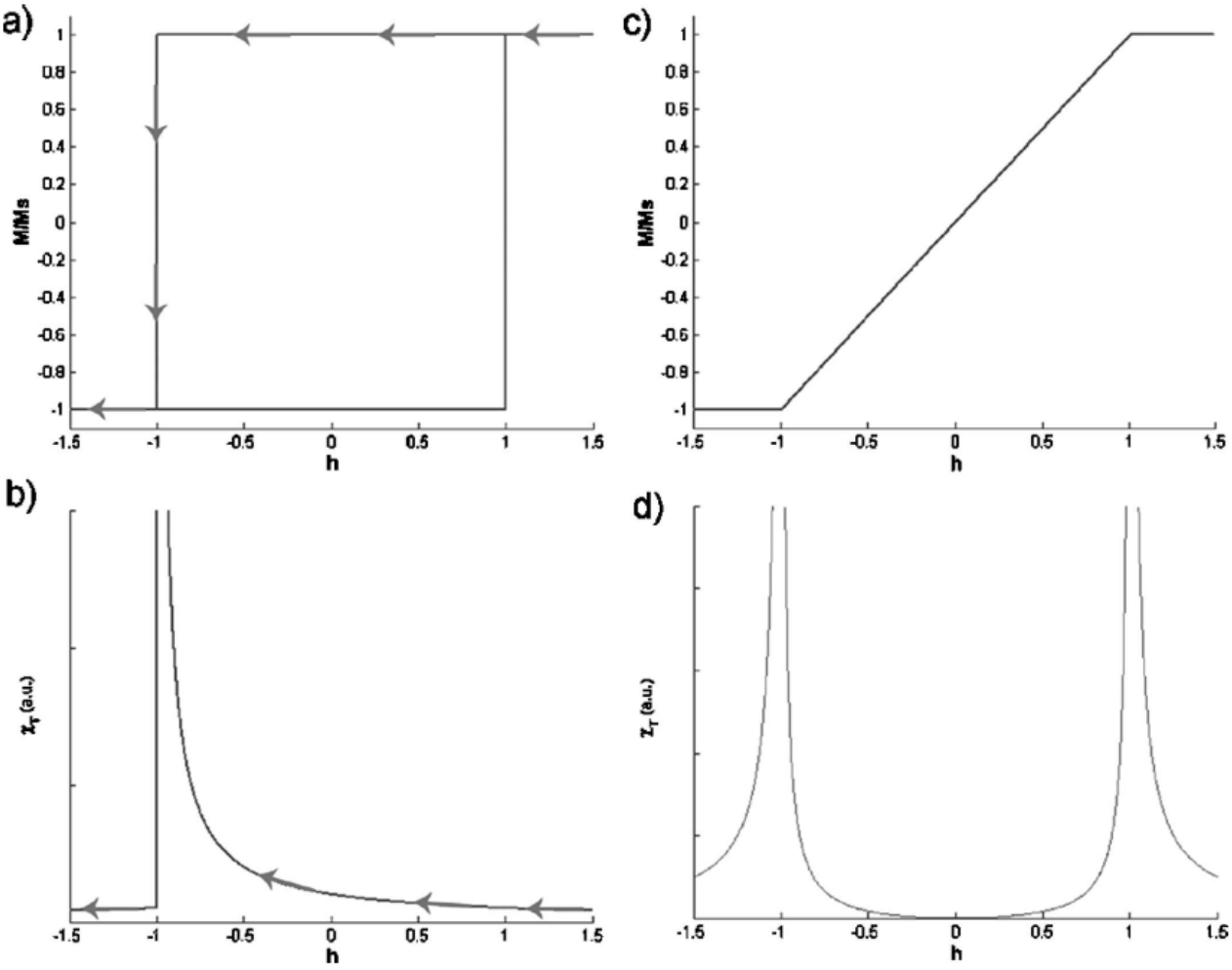

FIG. 5. Calculated hysteresis loops along the easy axis (a) and along the hard axis (c), and calculated transverse susceptibility curves with the bias field H along the easy axis (b) and along the hard axis (d) for a single domain particle with uniaxial anisotropy field H_k. Only coherent rotation processes have been taken into account in the calculations. In (a) and (b) the arrows indicate the sense of the applied field. The abscissa is the normalized field $h=H_1/H_k$ for the hysteresis loop and $h=H/H_k$ for the transverse susceptibility.

TS are observed for $H=\pm H_{sat}$, where H_{sat} is the saturation field which, in the case of a single domain particle, equals the anisotropy field. H_{sat} provides an estimation of the effective macroscopic anisotropy field, which is an average over the whole sample of the anisotropy fields of all the particles, and the TS does not depend linearly on H above saturation, but follows a more complicated behavior.[24–27] The value of H_{sat} and the shape of the peaks depend strongly on the anisotropy dispersion,[25,26] on the interparticle interaction,[27,28] and on texture.[25,26] It is remarkable that in the case of identical noninteracting particles H_{sat} coincides with the value of H_k of each particle.

We have performed TS measurements from saturation with H pointing in one sense ($H>0$) to saturation with H pointing in the opposite sense ($H<0$) through $H=0$. Let us first consider the TS measurement results obtained for the fcc Co samples, i.e., Al/100 Å Co/MgO, Al/20 Å Co/MgO, and Al/15 Å V/20 Å Co/MgO. TS measurements for all these systems show a fourfold symmetry, as expected for fcc Co, with two in-plane easy magnetization axes and two in-plane hard magnetization axes alternatively at 45°. This magnetic anisotropy could not be observed in the hysteresis loops for the samples with 20 Å of Co, as mentioned in the previous section. This clearly shows that TS measurements are much more sensitive than the hysteresis loops for detecting the magnetic anisotropy. Two different behaviors have been observed depending on the Co layer thickness. The two films with 20 Å Co exhibit a very similar behavior. In Fig. 6(a) we show the TS measurements for samples Al/20 Å Co/MgO and Al/15 Å V/20 Å Co/MgO with H along the $[110]_{MgO}$ direction—Co easy axis—and with H along the $[1\bar{1}0]_{MgO}$—another Co easy magnetization axis. Figure 6(b) displays TS measurements with H along the $[100]_{MgO}$ direction—Co hard axis. The TS curves with H along the other Co hard magnetization axis were identical to those of Fig. 6(b). The maxima about $-H_c$ are broadened, which shows that the magnetization reversal takes place over a wide range of field values. From Fig. 6(a) we can estimate the range of field values over which the magnetization re-

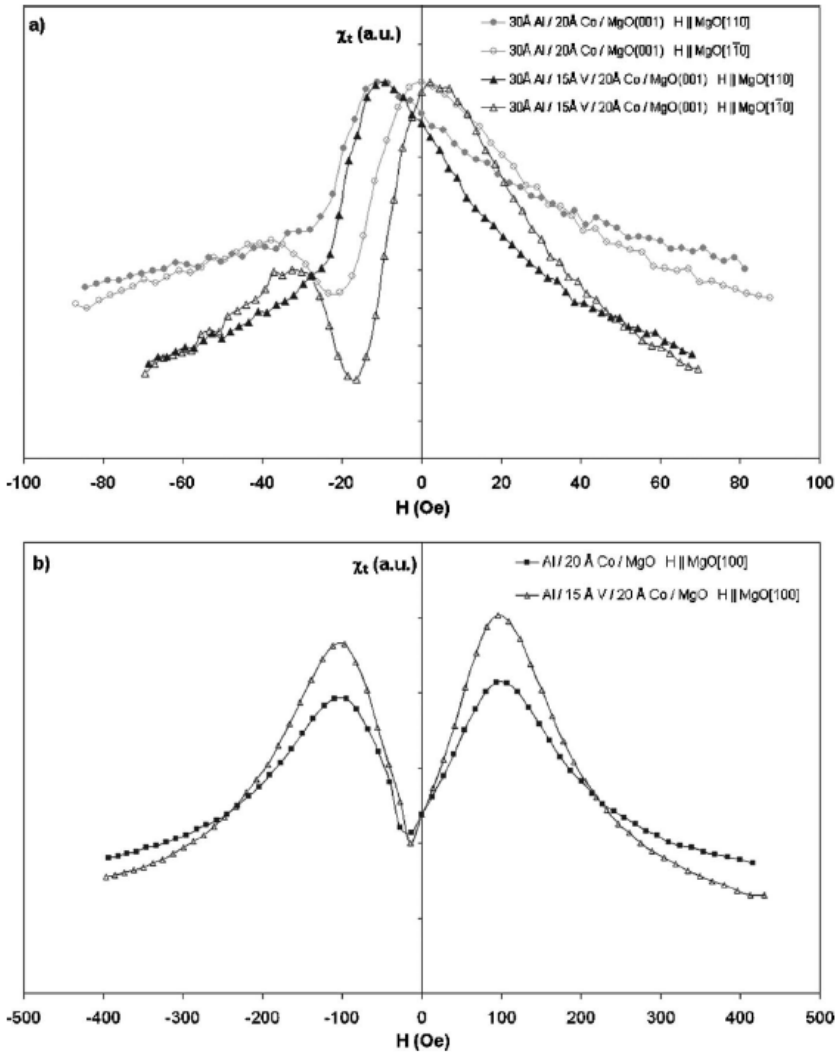

FIG. 6. Transverse susceptibility as a function of H for the samples Al/20 Å Co/MgO and Al/V/20 Å Co/MgO with H along the $[110]_{MgO}$ and $[1\bar{1}0]_{MgO}$ directions (a) and with H along the $[100]_{MgO}$ direction (b).

verses, which agree with those obtained from the Kerr hysteresis loops of Fig. 4: in the range of 10–25 Oe for H along the $[110]_{MgO}$ direction and in the range of 0–40 Oe for H along the $[1\bar{1}0]_{MgO}$ direction for both samples [see Fig. 6(a)]. In Fig. 6(a) we can also see that the TS signal associated with the magnetization reversal along the magnetization easy axis takes place for smaller magnetic fields for the film with the V capping layer. It is remarkable that, according to TS measurements, the two easy axes are not equivalent, since in the case of H along the $[1\bar{1}0]_{MgO}$ a minimum in the TS signal is observed, whereas it is absent for H applied along the $[110]_{MgO}$ direction. This minimum is due to an alignment of the magnetization along the $[110]_{MgO}$ direction during the magnetization reversal process along the $[1\bar{1}0]_{MgO}$. A similar behavior has also been observed in Fe grown on MgO (Ref. [29] and later explained as due to a superimposed uniaxial anisotropy.[30] Regarding the TS measurements with H along the $[100]_{MgO}$ direction, shown in Fig. 6(b), both films exhibit a very similar behavior. In this case, the inverse of the TS (not shown) does not depend linearly on H. On the other hand, the value of $H_{sat}=100$ Oe, determined by Co anisotropy, is the same for both films. Moreover, the peaks about $H=\pm H_{sat}$ are not sharp, but rounded. All these results suggest again a discontinuous growth of Co for this thickness, as already pointed out in the previous section.

In Fig. 7 we show the inverse of the TS for the Al/100 Å Co/MgO sample. In this case, the inverse of the TS depends linearly on H for high H values, for which the sample is saturated. This feature shows that this film is continuous. Moreover, the magnetization reversal for H along the Co magnetization easy axes (the $[110]_{MgO}$ direction) takes place very abruptly. In this case, we also performed TS measurements for H around H_c, as in Figs. 6(a) (not shown). From these measurements we could estimate that the magnetization completely reversed over a rage smaller than 3 Oe. As can be seen, the two easy axes are not equivalent either, and the inverse of the TS signal when H is applied along the $[1\bar{1}0]_{MgO}$ shows a sharp peak (which corresponds to a sharp minimum in the direct TS), as in the previous cases. For H parallel to $[100]_{MgO}$, we obtained $H_{sat}=230$ Oe which is higher than for the previous two thinner films, due to an increase of the magnetic anisotropy. In the case of this

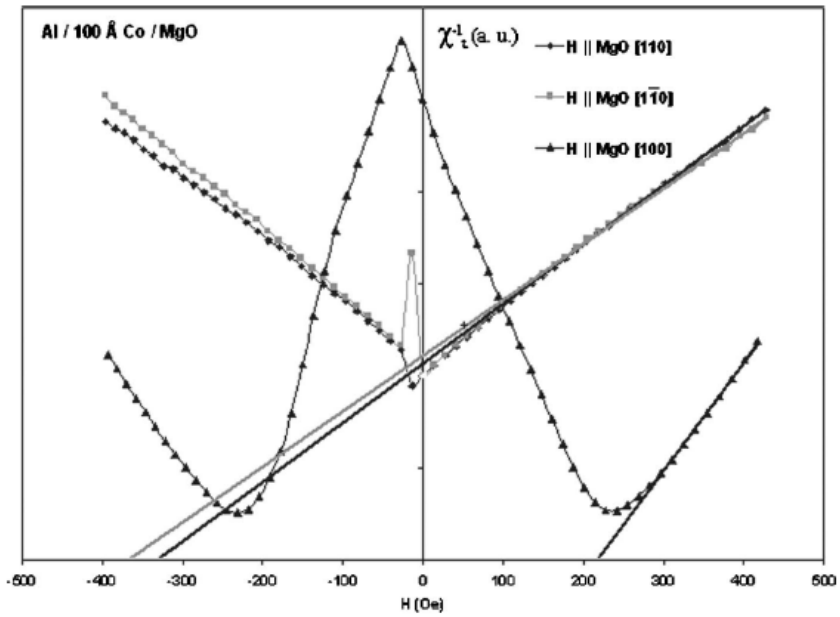

FIG. 7. Inverse of the transverse susceptibility as a function of H for the sample Al/100 Å Co/MgO with H along the $[110]_{MgO}$, $[1\bar{1}0]_{MgO}$, and $[100]_{MgO}$ directions.

sample a quantitative analysis of the anisotropies involved in the system has been carried out and is given in Sec. IV.

Let us now consider the TS measurements for the hcp Co, i.e., Al/Co/V/MgO samples. For these systems, two behaviors have been observed depending on the Co layer thickness. While all the samples exhibited an in-plane magnetic anisotropy with a fourfold symmetry, no difference was observed between the two easy magnetization axes in the TS measurements. In Fig. 8 we show the TS for the sample Al/20 Å Co/V/MgO(100). The saturation field for H applied along the hard magnetization axis can be estimated to be 250–260 Oe. The magnetization reversal for H along an easy axis takes place over a wide range of H values, between 11 and 35 Oe. In Figs. 9(a) and 9(b) the TS measurements for the sample with a thicker Co layer, Al/200 Å Co/V/MgO(100), are shown. The behavior for the sample Al/100 Å Co/MgO was similar to this one. Neither of the samples could be saturated in our experimental setup (the maximum attainable magnetic field is H_{max}=430 Oe) for H applied along the $[100]_{MgO}$ direction, which is a hard magnetization axis [see the inset in Fig. 9(a)]. The TS curves in Fig. 9(a) correspond to the H values between the two saturation peaks [see, for comparison, Fig. 6(b)]. The most striking feature in this case is the asymmetry of TS measurements for H along the hard magnetization axis. This asymmetry, which was not observed in the Kerr hysteresis loops is clearly observed in TS measurements for this sample. On the other hand, when H is applied along the $[110]_{MgO}$, which is an easy axis, a symmetric TS curve was obtained, as shown in Fig. 9(b). This result is in agreement with the symmetric Kerr hysteresis loop. The origin of this asymmetry in the first case is discussed in the next section.

IV. DISCUSSION

We can see from the above experimental results that both the structural and the magnetic properties of the systems un-

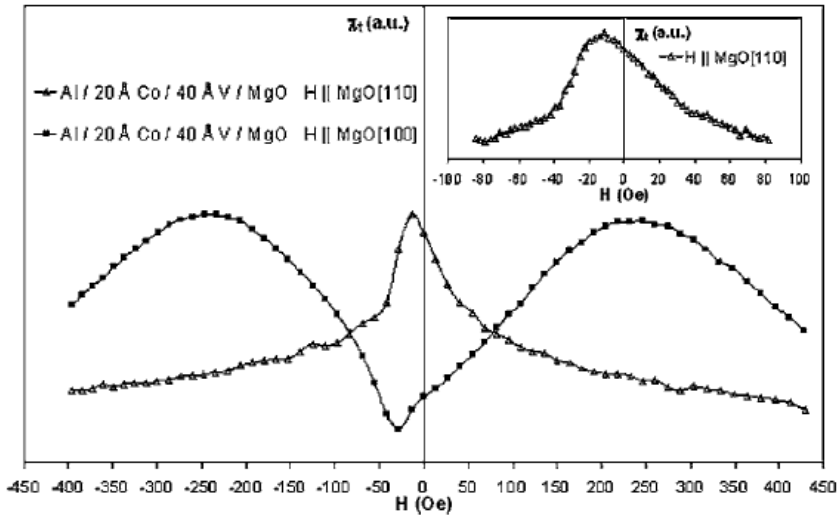

FIG. 8. Transverse susceptibility as a function of H for the sample Al/20 Å Co/40 Å V/MgO with H along the $[110]_{MgO}$ and $[110]_{MgO}$ directions. The inset shows a detailed view of the measurement along the $[110]_{MgO}$ direction around H=0.

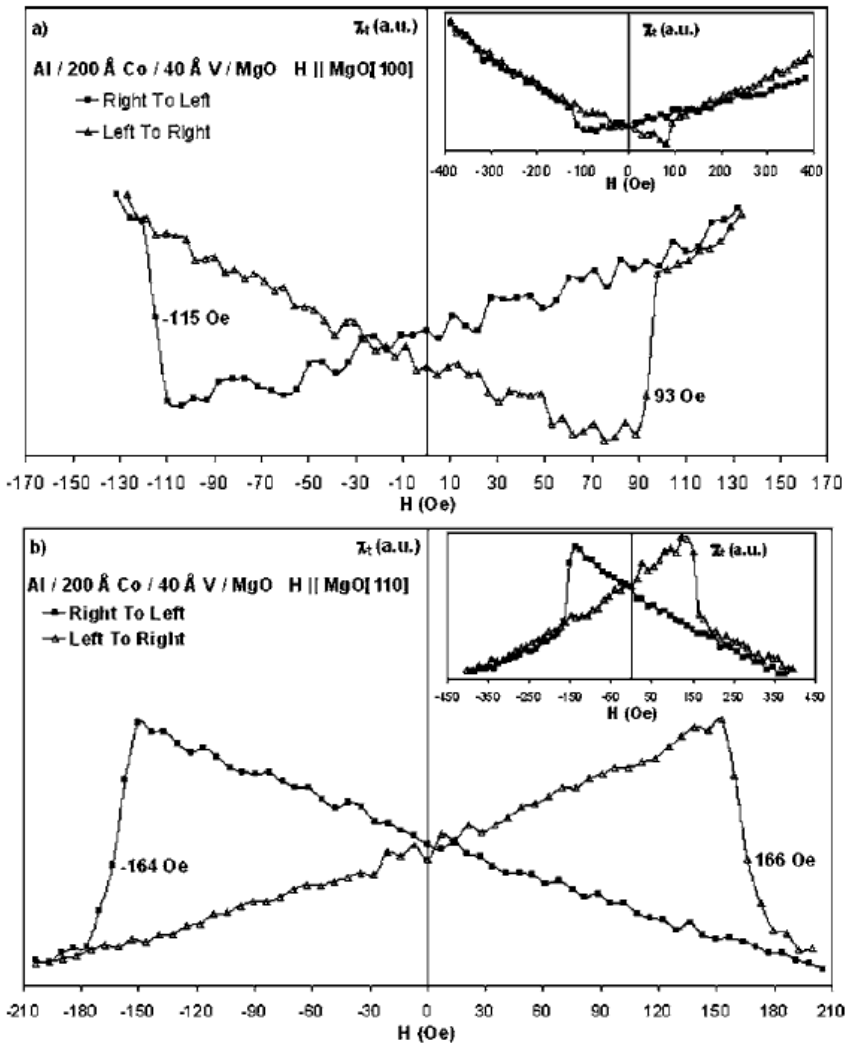

FIG. 9. Transverse susceptibility as a function of H for the sample Al/200 Å Co/40 Å V/MgO with H along the $[100]_{MgO}$ direction (a) and the $[110]_{MgO}$ direction (b).

der study basically depend on the order of deposition of Co and V on MgO(100), leading to fcc Co in V/Co/MgO(100) or to hcp Co in Co/V/MgO(100) stuctures.

Let us first consider the V/Co/MgO system. The magnetic properties in this case are determined by the Co layer and the Co/MgO(100) interface, since the subsequent deposition of the V layer leads only to very small changes. Some features are common to all the samples under study: (1) the fcc Co (001) growth exhibits the expected fourfold magnetic anisotropy (only observed with TS for the thinner samples) and (2) the Co/MgO interface seems to induce a uniaxial in-plane magnetic anisotropy. However, some differences are observed depending on the Co layer thickness and on the deposition of a V layer on Co.

Regarding the Co layer thickness, we conclude that the V/Co/MgO system develops the expected fourfold magnetic anisotropy when increasing the Co layer thickness. TS measurements for the samples with 20 Å Co are typical of a discontinuous film, and the fourfold anisotropy is not very well defined. The peaks for H applied along the $[100]_{MgO}$ direction are rounded [see Fig. 6(b)], which indicates that the magnetic saturation along that direction takes place over a wide range of H values due to the dispersion of anisotropy field values, associated with the discontinuous nature of the sample.[24,25]. Effectively, in this case, the local anisotropy field of each island is not only determined by the magnetocrystalline anisotropy but also by its shape, and a contribution from stress is expected as well. So each fcc Co island reverses the magnetization at a different H value. If we take[31] the saturation magnetization of Co as $M_s(\text{fcc}) = M_s(\text{hcp}) = 1430$ emu/cm^3, and suppose that the saturation field H_{sat} equals the anisotropy field H_1 of each Co island ($H_1 = H_{sat} = 100$ Oe), we obtain an anisotropy constant for each Co particle of $K_1 \sim 7 \times 10^4$ ergs/cm^3. Reported values[32,33] of the magnetocrystalline anisotropy of fcc Co, K_{1fcc}, range from -3.0×10^5 to -7.0×10^5 erg/cm^3 for thicknesses from 100 to 1000 Å. The absolute value estimated is much lower than the magnetocrystalline anisotropy constant for fcc Co. This can be explained if we consider that the magnetic anisotropy of the islands is highly influenced by shape and stress at this early stage of growth, and is also due to the anisotropy field dispersion and to the interisland interaction.[26–28] On the other hand, the sample with 100 Å Co shows a clearly developed fourfold magnetic anisotropy with the easy axis along the $\langle 110 \rangle_{Co}$ directions, as expected.

Therefore these results suggest that the Co layer is discontinuous at low coverages and becomes continuous at higher coverages, leading to the expected fourfold magnetic anisotropy at 100 Å. The saturation field increases with increasing Co layer thickness, which also indicates that the fourfold magnetic anisotropy value also increases as the Co layer thickness increases. In fact, the macroscopically observed anisotropy tends to that of bulk fcc Co as we will show in the case of the film with 100 Å of Co.

The superimposed uniaxial magnetic anisotropy is only manifested in the TS measurements, and as a consequence of it the two easy axes are not equivalent. It clearly affects the magnetization reversal along the $[1\bar{1}0]_{MgO}$ direction in the range of investigated Co thicknesses. This uniaxial magnetic anisotropy has also been found in fcc Co grown on MgO (Ref. 13) and on Fe grown on MgO (Ref. 23) and it is probably induced by steps in the MgO substrate surface.[34]

In the case of the film with 100 Å of Co we can calculate the fourfold anisotropy field H_{1fcc}, the ratio of the uniaxial anisotropy constant to the fourfold anisotropy constant $r = K_u/K_{1fcc}$, and the angle α between the $[100]_{Co}$ axis and the uniaxial easy axis following a formalism previously developed.[23] When applying this formalism, we have to take into account that for fcc Co, the easy axis is along the $\langle 110 \rangle$ directions, i.e., the fourfold anisotropy constant $K_{1fcc} < 0$, and that we call β the angle between the applied dc field during TS measurements and the $[100]_{Co}$ axis. In Fig. 7, $\beta = 0$ corresponds to the measurement with $H \| [100]_{MgO}$, $\beta = \pi/4$ corresponds to the measurement with H $H \| [110]_{MgO}$ and $\beta = 3\pi/4$ corresponds to the measurement with $H \| [1\bar{1}0]_{MgO}$. The linear extrapolations in Fig. 7 cut the abscissa at magnetic field values of $H(0)$, $H(\pi/4)$, and $H(3\pi/4)$ given by

$$H(0) = -H_{1fcc} - H_{1fcc} r \cos 2\alpha, \tag{1a}$$

$$H(\pi/4) = H_{1fcc} - H_{1fcc} r \sin 2\alpha, \tag{1b}$$

$$H(3\pi/4) = H_{1fcc} + H_{1fcc} r \sin 2\alpha. \tag{1c}$$

From Eqs. (1a)–(1c) we obtained $H_{1fcc} = 348$ Oe (absolute value), $r = -0.37$, and $\alpha \approx 4° \pm 1°$. With the value of M_s given above we obtained a fourfold anisotropy constant $K_{1fcc} = -2.5 \times 10^5$ erg/cm^3, close to the reported values.[32,33] The easy axis of the superimposed uniaxial anisotropy lies 4° from the $[100]_{Co}$, i.e., 4° from the $[100]_{MgO}$, in agreement with the case of Fe/MgO in which the superimposed uniaxial easy axis was found to lie 5° from the $[100]_{MgO}$.[23] This result is likely to confirm the hypothesis that the superimposed uniaxial anisotropy has a contribution from the MgO substrate.

As for the role of the V layer, it is noteworthy that the magnetization reverses in a narrower field range and for smaller field values for the film with a V layer on top [see Fig. 6(a)). This effect could be attributed to magnetic polarization of V which improves the magnetic contact between the Co islands, favoring the magnetization reversal process. Induced V magnetic moments at a V/Co interface have already been experimentally confirmed[5] and theoretically predicted.[35] V–Co intermixing, reducing the overall magnetic anisotropy of the system, and therefore the coercive field, might be an alternative interpretation.

Let us now consider the Co/V/MgO system. In this case the system is grown following the in-plane epitaxial relations $Co_{hcp}[c] \| V(001)_{bcc}[100] \| MgO(001)[110]$ and $Co_{hcp}[c] \| V(001)_{bcc}[100] \| MgO(001)[1\bar{1}0]$ All the samples showed a magnetic anisotropy with a fourfold symmetry, indicating that the hcp consists of equal volumes of material with easy axes at 90°. We can consider the films as made up of crystalline domains with the c axis along one direction and of crystalline domains with the easy axis at 90° randomly distributed over the whole surface of the sample. The two easy axes lie along the Co hcp c axes, i.e., along the $[110]_{MgO}$ and $[1\bar{1}0]_{MgO}$ directions. The hard axes lie 45° from the c axis orientations, i.e., along the $[100]_{MgO}$ and $[010]_{MgO}$ directions. The behavior of the system depends again on the Co layer thickness.

The sample with the 20 Å Co layer can be saturated along both the hard and the easy axes, as can be seen in Fig. 8. However, in both cases the TS results show a behavior typical of a nanostructured system with a great dispersion of magnetic anisotropy values.[23–25] As in the case of fcc Co, the peaks for H applied along the $[100]_{MgO}$ direction are rounded (see Fig. 8), which indicates that the magnetic saturation along that direction takes place over a wide range of H values. This result suggests that the Co layer is not continuous. Since the sample can be saturated in the range of 250–260 Oe, we can conclude that the magnetization reversal along the hard axes is not governed by the magnetocrystalline anisotropy of hcp Co. In such a case, the peaks of the TS would be detected at a magnetic field value equal to the anisotropy field of hcp Co. If we take[36] $K_{1,hcp} = 4.1 \times 10^6$ ergs/cm^3 and M_s (hcp) = 1430 emu/cm^3 we obtain an anisotropy field $H_{1,hcp} \sim 6000$ Oe and the sample could not have been saturated in our experimental setup. On the other hand, the samples with the 100 and 200 Å Co layers could only be saturated along the easy axes, but not along the hard axes. So the magnetization process along the hard axes may be controlled by the Co hcp magnetocrystalline anisotropy for the thicker samples. These results suggest that, as in the case of fcc Co, the magnetic anisotropy at the very early stages of growth is greatly influenced by some factors such as stress and shape.

According to Fig. 9(b), the magnetization reversal along the magnetization easy axes takes place in one step, and the samples are saturated along these directions and the hysteresis loops and the TS measurements are symmetric. However, the reversal along the hard axes needs a more careful inspection. The asymmetry in the TS measurements along the hard axes for the samples with 100 and 200 Å Co is associated with the fact that these samples are not saturated, as deduced from TS measurements. The magnetization reversal in this case takes place in two steps, but only one of them is observed in the range of field values attained in our experimental setup. A detailed study of this phenomenon is out of the scope of this paper and is still under investigation.

V. CONCLUSIONS

We have investigated the crystallographic structure, the magnetic anisotropy, and the magnetization reversal of the V/Co/MgO and Co/V/MgO structures. Cobalt grows in the fcc structure on MgO(100). Vanadium grows in the bcc structure on MgO and Co in the hcp structure on V with two hcp crystalline domains with the *c* axis on the plane but rotated 90° to each other. Although the expected fourfold symmetry of the anisotropy for fcc Co is already observed for a thickness of Co of 20 Å, its value is too low to be exclusively attributed to Co magnetocrystalline anisotropy. For a thickness of 200 Å of Co the anisotropy observed is close to the bulk value. In the case of hcp Co fourfold anisotropy is also already observed for a thickness of Co of 20 Å. However, the observed value is again too low compared to that of the magnetocrystalline anisotropy of hcp Co. In both cases and in the early stages of growth, the Co layer is not continuous and the magnetic anisotropy macroscopically observed is influenced by stress and shape anisotropies. Deposition of a vanadium layer onto the fcc Co layer induces a slight decrease of the coercive field and favors the magnetization reversal.

ACKNOWLEDGMENTS

The Spanish Commission of Science and Technology (CICyT) is acknowledged for financial support. One of the authors (Y.H.) acknowledges the Ramón y Cajal program and Consejo Superior de Investigaciones Científicas (CSIC) for financial support. Another author (B.P.) acknowledges Plan Investigación, Desarrollo Tecnológico e Innovación de Asturias 2001–2004 for financial support.

[1]S. S. P. Parkin, Phys. Rev. Lett. **67**, 3598 (1991).
[2]R. Krishman, T. Catinaud, M. Seddat, M. Porte, and M. Tessier, J. Magn. Magn. Mater. **159**, 175 (1996).
[3]J. Du, M. Lu, L. N. Tong, W. Ji, H. R. Zhai, and H. Xia, J. Magn. Magn. Mater. **177–181**, 1209 (1996).
[4]Y. Huttel, G. van der Laan, T. K. Johal, N. D. Telling, and P. Bencok, Phys. Rev. B **68**, 174405 (2003).
[5]B. Heinrich and J. F. Cochran, Adv. Phys. **42**, 523 (1993); H. Fritzsche, J. Kohlepp, H. J. Elmers, and U. Gradmann, Phys. Rev. B **49**, 15665 (1994); *Ultrathin Magnetic Structure I*, edited by J. A. C. Bland and B. Heinrich (Springer, Berlin, 1994).
[6]Y. Huttel, E. Navarro, and A. Cebollada, J. Cryst. Growth **273**, 474 (2004).
[7]C. K. Lo, I. Klik, Y. Liou, C. P. Chang, C. S. Yang, and Y. D. Yao, J. Magn. Magn. Mater. **177–181**, 1257 (1998).
[8]Y. Ikuhara, Y. Sugawara, I. Tanaka, and P. Pirouz, Interface Sci. **5**, 5 (1997).
[9]Y. Ikuhara and P. Pirouz, Microsc. Res. Tech. **40**, 206 (1998).
[10]M. Gutsche, H. Kraus, J. Jochum, B. Kemmather, and G. Gutekunst, Thin Solid Films **248**, 18 (1994); M. Gutsche, H. Kraus, J. Jochum, and B. Kemmather, Superconductivity and Superconducting Materials Technologies: Proceedings of Topical Symposium IV on Superconductivity, 1995 (unpublished), pp. 187–194.
[11]M. Hashimoto, H. Qiu, T. Ohbuchi, M. Adamik, H. Nakai, A. Barna, and P. B. Barna, J. Cryst. Growth **166**, 792 (1998).
[12]Y. D. Yao, Y. Liou, J. C. A. Huang, S. Y. Liao, I. Klik, C. P. Chang, and C. K. Lo, IEEE Trans. Magn. **32**, 4669 (1996).
[13]C. K. Lo, Y. Liou, C. P. Chang, I. Klik, Y. D. Yao, and J. C. A. Huang, Appl. Phys. Lett. **68**, 2155 (1996).
[14]C. K. Lo, I. Klik, C. P. Chang, Y. Liou, C. S. Yang, Y. D. Yao, and J. A. C. Huang, Appl. Surf. Sci. **113**, 160 (1997).
[15]Q. Jiang, H.-N. Yang, and G.-C. Wang, Surf. Sci. **373**, 181 (1997).
[16]I. Klik, U. M. Chen, Y. D. Yao, C. K. Lo, C. P. Chang, S. Y. Liao, and Y. Liou, Appl. Surf. Sci. **113**, 165 (1997).
[17]Y. Z. Wu, H. F. Ding, C. Jing, D. Wu, G. S. Dong, X. F. Jin, K. Sun, and S. Zhu, J. Magn. Magn. Mater. **198**, 297 (1999).
[18]E. C. Stoner and E. P. Wohlfarth, Philos. Trans. R. Soc. London, Ser. A **240**, 599 (1948).
[19]K. L. Chopra, *Thin Film Phenomena* (McGraw-Hill, New York, 1969), pp. 654–659.
[20]H. Hoffmann, Phys. Status Solidi **33**, 175 (1969).
[21]M. C. Contreras, J. F. Calleja, M. Rivas, M. O. Gutiérrez, and J. A. Corrales, J. Magn. Magn. Mater. **175**, 64 (1997).
[22]A. Stancu and L. Spinu, J. Magn. Magn. Mater. **266**, 200 (2003).
[23]J. F. Calleja, J. L. Menéndez, A. Cebollada, and C. Contreras, Jpn. J. Appl. Phys., Part 1 **40**, 6829 (2001).
[24]L. Paretti and G. Turilli, J. Appl. Phys. **61**, 5098 (1987).
[25]P. Poddar, J. L. Wilson, H. Srikanth, D. F. Farrell, and S. A. Majetich, Phys. Rev. B **68**, 214409 (2003).
[26]A. Hoare, R. W. Chantrell, W. Schmitt, and A. Eiling, J. Phys. D **26**, 461 (1993).
[27]R. Matarranz, M. C. Contreras, G. Pan, B. Presa, J. A. Corrales, and J. F. Calleja, J. Appl. Phys. **99**, 08Q504 (2006).
[28]Ch.-R. Chang and J.-S. Yang, Appl. Phys. Lett. **65**, 496 (1994).
[29]C. Contreras, J. L. Menéndez, A. Cebollada, and J. F. Calleja, Jpn. J. Appl. Phys., Part 1 **38**, 106 (1999).
[30]C. Martínez Boubeta, A. Cebollada, J. F. Calleja, C. Contreras, F. Peiró, and A. Cornet, J. Appl. Phys. **93**, 2126 (2003).
[31]H. P. Oepen, M. Benning, H. Ibach, C. M. Schneider, and J. Kirschner, J. Magn. Magn. Mater. **86**, L137 (1990).
[32]T. Suzuki, D. Weller, C. A. Chang, R. Savoy, T. Huang, B. A. Gurney, and V. Speriosu, Appl. Phys. Lett. **64**, 2736 (1994).
[33]J. A. Wolf, J. J. Krebs, and G. A. Prinz, Appl. Phys. Lett. **65**, 1057 (1994).
[34]C. Martínez Boubeta, C. Clavero, J. M. García-Martín, G. Armellas, A. Cebollada, Ll. Balcells, J. L. Menéndez, F. Peiró, A. Cornet, and M. F. Toney, Phys. Rev. B **71**, 014407 (2005).
[35]T. A. Carillo-Cázares, S. Meza-Aguilar, and C. Demangeat, J. Magn. Magn. Mater. **290/291**, 110 (2005); T. A. Carrillo-Cázares, S. Meza-Aguilar, and C. Demangeat, Eur. Phys. J. B **48**, 249 (2005); J. Hong, J. Magn. Magn. Mater. **303**, 191 (2006).
[36]R. C. O'Handley, *Modern Magnetic Materials: Principles and Applications* (Wiley, New York, 2000).

4.3 Artículo IV

IOP PUBLISHING JOURNAL OF PHYSICS D: APPLIED PHYSICS
J. Phys. D: Appl. Phys. **40** (2007) 6857–6864 doi:10.1088/0022-3727/40/22/001

Fourfold magnetic anisotropy, coercivity and magnetization reversal of Co/V bilayers grown on MgO(0 0 1)

J F Calleja[1], M García del Muro[2], B Presa[1], R Matarranz[1], J A Corrales[3], A Labarta[2] and M C Contreras[1]

[1] Departamento de Física, Facultad de Ciencias, Universidad de Oviedo, Calvo Sotelo s/n, 33007 Oviedo, Spain
[2] Departament de Física Fonamental and Institut de Nanociència i Nanotecnologia IN2UB de la Universitat de Barcelona, Martí i Franquès, 1, E-08028 Barcelona, Spain
[3] Departmento de Informática, Universidad de Oviedo, Edificio Departamental 1, Campus de Viesques s/n, 33204 Gijón, Spain

Received 27 May 2007, in final form 7 September 2007
Published 2 November 2007
Online at stacks.iop.org/JPhysD/40/6857

Abstract
Magnetic anisotropy and magnetization reversal of Al/Co/V /MgO(0 0 1) thin films have been investigated. The films were fabricated by magnetron sputtering. The roles of both Co and V layers thicknesses have been studied. Magnetic characterization has been carried out by transverse susceptibility (TS) measurements and hysteresis loops. Cobalt is grown in the hcp structure on V with the *c* axis parallel to the film plane. Two types of hcp Co crystal are grown with the *c* axes perpendicular to each other. This structure gives rise to a fourfold magnetic anisotropy. When the V layer thickness is below 40 Å a superimposed uniaxial anisotropy develops, the effect of which is a depression in the TS, in agreement with theoretical calculations. This uniaxial anisotropy is induced by the substrate and due to a discontinuous growth of the V layer. For hcp Co grown on V, the magnetic anisotropy rapidly increases with Co layer thickness. In this case, unexpected shifted hysteresis loops along the hard axes were observed when the films were not saturated. This has been explained by taking into account the magnetization reversal along the hard axis: it proceeds via magnetization rotation of some portions of the film at high fields, and by domain wall motion of the rest of the film at lower field values.

(Some figures in this article are in colour only in the electronic version)

1. Introduction

In the last decade close attention has been paid to the study of Co/V multilayers [1–4] due to the oscillatory exchange through V layers. These studies clearly indicated that a better understanding of the interface magnetism at the Co/V interface is mandatory to understand the physics of this system. It is our aim to gain insight on this issue in the case of hcp Co grown on V, focusing our efforts on magnetic anisotropy and magnetization reversal.

The symmetry of the anisotropy of nanostructured hcp Co has been a source of controversy in the last few years. When Co is grown in the hcp structure with the *c* axis parallel to the film plane, both uniaxial [5–7] and biaxial [8–10] anisotropies have been observed, depending on the substrate and the buffer layer used. When biaxial anisotropy is observed, two types of hcp Co crystals are grown with the *c* axes perpendicular to each other. In this case, according to theoretical calculations, a fourfold anisotropy develops with the hard axes parallel to the hcp *c* crystalline axes [11]. However, experimentally, the directions of the easy and hard axes seem to depend on the substrate used. For instance, hcp Co grown on GaAs(0 0 1) displays a biaxial anisotropy with the hard axes parallel to the c axis of the two types of hcp Co crystals. This anisotropy becomes

uniaxial along one of the c axis directions as the films get thicker [8]. However, hcp Co grown on Mo(1 0 0) [9] exhibits a biaxial anisotropy with the easy axes along the c axis of the two types of hcp Co crystals. Moreover, the magnetization reversal has also been investigated experimentally [7, 8] and theoretically [11, 12].

In this work we intend to carry out a systematic study of the magnetic anisotropy and the magnetization reversal of the Co/V/ MgO(0 0 1) system. The roles of both the Co and the V layer thicknesses are discussed and correlated with the structure of the bilayer. The choice of Co/V/MgO is also motivated by the high chemical stability of the system. Effectively, the Co/V interface exhibits interfacial mixing that penetrates 2 Å into the Co layer [13]. The lower the deposition rate used, the sharper the interface obtained [14]. Moreover, a flat and sharp V/MgO interface at room temperature (RT) has been obtained previously [15].

2. Experimental procedure

The samples were grown in a combined ultra high vacuum system (base pressure in the low 10^{-9} mbar) with triode sputtering and laser ablation facilities. In the first step, an 80 Å MgO buffer layer was grown by laser ablation at 450 °C on the substrate to planarize the surface. The laser wavelength was $\lambda = 193$ nm, the pulse duration 17 ns, the laser was pulsed at a rate of 10 Hz and with an energy of 300 mJ/pulse. In the second step, the Co and V films were deposited by triode sputtering on MgO(0 0 1) single crystals and at normal incidence. The argon pressure during the sputtering was kept at 4×10^{-4} mbar and the deposition rates were 4 Å min^{-1} for V and 15 Å min^{-1} for Co. Subsequent to the RT deposition of V and Co, a 30 Å thick Al capping layer was deposited at RT in order to protect the films from oxidation. In order to study the influence of Co and V layer thickness separately we deposited the stacking structures: Al/20 Å Co/t_V V/MgO(0 0 1) ($t_V = 10$, 20 and 40 Å) and Al/t_{Co} Co/40 Å V/MgO(0 0 1) ($t_{Co} = 20$, 40, 100 and 200 Å).

Crystallographic structure, coercivity and magnetic anisotropy were measured after the samples were removed from the vacuum system. The crystallographic structure was investigated using x-ray diffraction (XRD) with a 4-circle diffractometer, Cu Kα radiation and 1/4° divergence slits. Both symmetric ($\theta/2\theta$ scans) and asymmetric phi scans (φ scans) were recorded.

In-plane hysteresis loops and transverse susceptibility (TS) measurements were performed at RT using a transverse magneto-optical Kerr effect. Two orthogonal magnetic fields H_1 and H can be applied in the plane of the sample. While H lies on the plane of incidence, H_1 is perpendicular to the plane of incidence. The Kerr signal is proportional to the magnetization component parallel to H_1 (M_t). In order to obtain a hysteresis loop only a low frequency magnetic field H_1 is applied. In the case of TS measurements two magnetic fields are applied: H_1, which in this case is a small amplitude alternating field (the frequency of H_1 used was 127 Hz), and an orthogonal bias field H, both in the film plane. The experimental set-up is described elsewhere [16]. Further in-plane hysteresis loops at high fields and at both 350 and 5 K were performed using a Superconducting Quantum Interference Device (SQUID) magnetometer.

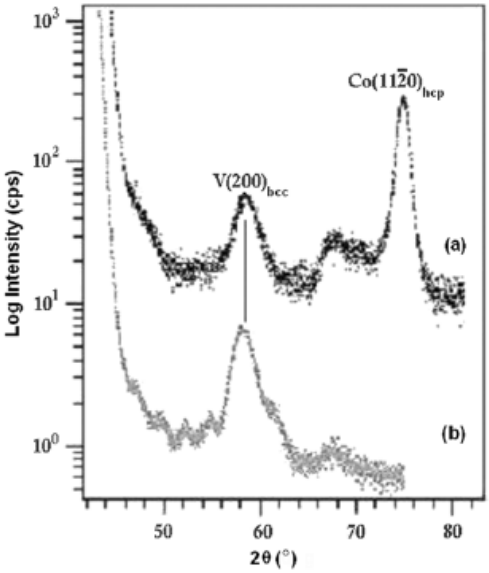

Figure 1. Symmetric XRD scans for the films (*a*) 30 Å Al/ 100 Å Co/40 Å V/MgO(1 0 0) and (*b*) MgO/40 Å V/ MgO(1 0 0).

3. Results

3.1. Structure

The crystallographic structure of the samples has been investigated by means of XRD. Both symmetric (2θ scans) and asymmetric phi scans (φ scans) have been recorded and the corresponding spectra are displayed in figures 1 and 2. In figure 1, the crystallographic structure of the Co layer deposited on the V layer is illustrated through the symmetric scan corresponding to the 30 Å Al/100 Å Co/40 Å V/MgO(1 0 0) system. The feature located at 74.8° corresponds to the hexagonal close packed (hcp) Co(1 1 -2 0) diffraction peak, indicating the growth of Co on V in hcp structure [17] with the c axis located in the plane of the surface. For reference, in figure 1 the symmetric scan for 40 Å of V grown on MgO(1 0 0) and capped with a MgO layer is shown. As reported previously [15], in the case of V grown on MgO, the feature located at around 58° corresponds to the V(2 0 0) diffraction of the body centred cubic V structure.

Further characterization of the crystallographic structure is given by the asymmetric φ scans displayed in figure 2. When performing a φ scan, the sample is tilted at an angle χ, which is the angle between the sample surface and the plane to be explored. The x-ray detector is kept fixed in the 2θ position corresponding to the Co, V or MgO peak being explored. The sample is rotated around an axis normal to its surface. For instance, in the case of the φ scan for Co in figure 2, $2\theta = 91.36°$ and $\chi = 32.28°$. As can be observed in the asymmetric φ scan corresponding to the MgO(1 1 1) diffraction peak, the MgO substrate displays the expected fourfold symmetry. As previously reported [15,18–21], V grown on MgO(1 0 0) also displays a fourfold symmetry with an additional rotation of 45°, leading to the V[1 0 0]||MgO[1 1 0] epitaxial relation, i.e. a 45° in-plane rotation of the V[1 0 0] directions with respect to the MgO ones. Regarding the V growth on MgO, the φ scans in figure 2 show that (i) V and MgO are c-axis oriented, (ii) V⟨0 0 1⟩ directions

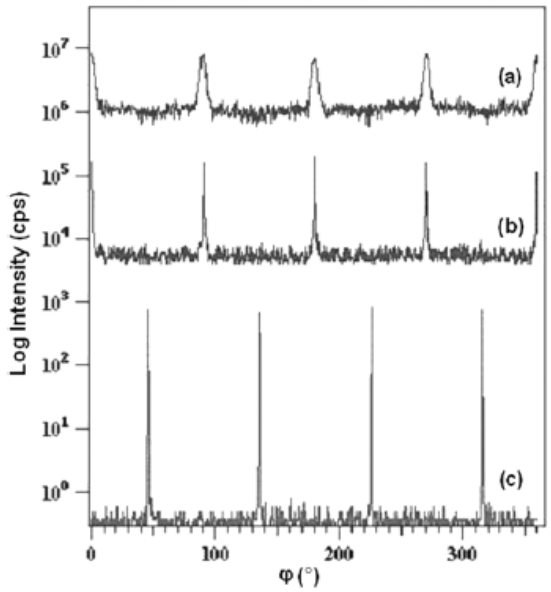

Figure 2. Representative asymmetric φ scans for Co(1 1 0 $\bar{2}$) (*a*), V(1 1 0) (*b*) and MgO(1 1 1) (*c*) reflections. The φ scans illustrate the epitaxial relationships that govern the growth of the structures. See text for details.

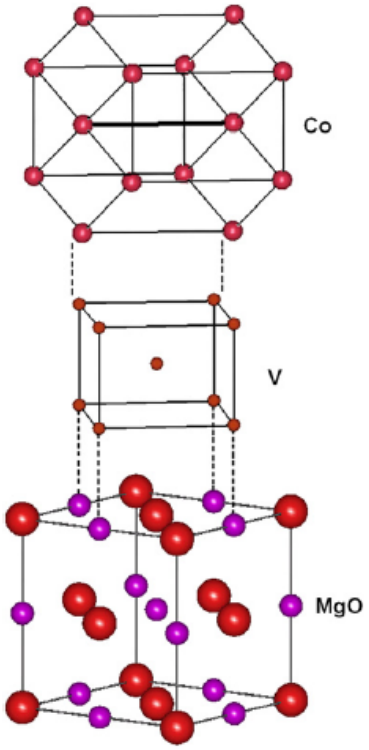

Figure 3. Schematic representation of the stacking structure of the Co/V/MgO system. In the case of MgO, small balls represent O atoms, large balls represent Mg atoms.

are 45° rotated from MgO⟨0 0 1⟩ directions and (iii) V{1 1 0} planes are 45° rotated from the MgO{1 1 1} planes. As for Co growth on V, the φ scans show that (i) Co *c* axis is parallel to V⟨0 0 1⟩ directions, (ii) as can be seen in figure 2 the Co(1 1 0 $\bar{2}$) reflection shows a fourfold symmetry, indicating that the hcp Co breaks into 2 hcp domains rotated by 90° to each other [17], and (iii) Co{1 1 0 $\bar{2}$} planes are parallel to V{1 1 0} planes. According to these results, the system is grown following the epitaxial relation Co[0 0 1]||V[1 0 0]||MgO[1 1 0]. Also, it can be noted that the Co(1 1 0 $\bar{2}$) reflections of the corresponding φ scan have similar intensities, indicating that the two hcp Co domains are equally distributed in the two perpendicular in-plane directions. Figure 3 shows a schematic representation of the stacking structure of the Co/V/MgO system.

3.2. Transverse Kerr hysteresis loops

The transverse Kerr hysteresis loops of the samples are depicted in figure 4. Two in-plane easy axes and two in-plane hard axes were observed (only one of each is shown). The easy axes are parallel to the [1 1 0] and [1 $\bar{1}$ 0] directions, i.e. along the *c* axis of the two types of Co crystals. The hard axes lie along the [1 0 0] and [0 1 0] directions. The coercive field H_c of each sample is given in table 1. The samples with 40, 100 and 200 Å of Co exhibit asymmetric hysteresis loops along the hard axes. The two values of H_c in table 1 are the values measured at each side of the hyseresis loop. The origin of this asymmetry will be discussed later on.

3.3. Transverse susceptibility

Let us now analyse TS measurements. In order to understand the information obtained from the TS measurements, let us consider the case of a single domain particle with biaxial anisotropy in which only coherent magnetization rotation is taken into account. Let us keep in mind that while the hysteresis loop is a representation of M_t versus H_l, TS is a representation of dM_t/dH_l versus H. Any small change in the component of the saturation magnetization along H induces a small change in M_t which can be detected as a peak in dM_t/dH_l. The case of a single domain particle with biaxial anisotropy has been studied theoretically [22] and experimentally [23]. If K_1 is the anisotropy constant and M_s the saturation magnetization, let the anisotropy field be defined as $H_k = 2K_1/M_s$. Applying the Stoner–Wohlfarth model [24], we have calculated the hysteresis loops and the corresponding TS for H_l and H along the hard and easy axes. The results are shown in figure 5. The normalized applied field in figure 5 is $h = H_l/H_k$ for the hysteresis loops (figures 5(*a*) and (*c*)) and $h = H/H_k$ for the TS (figures 5(*b*) and (*d*)). The calculated TS exhibits singularities at $h = \pm 1$. In real films such singularities become maxima in the detected signal and the position of the maximum for H along the easy axis occurs not for $h = -1$ as in figure 5(*b*) but for the field at which the magnetization reverses, i.e. at the coercive field H_c. Moreover, when H is applied along a hard axis two peaks in the TS are observed for $H = \pm H_{sat}$, where H_{sat} is the saturation field which, in the case of a single domain particle, equals the anisotropy field. H_{sat} provides an estimation of the effective macroscopic anisotropy field, which is an average over the whole sample of the anisotropy fields of all the particles in the case of a particulate media. According to this, we will refer to the magnetic field at which the peak in the TS curves with H along a hard axis is attained as the effective anisotropy field H_{Keff}.

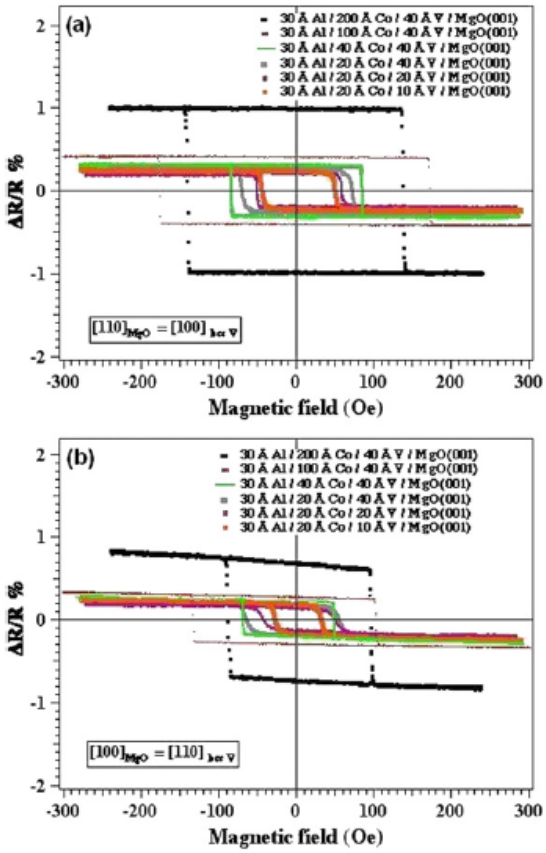

Figure 4. Transverse Kerr hysteresis loops of the Al/V/Co/MgO(0 0 1) systems along the $[1\,1\,0]_{MgO}$ (*a*) and $[1\,0\,0]_{MgO}$ (*b*) directions.

Table 1. Coercive field of Al/Co/V/MgO (0 0 1) thin films along the MgO [1 1 0] direction (easy axis) and along the MgO [1 0 0] direction (hard axis). Two values are given when asymmetric hysteresis loops were obtained.

	H_c (Oe) (H|| $[1\,1\,0]_{MgO}$)	H_c (Oe) (H || $[1\,0\,0]_{MgO}$)
20 Å Co /10 Å V/MgO	47	30
20 Å Co/20 Å V/MgO	53	45
20 Å Co/40 Å V/MgO	70	60
40 Å Co/40 Å V/MgO	84	70/50
100 Å Co/40 Å V/MgO	173	133/103
200 Å Co/40 Å V/MgO	140	90/100

According to the results shown in figures 6, 7 and 8 all the films exhibit a fourfold magnetic anisotropy with the easy axis along the [1 1 0] and [1 $\bar{1}$ 0] directions. The hard axes lie along the [1 0 0] and [0 1 0] directions. These results agree with those obtained from the hysteresis loops.

4. Discussion

For the sake of clarity, we shall introduce and discuss the results obtained in two groups: in the first place we focus on the samples with fixed Co thickness of 20 Å and varying V thickness to proceed afterwards with the samples with fixed V thickness of 40 Å and varying Co thickness.

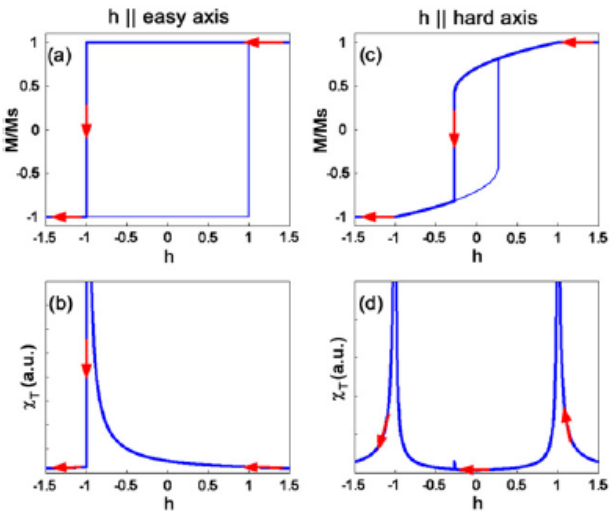

Figure 5. Calculated hysteresis loops along an easy axis (*a*) and along a hard axis (*c*) and calculated TS curves with the bias field along an easy axis (*b*) and along a hard axis (*d*) for a single domain particle with fourfold anisotropy. Only coherent rotation processes were taken into account in the calculations. The arrows indicate the sense of the applied field. The abscissa is the normalized field $h = H_1/H_k$ for the hysteresis loop and $h = H/H_k$ for the TS, H_k being the anisotropy field.

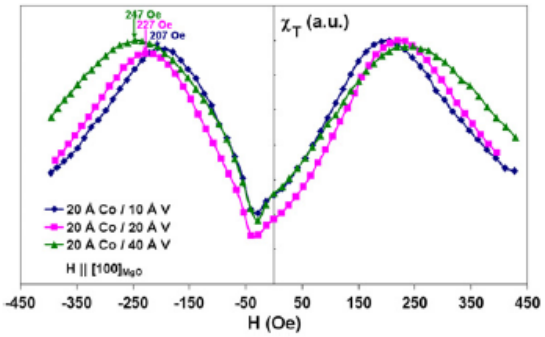

Figure 6. TS curves for the samples Al/20 Å Co/t_V ÅV/MgO(0 0 1) with H along the $[1\,0\,0]_{MgO}$ direction. Vanadium thickness layer $t_V = 10$, 20 and 40 Å. The effective anisotropy fields are marked by arrows.

4.1. The role of V thickness

The TS with H along the [1 0 0] direction is shown in figure 6 for the films Al/20 Å Co/t_V V/MgO (0 0 1), with $t_V = 10$, 20 and 40 Å. The effective macroscopic anisotropy field increases as the V layer thickness is increased, from a value of $H_{Keff} =$ 207 Oe for $t_V = 10$ Å up to $H_{Keff} = 247$ Oe for $t_V = 40$ Å. This could be put down to a discontinuous growth of the V layer, so that some Co is grown directly on the MgO buffer layer. As is well known, Co grows in the fcc structure on MgO (0 0 1) [25], the anisotropy constant of fcc Co being lower than that of hcp Co. Moreover, the easy axes of Co(hcp)/V/MgO(0 0 1) and those of Co(fcc)/MgO(0 0 1) are parallel [25], so a fraction of fcc Co should decrease the value of the effective magnetic anisotropy. A proof of the discontinuity of the V layer is obtained from a detailed analysis of the TS with H parallel to the easy axes (figures 7(*a*) and (*b*)). Four important features stand out: (1) the magnetization reversal

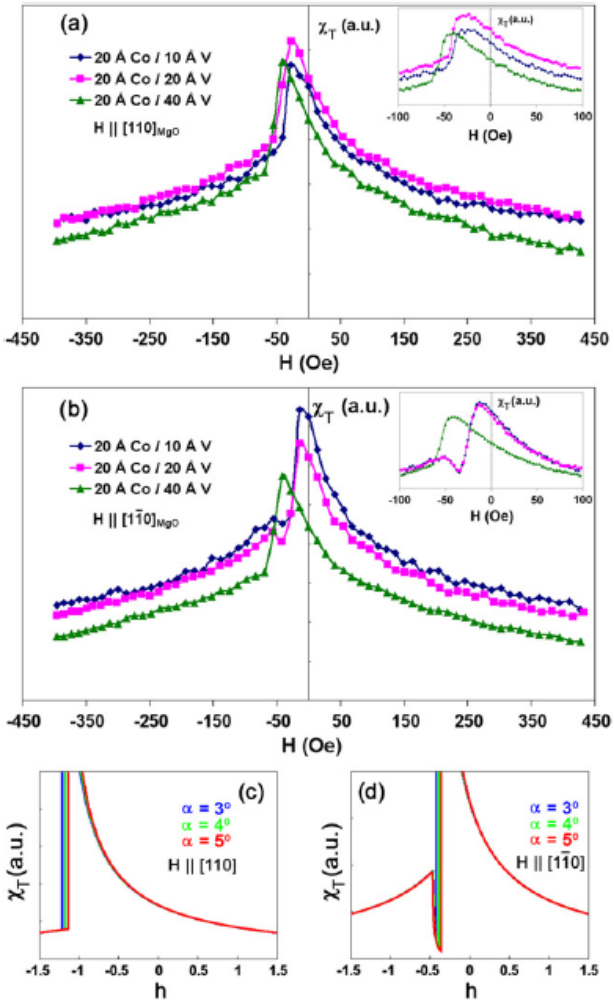

Figure 7. TS curves for the samples Al/20 Å Co/t_V Å V/MgO(0 0 1) with H along the [1 1 0]$_{MgO}$ (*a*) and the [1 $\bar{1}$ 0] (*b*) directions. Vanadium layer thickness $t_V = 10$, 20 and 40 Å. The insets show a closer view of the coercive field. (*c*) and (*d*) Calculated TS curves for a system with fourfold anisotropy and a uniaxial anisotropy superimposed with H along both easy axes, named [1 1 0] and [1 $\bar{1}$ 0]. The uniaxial anisotropy easy axis was at an angle $\alpha = 3°$, 4° and 5° from the [1 1 0] easy axis, and the ratio of the uniaxial to the fourfold anisotropy was $r = 0.4$.

takes place smoothly, in a magnetic field range of about 20 Oe for each of the samples, (2) the coercive force increases as the V layer thickness increases, (3) the coercive force along the [1 1 0] direction is greater than along the [1 $\bar{1}$ 0] direction for the films with $t_V = 10$ and 20 Å and (4) a minimum at $H \approx 40$ Oe for H parallel to the [1 $\bar{1}$ 0] is observed for $t_V = 10$ and 20 Å, which disappears for $t_V = 40$ Oe. This minimum has been observed previously on Fe/MgO [16] and and its origin put down to a superimposed uniaxial anisotropy.

Hence, in agreement with previous observations and in order to understand the behavior of TS, we calculated the TS curves for a system with fourfold anisotropy and a uniaxial anisotropy superimposed using the Stoner–Wohlfarth model. The results are shown in figures 7(*c*) and (*d*). Let us assume that the uniaxial anisotropy appears when Co is grown directly on MgO. In such a case, Co is grown in the fcc phase, with the easy axes along the [1 1 0] and [1 $\bar{1}$ 0] directions. Let $r = K_u/K_1$ be the ratio of the uniaxial anisotropy energy to the biaxial anisotropy energy and α the angle between the uniaxial anisotropy easy axis and the [1 1 0] direction. We calculated the TS curves for such a system with $r = 0.4$ and taking the uniaxial easy axis lying close to the [1 1 0] biaxial easy axis (for example $\alpha = 3°$, 4° and 5°). We obtained that (1) H_c along the [1 1 0] direction is greater than along the [1 $\bar{1}$ 0] one and (2) TS with H along the [1 $\bar{1}$ 0] direction exhibits a characteristic minimum. The minimum in TS is produced by an alignment of the magnetization close to the [1 1 0] direction during the magnetization reversal along the [1 $\bar{1}$ 0] direction.

According to the theoretical calculations, the experimental finding that H_c along the [1 1 0] direction is greater than along the [1 $\bar{1}$ 0] direction and the minimum in the TS curve for H along the [1 $\bar{1}$ 0] direction can be put down to a superimposed uniaxial anisotropy. The biaxial anisotropy and the superimposed uniaxial anisotropy could both be intrinsically produced as a consequence of the anisotropies involved when hcp Co is grown with the *c* axis along two perpendicular directions. Effectively, it has been theoretically shown [11] and experimentally reported [8] that an assembly of uniaxial crystallites with the easy axes lying along two orthogonal directions amounts to a fourfold anisotropy and a uniaxial anisotropy superimposed. In such a case, the hard axes of the fourfold anisotropy lie along the uniaxial easy axes of the crystallites. If this were the case for the Co/V thin films under study, the hard axes should lie along the [1 1 0] and [1 $\bar{1}$ 0] directions. Our experimental results contradict such predictions. On the other hand, we must take into account that the minimum in the TS curve disappears when the V layer thickness increases and that this minimum has been observed previously on Fe/MgO [16]. These experimental findings can be put together by assuming that the uniaxial anisotropy is induced by the MgO buffer layer.

4.2. *The role of Co thickness*

We now proceed with the samples with the stacking structure 30 Å Al/t_{Co} Co/40 Å V/ MgO(0 0 1) with $t_{Co} = 20$, 40, 100 and 200 Å. According to the results above, we can assume that in this case the V layer is continuous and only hcp Co is grown onto MgO.

The TS with H along the [1 0 0] direction is shown in figure 8(*a*) for $t_{Co} = 40$, 100 and 200 Å (for $t_{Co} = 20$ Å see figure 6). For $t > 20$ Å the effective magnetic anisotropy is so high that the samples could not be saturated in our experimental set-up, in which a magnetic field H up to 430 Oe can be attained. Effectively, the peaks in the TS at $H = \pm H_{Keff}$ were not observed, and only the 'valley' between $\pm H_{Keff}$ is observed in figure 8(*a*) (see the inset). The jump observed corresponds to H_c. For $t_{Co} = 20$ Å the magnetization reversal along the hard axes is not governed by the magnetocrystalline anisotropy of each hcp Co crystallite, and the sample is saturated at $H = H_{Keff} = 247$ Oe (see the peaks in figure 6). When t_{Co} is increased the grain size increases as well and the magnetization reversal along the hard axes is governed by the magnetocrystalline anisotropy of each hcp Co crystallite. Due to the high magnetocrystalline anisotropy of hcp Co, the samples cannot be saturated in our experimental set-up. In the latter case, we observed that the magnetization reversal

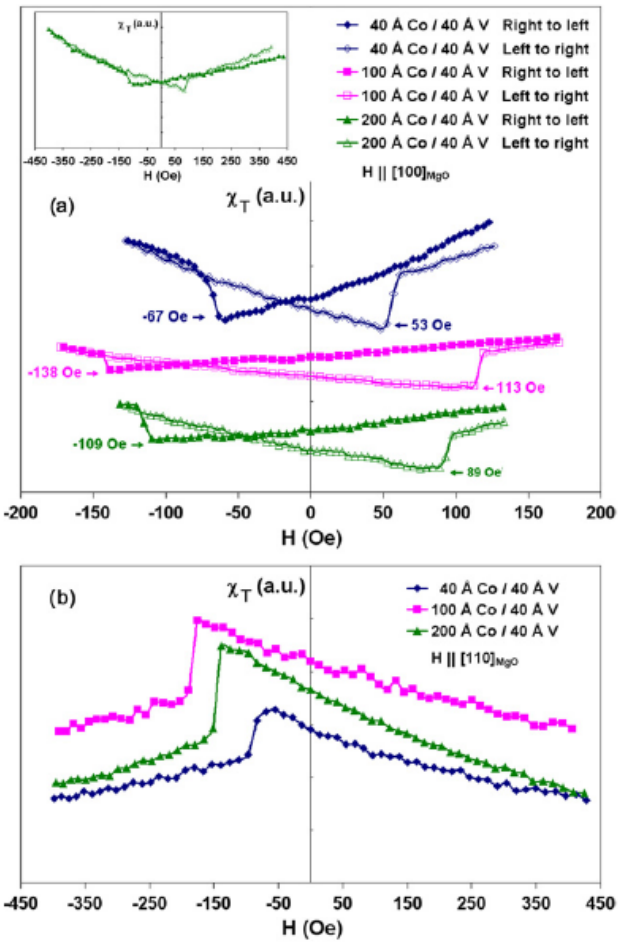

Figure 8. TS curves for the samples Al/t_{Co} Å Co/40 Å V/MgO(0 0 1) with H along the [1 0 0]$_{MgO}$ (*a*) and along the [1 1 0]$_{MgO}$ (*b*) directions. Cobalt layer thickness $t_{Co} = 40$, 100 and 200 Å. In (*a*) the coercive field values are marked by arrows. The inset in (*a*) shows the measurement in the complete range of fields attained in order to show the lack of saturation.

along the [1 0 0] direction is asymmetric as can be seen from the position of the jumps at $H = \pm H_c$ in figure 8(*a*). This asymmetry was also noticed in the hysteresis loops. TS measurements with H parallel to the [1 1 0] direction are shown in figure 8(*b*). TS along the other easy axis (not shown) are very much the same. The magnetization reversal along the easy axis is influenced by the thickness of the Co layer. While for $t_{Co} = 20$ Å the magnetization reversal takes place from 47 to 64 Oe (an indication of the discontinuity of the sample), for $t_{Co} > 20$ Å the magnetization reversal takes place more abruptly, in a narrower magnetic field range, due to a quick domain wall displacement throughout the sample.

Let us now get more insight into the asymmetry of magnetization reversal along the [1 0 0] direction. It is remarkable that the samples exhibiting the asymmetric hysteresis loops along the hard axes exhibited stepped hysteresis loops along an intermediate direction between the hard and easy axes as shown in figures 9(*a*) and (*b*) for the film with $t_{Co} = 100$ Å. The existence of both asymmetric and stepped hysteresis loops could lead us to think of exchange anisotropy in the system [26, 27] or to grain boundary effects (spin freezing). However such a hypothesis must be ruled out

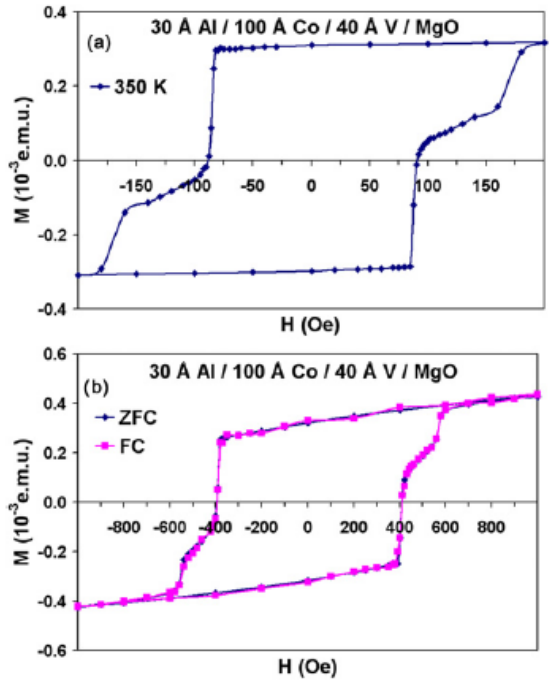

Figure 9. SQUID hysteresis loops for the sample Al/100 Å/40 ÅV/MgO(0 0 1) along a direction between an easy and a hard axis. (*a*) Hysteresis loop at 350 K and (*b*) ZFC and FC hysteresis loops at 5 K.

according to the results shown in figure 9. Effectively, the exchange anisotropy could be due to the existence of a top layer of CoO on the Co one. This CoO layer was not detected by XRD. However the exchange anisotropy has to be ruled out since the stepped hysteresis loop, as shown in figure 9(*a*), was still observed at a temperature of 350 K, which is above the CoO Néel temperature of 270 K [28]. On the other hand, we have performed the hysteresis loop along the intermediate direction at 5 K, by cooling the sample from RT in the presence of a magnetic field of 5 T (FC hysteresis loop) and by cooling the sample from RT in the absence of a magnetic field (ZFC hysteresis loop). Both loops are shown in figure 9(*b*). The shape of the hysteresis loop along the intermediate direction does not change appreciably, so the exchange anisotropy must be ruled out as an explanation for the stepped hysteresis loop. On the other hand, if grain boundary effects were the source of this behaviour, a stepped hysteresis loop should have been observed along any direction, which is not the case.

Now we can show that the asymmetry is due to the fact that the samples are not saturated for $t_{Co} = 40$, 100 and 200 Å. In order to check the relation between the asymmetry in the magnetization process and the non saturation of the samples, we measured the hysteresis loops at higher magnetic fields with a SQUID magnetometer. The hysteresis loops for $t_{Co} = 200$ Å are shown in figure 10. The loops in figure 10(*a*) were recorded between +3000 and −3000 Oe in order to ensure saturation (only the part of the loop between +300 and −300 Oe is shown). The asymmetry along the hard axis has vanished. The asymmetry is present when the hysteresis is recorded between +300 and −300 Oe (figure 10(*b*)).

It is worth noting here that, although a sample seems to be saturated by a simple inspection of the hysteresis loop if the magnetic moment is not directly measured (see figure 4

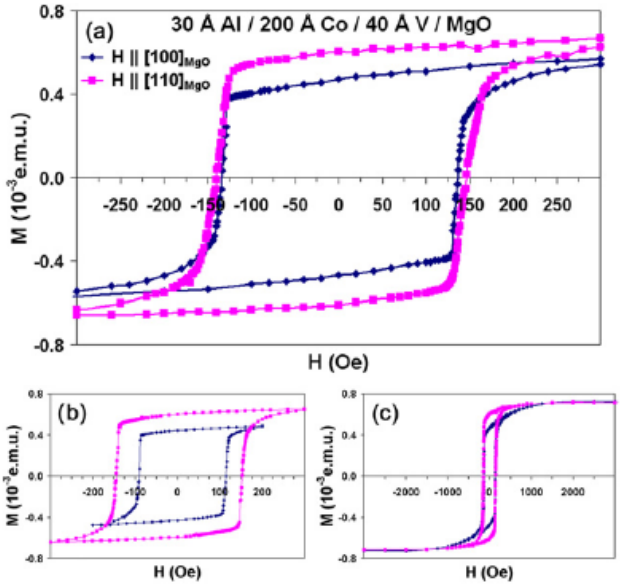

Figure 10. Room temperature SQUID hysteresis loops for the sample Al/200 Å Co/40 Å V/ MgO(0 0 1) along an easy and a hard axis. (*a*) A close view of the hysteresis loops for fields between 3000 and −3000 Oe, (*b*) hysteresis loops for fields between 300 and −300 Oe and (*c*) complete hysteresis loops between 3000 and −3000 Oe.

for instance), TS measurements with H parallel to the hard axes clearly evidence the non saturated state, since in such a case, the peaks at $H = \pm H_{K\text{eff}}$ are not observed. Figure 10(*c*) shows the complete hysteresis loops along one easy axis and one hard axis between +3000 and −3000 Oe. According to this figure the magnetization process comprises two mechanisms: magnetization rotation at high field values and domain wall displacement at low fields, corresponding to the observed coercive field. The saturation along the hard axis is attained at a field of 1500 Oe. The saturation magnetization obtained from the saturation magnetic moment and taking into account the dimensions and Co thickness of the sample was 1460 emu cm^{-3}, very close to the saturation magnetization of bulk hcp Co [28].

According to these results we can conclude that the samples behave as a system with a fourfold magnetic anisotropy. The magnetization reversal along the easy axis proceeds via magnetic domain walls displacement. The magnetization reversal along the hard axes involves two mechanisms. In some regions of the sample the magnetization is reversed via domain wall displacement. In the rest of the sample the magnetization is reversed via magnetization rotation towards the hard axis. If the applied magnetic field is not high enough to ensure the complete magnetization rotation, the unreversed regions create a bias field so that an asymmetrical hysteresis loop is observed. The asymmetry vanishes when the sample is completely saturated, so no bias field affects the magnetization reversal process.

5. Conclusions

Hcp Co grown on bcc V exhibits a fourfold anisotropy related to the fact that two types of Co crystals are grown with the *c* axis in the plane of the film and perpendicular to each other. The vanadium layer is discontinuous for a thickness below 40 Å, so that fcc Co is grown directly on MgO(0 0 1). In this latter case, a superimposed magnetic anisotropy develops due to the substrate. The effective magnetic anisotropy of hcp Co increases as the Co layer thickness increases. For the lower Co layer thickness, neither the effective magnetic anisotropy nor the magnetization reversal is governed by the Co magnetocrystalline anisotropy. Unexpected hard axis shifted hysteresis loops were observed for the thicker samples. Only when the samples are saturated does the shift vanish. ZFC and FC hysteresis loops and 350 K hysteresis loops ruled out the possibility of an exchange bias mechanism. The behaviour can be explained by taking into account that the magnetizations reversal along the hard axes takes place in two steps: at higher fields some regions of the samples rotate the magnetization towards the applied field and some others reverse the magnetization via domain wall motion at lower fields. If the applied field is not high enough to ensure saturation, the non reversed zones create a bias field that causes the observed shift.

Acknowledgments

This work has been supported by the Universidad de Oviedo and by projects MAT2006-03999 and NAN2004-08805-C04-02. The authors would like to thank Drs A Cebollada from Instituto de Microelectrónica de Madrid and Y Huttel from Instituto de Ciencia de Materiales de Madrid for growing and providing the samples and for the XRD data. BP would like to thank II Plan Regional de Investigación del Principado de Asturias for financial support.

References

[1] Parkin S S P 1991 *Phys. Rev. Lett.* **67** 3598
[2] Krishman R, Catinaud T, Seddat M, Porte M and Tessier M 1996 *J. Magn. Magn. Mater.* **159** 175
[3] Du J, Lu M, Tong L N, Ji W, Zhai H R and Xia H 1996 *J. Magn. Magn. Mater.* **177–181** 1209
[4] Huttel Y, van der Laan G, Johal T K, Telling N D and Bencok P 2003 *Phys. Rev.* B **68** 174405
[5] Huang J C A, Liou Y, Tao Y D, Yang W T, Chang C P, Liao S L and Hu Y H 1995 *Phys. Rev.* B **52** R13110
[6] Lo K, Liou Y, Chang C P, Klik I, Yao Y D and Huang J C A 1996 *Appl. Phys. Lett.* **68** 2155
[7] Lo C K, Klik I, Chang C P, Liou Y, Yang C S, Yao Y D and Huang J A C 1997 *Appl. Surf. Sci.* **113–114** 160
[8] Gu E, Gester M, Hicken R J, Daboo C, Tselepi M, Gray S J, Bland J A C, Brown M L, Thomson T and Riedi P C 1995 *Phys. Rev.* B **52** 14704
[9] Klik I,Chen U M, Yao Y D, Lo C K, Chang C P, Liao S Y and Liou Y 1997 *Appl. Surf. Sci.* **1113–1114** 165
[10] Wu Y Z, Ding H F, Jing C, Wu D, Dong G S, Jin X F, Sun K and Zhu S 1999 *J. Magn. Magn. Mater.* **198–199** 297
[11] Zhu J G and Ye X G 1993 *IEEE Trans. Magn.* **29** 324
[12] Jagla E A 2005 *Phys. Rev.* B **72** 094406
[13] Thomson T, Riedi P C and Krishnan R 2000 *J. Appl. Phys.* **87** 6594
[14] Du J, Lu M, Tong L N, Ji W, Zhai H R and Xia H 1998 *J. Magn. Magn. Mater.* **177** 1209
[15] Huttel Y, Navarro E and Cebollada A 2005 *J. Cryst. Growth* **273** 474
[16] Contreras M C, Calleja J F, Rivas M, Gutiérrez M O and Corrales J A 1997 *J. Magn. Magn. Mater.* **175** 64

[17] Lo C K, Klik I, Liou Y, Chang C P, Yang C S and Yao Y D 1998 *J. Magn. Magn. Mater.* **177–181** 1257
[18] Ikuhara Y, Sugawara Y, Tanaka I and Pirouz P 1997 *Interface Sci.* **5** 5
[19] Ikuhara Y and Pirouz P 1998 *Microsc. Res. Tech.* **40** 206
[20] Gutsche M, Kraus H, Jochum J, Kemmather B and Gutekunst G 1994 *Thin Solid Films* **248** 18
[21] Gutsche M, Kraus H, Jochum J and Kemmather B 1995 *Proc. Topical Symp. IV on Superconductivity (Florence, Italy, 1995)* pp187–94
[22] Stancu A and Spinu L 2003 *J. Magn. Magn. Mater.* **266** 200
[23] Calleja J F, Menéndez J L, Cebollada A and Contreras C 2001 *Japan. J. Appl. Phys.* **40** 6829
[24] Stoner E C and Wohlfarth E P 1948 *Trans. R. Soc.* A **240** 599
[25] Doyle W D 1966 *IEEE Trans. Magn.* **MAG-2** 68
[26] Nogués J, Sort J, Langlais V, Skumryev V, Surinach S, Munoz J S and Baro M D 2005 *Phys. Rep.* **422** 65
[27] Bruck S, Sort J, Baltz V, Surinach S, Munoz J S, Dieny B, Baro M D and Nogues J 2005 *Adv. Mater.* **17** 2978
[28] O'Handley R C 2000 *Modern Magnetic Materials* (New York: Wiley)

Capítulo 5

Conclusiones

La idea general del trabajo ha sido explicar los diferentes comportamientos magnéticos que pueden tener las láminas delgadas de Co dependiendo de las características estructurales, substratos y condiciones de deposición. Para ello se han depositado y caracterizado láminas delgadas de Co crecidas por diferentes medios y sobre diferentes sustratos, con los siguientes resultados:

Co con crecimiento no epitaxial crecido sobre vidrio:

- No se observa formación de islas. Los patrones XRD muestran que las láminas son policristalinas con fase principalmente hcp.
- El tamaño del grano aumenta con el espesor de las láminas y desempeña un papel determinante en la evolución de la anisotropía de las muestras, que varía desde una anisotropía uniáxica muy bien definida hasta un comportamiento cuasi-isótropo.
- Los valores del campo de anclaje llegan a ser el doble del campo coercitivo, aumentado con el espesor de Co.

Co con crecimiento no epitaxial en forma de islas crecido sobre Si_3N_4:

- Todas las láminas delgadas mostraron un comportamiento magnético isótropo.
- El sistema presenta un claro crecimiento 3D debido a la alta temperatura del sustrato durante el proceso de deposición.
- Los resultados AFM muestran un patrón nanoestructurado bien definido para las muestras con espesores nominales por debajo de los 5 nm. A medida que el espesor de Co aumenta, las partículas incrementan su tamaño y terminan percolando.
- La anisotropía magnética efectiva está ligada al tamaño de la partícula, a la distribución de tamaños y a la interacción interpartícula. El recubrimiento de Au

(poco polarizable) o Pt (altamente polarizable) modifica de manera significativa la interacción entre partículas.

Bicapas Co/V y V/Co con crecimiento epitaxial crecidas sobre MgO:

- Cuando se crece Co sobre óxido de magnesio exhibe una estructura cristalina fcc, mientras que si está depositado sobre vanadio su estructura es hcp, afectando de manera fundamental a las propiedades magnéticas de estos sistemas.

- No se encontró, mediante efecto Kerr polar, señal remanente de imanación en ninguna muestra, lo que indica una fuerte anisotropía de forma debido a la estructura 2D de los sistemas estudiados, que coloca a la imanación siempre en el plano de la película.

- Los ciclos de histéresis medidos para el sistema Co_{hcp}/V_{bcc}/MgO muestran dos claros ejes de fácil imanación los cuales se corresponden con los ejes ‘c’ del cobalto hcp crecido sobre las aristas de vanadio bcc.

- En muestras con espesores de Co 40 Å, 100 Å y 200 Å crecidas sobre V se observa una pequeña asimetría del ciclo de histéresis a lo largo de las direcciones de difícil imanación.

- El espesor de cobalto hcp depositado sobre vanadio influye tanto en los procesos de inversión de la imanación como en los valores de campo coercitivo y de la anisotropía magnética.

Bibliografía

[1] J. Freeland, Y.B.Xu, E.T.M. Kernohan, M. Tselepi and J.A.C.Bland, "Scaling behaviour and evolution of ferromagnetism in epitaxial Fe/GaAs(100) and Fe/InAs(100)", Thin Solid Films, 344:210, 1999

[2] Bland JAC, Hope S, Choi BC, et al. Magnetic anisotropy engineering in in-plane magnetized ultrathin ferromagnetic films (invited) J. Appl. Phys. 85, 4613 (1999)

[3] J. Frenkel and J. Dorfman, Nature (London) 126, 274 (1930)

[4] Ch. Kittel, Phys. Rev. 70, 965 (1946)

[5] L. Néel, Ann. Geophys. (C.N.R.S.) 5, 99 (1949)

[6] W.F. Brown, J. Appl. Phys. 30, 130S (1959)

[7] W.F. Brown, Phys. Rev. 130, 1677 (1963)

[8] G.C.Hadjipanayis and G.A.Prinz (eds.), Science and Technology of Nanostructured Magnetic Materials, Series B: Physics, Plenum Press, New York, NATO Advanced Study Institute (1991), Vol.259

[9] Enders, R. Skomski and J. Honolka . Magnetic Surface nanostructures
J. Phys. Condens. Matter 22 (2010) 433001

[10] Exchange bias in nanostructures by J Nogues, J Sort, V Langlais, V Skumryev, S Surinach, J Muñoz, M Baro Physics Reports (2005) Volume: 422, Issue: 3, Publisher: Elsevier, Pages: 65 - 117

[11] A.Jordan, R.Scholz, and K.Maier-Hauff, F.K.H. van Landeghem, N.Waldoefner, U.Teichgraeber, J.Pinkernelle, H.Bruhn, F.Neumann, B.Thiesen, A. von Deimling, and R.Felix, *J. Neuro-Oncology* 78, 7 (2006)

[12] H.J.Lee and S.H.Jeong, *Textile Research Journal* 75, 551 (2005)

[13] R.H.Müller, S.Runge, V.Ravelli, W.Mehnert, A.F .Thünemann, and E.B.Souto, *Int. J. Pharm.* 317, 82 (2006)

[14] .D.Kuempel, C.L.Tran, and V.Castranova, *Inhalation Toxicology* 18, 717 (2006)

[15] I. J. Vera Marún, F. M. Postma, J. C. Lodder, and R. Cansen, Phys. Rev. B **76**, 064426, 2007

[16] N. D. Hughes and R. J. Hicken, J. Phys. D: Appl. Phys. **35**, 3153, 2002

[17] F. Prieto, L. M. Lechuga, A. Calle, A. Llobera, and C. Domínguez, J. Lightwave Technol. **19**, 75, 2001

[18] D. O. Hogenboom, S. A. Oliver, and C. A. Dimarzio, Appl. Opt. **37**, 7218, 1998

[19] R. P. H. Kooyman, and L. M. Lechuga, Handbook of Biosensors and Electronic Noses, Ch. 8. CRC Press, 1997

[20] S. S. Parkin, Phys. Rev. Lett. **67**, 3598, 1991

[21] R. Krishnan, T. Catinaud, M. Seddat, M. Porte, M. Tessier, J. Magn. Magn. Mater. **159**, 175, 1996

[22] J. Du, M. Lu, L. N. Tong, W. Ji, H. R. Zhai, H. Xia, J. Magn. Magn. Mater. **177-181**m 1209, 1996

[23] Y. Obi, M. Ikebe, T. Kubo, H. Fujimori, Physica C **317-318**, 149, 1999

[24] Y. Huttel, C. Clavero, G. van der Laan, P. Bencok, T. K. Johal, J. S. Claydon, G. Armelles, A. Cebollada, Phys. Rev. B **77**, 064411, 2008

[25] Clavero C, Martínez L, García-Martín A, García-Martín J M, Huttel Y, Telling N D, van der Laan G, Cebollada A and Armelles G 2008 Phys. Rev. B **77**, 094417

[26] Denardin J C, Brandl A L, Knobel M, Panissod P, Pakhomov A B, Liu H and Zhang X X 2002 Phys. Rev. B **65** 064422

[27] Denardin J C, Nunes W C and Knobel M 2006 Physica B **384** 290

[28] Bastos C S M, Bahiana M, Nunes W C, Novak M A, Altbir D, Vargas P and Knobel M 2002 Phys. Rev. B **66** 214407